Modeling Methane Utilization by Methanotrophs in Groundwater: Applications for Groundwater Bioremediation

Thesis by

Edye C. Udell

In Partial Fulfillment of the Requirements

for the Degree of

Doctor of Philosophy

California Institute of Technology

Pasadena, California

1997

(Submitted July 12, 1996)

Acknowledgments

First and foremost I want to thank my advisor, Professor Mary Lidstrom. She gave me the freedom to pursue the research I was most interested in doing, trusted me enough to let me run with it, and set me back on the right path when I found myself stumbling along a side road leading nowhere. Throughout my tenure at Caltech, Mary was a source of inspiration. I want to thank Dr. Brooks for helping me see the beauty of transport phenomena. His Hydrology class gave me a new perspective on transport and many of the issues I never before understood finally clicked.

I want to thank several of the Caltech staff. I could not have completed my thesis without the help of Rick Gerhart, the Chemistry Department glassblower. He saved my research career when my column reactor broke and he miraculously found a way to fix it. That was a bad week... Fran Matzen helped me keep track of my sanity as I was finishing up my thesis.

I can't forget my lab - I could not have gotten to this point without you all. Thanks to all my friends at Caltech! Susan Paulsen and Selena Forman helped me stay sane during the last three years of graduate school. Thanks for all the long talks, the willing ears, and the hugs. And thank you so much Susan for proofreading my chapters. Thanks to Kim Mislick for her friendship over the years. Caltech would not have been the same without her. She has been not only a great friend and roommate, but also a great party-mate. I think that any two people who can live together while both writing up a thesis are meant to be friends forever.

Thanks to Bob Blake for going through my hell period with me. After knowing first hand what its like to finish a thesis I can't figure out how he was able to keep his sanity between that and my demands. Some people are just crazy.

One more thing for Bob - I never would have met Chris Karp and Maria Khader if it wasn't for him. Life has funny twists. Those two are amazing. Chris is always willing to lend a helping hand, even when the amount of help he's giving is way beyond the call of duty. And Maria, well, to know Maria is to love her. She's been there through the thick and thin of the last year. And that's saying a lot. Anyone willing to start a friendship with someone trying to finish a thesis is taking a big risk. The thesis writer becomes a taker whether or not that's his/her innate persona. Thanks Maria for taking the risk - I hope you'll find it's been worth it.

And to the people who have been pushing me along for the last few years, how can I ever thank you enough. Michael Tsapatsis kept calling from Massachusetts asking me, "Are you going to finish soon? Are you going to apply for an academic job? Go for it!! Are you going to visit me soon? You have to finish so you can come to Greece." Ahhhhh, Greece. Michael, it's finally going to happen!

I wasn't sure where I wanted to thank her in this maze of people, but here seems most appropriate. I want to thank Chariklia Economou for her smile, her love of life, her memory, and for reminding me that what's most important is to try to find something you can enjoy each day. Chara was an inspiration to me. She helped me look at my life and make some hard decisions about where life was going to lead me. Thank you for your smiles.

The other big pusher was Kelly Goodwin. Every time I thought about how it would be easier to not finish this monster than to finish it, I heard Kelly's voice: You are going to do this. You haven't come this far for nothing! Well, Kelly, I had my doubts, but I guess you were right all along. Kelly has been so much more, though, than just someone who has helped me complete this thesis. She has been my confidant, a source of strength, a friend, and a teacher. I hope someday she will feel that I have given her as much as she has given to me.

Rob Johnson has been not only a great friend, but also a great help with my thesis. He was always willing to spend his time talking over questions. He provided beneficial insight to many issues that arose as I completed my thesis. And all along, he has been a supportive friend. Kelly and Rob, you two are awesome. Who knows, maybe relationships can last forever! If any can, yours is one of 'em.

I'm getting a bit longwinded here. So I'll try to keep the rest short. Just kiddin', Jeff! I had to start you off with a joke. I don't know how I would have survived the last seven months of writing without Jeff. It's amazing what finishing a thesis can do to a personality. And somehow Jeff has trusted that underneath this sharp, easily irritated, selfish persona I have been trying to control lies a friendly warm-hearted person. Jeff, I can't pretend I haven't been the nicest person while writing this thesis, but I'm hoping that your trust will pay off and the person I think I am will reappear once this is all over. Have I really been as bad as everyone says? I hope I can laugh in a few years when I look back at this. In all seriousness, Jeff has truly helped make thesis writing a bearable experience.

And finally, I want to thank my family. I miss you all and wish Caltech was in Chicago. Such is the life of a scientist. My mother always supported my life decisions once they were set in stone and helped me tremendously throughout my schooling. I give her much credit for helping me reach this pinnacle in my life. My father was a large motivation for my choosing to major in Chemical Engineering. I remember playing with that chemistry set when I was young. Maybe chemicals remind me of doing cool experiments with him!

One of the most important things I think I have learned from my graduate school career is that it's okay, and may even be necessary, to depend on other people. I know I could never have finished my thesis without everyone's help. It is amazing how much life thesis writing can take out of a person. My advice to those who do it next is: don't forget to take a break every so often and accept any and all help from your friends. You'll need it and you'll have the rest of life to make it up to them.

Abstract

A model was developed to predict substrate concentrations for bacterial growth in a groundwater system. The model coupled substrate transport and oxidation by cells with bacterial growth. A reactor was designed that could test the model's ability to correctly predict the biological and physical phenomena governing the reactor setup. In order to design the reactor, I needed a methanotroph strain capable of attaching well to sand contained in the reactor. I found that *Methylomicrobium albus* BG8 cells attached strongly to the pretreated Ottawa sand used for the reactor solid phase. I also analyzed the effect of copper on methane utilization kinetics for this strain because prior evidence suggested copper may influence kinetic parameters. I found that copper did not have a statistically significant effect on methane utilization kinetics under the experimental conditions used. I also found that the mathematical model worked well to predict methane concentrations throughout the reactor over time. Model input parameters were then analyzed for their influence on model predictions. I found that the Michaelis-Menten maximum rate of methane utilization and Monod maximum specific growth rate had the largest effect on model predictions. I also found that mass transfer from the bulk liquid to bacteria attached to particles could have a large impact on model predictions. The mass transfer effect was greatest when the substrate concentration was less than or equal to the Michaelis-Menten affinity coefficient and Monod half-maximum growth rate constant.

Table of Contents

Acknowledgments iii

Abstract vii

Table of Contents viii

Chapter 1 - Introduction 1-1

1.1 Groundwater Contamination 1-2

1.2 Forms of Remediation 1-2

1.3 Bioremediation 1-3

1.4 Modeling Bioremediation 1-6

1.5 References 1-8

Chapter 2 - Modeling Transport Coupled with Substrate Oxidation 2-1

2.1 Abstract 2-2

2.2 Introduction 2-3

2.3 Review of Models Previously Published 2-3

2.4 Overview of Michaelis-Menten and Monod Kinetics 2-5

2.4.1 Derivation of Michaelis-Menten Kinetics 2-6

2.4.2 Modified Monod Kinetic Equations Used in Published Models 2-8

2.5 Proposed Model for Substrate Utilization and Bacterial Growth 2-10

2.6 Transport 2-11

2.7 Modeling Transport Combined with Degradation 2-12

2.8 Numerical Simulation Method 2-16

2.9 Testing the Simulation 2-18

2.10 Results 2-21

2.11 Conclusions 2-22

2.12 References 2-28

Chapter 3 - Reactor Design Part 1: Methanotroph Attachment to Sand 3-1
3.1 Abstract 3-2
3.2 Introduction 3-3
3.3 Background on Methanotrophs 3-3
3.4 Strains Selected for Study 3-5
3.5 Materials and Methods 3-5
3.5.1 Materials 3-5
3.5.2 Cell Growth Conditions 3-5
3.5.3 Attachment Experiments 3-5
3.5.4 Protein Assays of Sand and Liquid Samples 3-8
3.6 Results and Discussion 3-8
3.7 Conclusions for Cell Attachment 3-11
3.8 References 3-19

Chapter 4 - Reactor Design Part 2: Methane Utilization Kinetic Parameter Determinations 4-1
4.1 Abstract 4-2
4.2 Introduction 4-3
4.3 Materials and Methods 4-5
4.3.1 Materials 4-5
4.3.2 Cell Growth Conditions 4-5
4.3.3 Determining the Mass Transfer Coefficient 4-6
4.3.4 Determining the Kinetic Parameters V_{max}' and K_S 4-8
4.3.4.1 Experimental Setup - Methane Stock Vials 4-8
4.3.4.2 Experimental Setup - Cell Preparation 4-9
4.4 Results and Discussion 4-11
4.4.1 Mass Transfer Coefficient Determination 4-11
4.4.2 Kinetic Parameter Determination 4-14

4.4.2.1 Calculating a Maximum Cell Density for Non-Mass Transfer Limited Kinetics 4-14
4.4.2.2 Cell Densities and Copper Concentrations 4-16
4.4.2.3 Kinetic Parameters 4-17
4.5 Conclusions and Summary 4-20
4.6 References 4-42

Chapter 5 - Reactor Design Part 3: Transport Parameter Determinations, Reactor Setup, and Comparison of Model Predictions to Reactor Data 5-1
5.1 Abstract 5-2
5.2 Introduction 5-3
5.3 Materials and Methods 5-3
5.3.1 Materials 5-3
5.3.2 Transport Parameter Determinations 5-4
5.3.3 Growth Kinetics: μ_{max} and $K_{S\text{-}Monod}$ 5-6
5.3.4 Medium Preparation and Column Setup 5-7
5.3.5 Column Sampling Procedure: Methane Analysis 5-9
5.3.6 Column Sampling Procedure: Cell Density Analysis 5-11
5.3.7 Model Simulation Procedure 5-12
5.4 Results and Discussion 5-13
5.4.1 Longitudinal Dispersion Coefficient 5-13
5.4.2 Maintenance Energy 5-14
5.4.3 Maximum Specific Growth Rate: μ_{max} 5-15
5.4.4 Controls: Methane Leakage, Sampling Assays 5-16
5.4.5 Comparison of Reactor Data to Model Predictions 5-19
5.4.5.1 Short Term Column Experiments, Limited Growth 5-19
5.4.5.2 Column Experiments Run for Times on the Order of Cell Doubling Times 5-21

5.5 Conclusions 5-24
5.6 References 5-44

Chapter 6 - Model Parametric and Dimensional Analysis, Groundwater Simulations, and Mass Transfer Limitation Analysis 6-1
6.1 Abstract 6-2
6.2 Introduction 6-3
6.3 Methods 6-3
6.4 Results 6-4
6.4.1 Dimensional Analysis 6-4
6.4.2 Parametric Analysis 6-7
6.4.3 Groundwater Simulations: Mass Transfer Limitation 6-10
6.5 Conclusions 6-12
6.6 References 6-27

Chapter 7 - Summary and Conclusions 7-1

Appendix A - Fortran Program Used for Numerical Simulations A-1

Appendix B - List of Variables B-1

Chapter 1

Introduction

1.1 Groundwater Contamination

Several studies have demonstrated the vast nature of hazardous waste contamination of the nation's groundwater supply (Westrick *et al.*, 1984). The main pollutants found in groundwater are volatile organic carbon compounds, generally chlorinated hydrocarbons. In addition, several semi-volatile organic carbon compounds such as polynuclear aromatic hydrocarbons are widely distributed in groundwater systems. Enhanced methods of remediation are needed for hazardous waste containment and decontamination of the groundwater supply because currently accepted methods do not remove the bulk of the contamination. Until the last decade, technological advancements in the treatment of groundwater contamination were not achieved. However, recent political pressure has caused government to emphasize new technological developments in remediation. This has come about due to recognition of the amount of expenditures put into studying groundwater contamination rather than remediating polluted sites.

1.2 Forms of Remediation

The main method of remediation currently under use for contaminated groundwater is a process called "pump and treat" (Travis and Doty, 1990). This involves pumping clean water into a contaminated aquifer and pumping contaminated groundwater out of the system through a well downstream from the input water. The water pumped out is treated above ground and then either returned to the aquifer as clean water or used for other approved purposes. The above ground treatment takes many forms, including, but not limited to bioremediation, chemical treatment such as

ozonation, and physical treatment such as contaminant volatilization. While the "pump and treat" method can work well to prevent contaminants from spreading beyond the original site of contamination, the method does not adequately remove the bulk of the contamination from the system (Travis, 1992). This is due to the strong adsorption of many contaminants to the solids fraction of the aquifer as well as the presence of non-aqueous phase liquids (NAPLs), which have a tendency to remain stagnant.

Several solutions to this problem exist. One possibility is adding compounds to the aquifer to increase the desorption of contaminants from the solids or NAPLs into the liquid phase coupled with pumping clean water through the water column. Another strategy is using *in situ* bioremediation. The research presented in this thesis focuses on predicting the best strategies for this area.

1.3 Bioremediation

Bioremediation is defined in this thesis as the use of microorganisms for degrading hazardous wastes to less hazardous wastes, or, preferably, to inert compounds such as carbon dioxide, chloride ions and water. Two types of bioremediation may take place. These are intrinsic and enhanced bioremediation. Intrinsic bioremediation occurs naturally, without the addition of compounds that may enhance the ability for bacteria to break down contaminants. This type of bioremediation has been given more attention recently because it is becoming more widely recognized and it is less expensive than the alternative form. Enhanced bioremediation, as its name suggests, is bioremediation done in a way which enhances

the bioremediation that would take place without the addition of any compounds to a contaminated site.

Many options exist for enhancing *in situ* bioremediation. These include:

- adding a combination of nutrients, carbon sources, cometabolic substrates, and/or terminal electron acceptors to a site to promote the growth of bacteria naturally present in the system capable of degrading the contaminant of concern,
- adding microorganisms known to degrade specific wastes to a contaminated site, and
- adding microorganisms that have been genetically engineered to degrade the contaminants of concern to a site.

The research presented herein focuses on the first of these three alternatives. Nutrients are an essential component for cellular growth. Often they are at limiting quantities in natural environments. The terminal electron acceptor for aerobic processes, oxygen, is usually limiting and is often added to systems undergoing enhanced bioremediation. Carbon sources are needed only if the contaminants cannot serve as a carbon source and a natural carbon source for the desired bacteria is not present in sufficient quantity to support the bioremediation treatment. Cometabolic substrates are needed when the contaminant does not serve as a carbon or energy source. Addition of the cometabolic substrate enables growth of bacteria capable of degrading the contaminant. Upon growing, the cells produce an enzyme that can oxidize or reduce the contaminant.

This work focuses on the problem of bioremediation of trichloroethylene (TCE) by methanotrophs, bacteria that grow on methane as a carbon and energy

source. These cells produce methane monooxygenase (MMO), an enzyme that oxidizes methane to methanol. Two forms of this enzyme may be made by methanotrophs. These are soluble MMO (sMMO), which is present in the cytoplasm, and particulate MMO (pMMO), which resides in cell membranes. Soluble MMO has a broad substrate range while pMMO has a much narrower substrate range (Burrows *et al.*, 1984). The particulate form of the MMO is believed to oxidize TCE to TCE-epoxide. Soluble MMO oxidizes TCE to TCE-epoxide or to chloral (Fox *et al.*, 1990). TCE-epoxide undergoes a number of different chemical reactions to form less toxic intermediates. These intermediates and chloral can be oxidized by other ubiquitous bacteria to form chloride, water, and carbon dioxide.

Site remediators add methane to TCE-contaminated sites in order to enhance the growth of methanotrophs naturally present. This process is known as cometabolism because TCE does not support growth. The addition of methane, a cometabolic substrate, does enable methanotrophs to grow and then degrade TCE present in the system.

In order to optimize *in situ* bioremediation site evaluators need predictive models to understand the fate and transport of contaminant(s) of concern and nutrients and substrates needed for cell growth. In addition, laboratory scale reactors representing simplified aquifer systems are needed for testing predictive models. After the initial fate and transport questions are answered these reactors can be made more complex to address additional questions.

1.4 Modeling Bioremediation

In a real groundwater system many fates exist for chemicals, including chemical and biological reactions and different types of physical placement in the system. One important factor is sorption, which can cause a large fraction of the contaminants to remain attached to the aquifer's solid phase. Recent evidence suggests that a certain fraction of specific contaminants is sorbed strongly to inner portions of soil aggregates. The desorption time for these species is much larger than for recently sorbed molecules. Another important factor is whether the contaminants have the same density as water. If not, the contaminants may form non-aqueous phase liquid contaminant fractions (NAPLs). These can exist throughout the contaminated area, ranging in size from small, millimeter diameter NAPLs, to large pools of NAPLs floating on the surface of the aquifer (gasoline, for example), or sinking to an impermeable zone (dense liquids such as TCE).

The fate and transport characteristics of all added nutrients, substrates, and terminal electron acceptors are also key factors for modeling bioremediation. Depending on the aquatic chemistry of the system, these added components may adsorb to aquifer solids. This would decrease the distribution of these species throughout the aquifer.

Cells present in the system may be attached to solid surfaces or floating freely in the water phase. Past evidence suggests that most of the cell mass in natural systems will be attached to the solid phase of the aquifer (van Loosdrecht *et al.*, 1990). The contaminant degradation time will be dependent upon whether cells are

moving with the water in the system or remaining in one point in space as the water moves past the biomass.

Kinetic parameters for cell growth, substrate utilization, and contaminant breakdown by bacteria also strongly affect the time needed for bioremediation. If cometabolic substrates are added, specific strains of cells capable of degrading contaminants will likely outcompete other strains. Different conditions such as fixed nitrogen limitation, phosphate limitation, carbon or energy limitation and contaminant bioavailability will all affect the bioremediation potential.

Modeling *in situ* bioremediation is a complex task due to the number of different parameters affecting this process. Past modeling attempts have succeeded in predicting liquid phase contaminant concentrations (Semprini *et al.*, 1992). However, the kinetic parameters described above are generally fit for the models and much leeway exists for fitting data.

The work presented herein describes a method to test predictive models without the need for fitting parameters. A reactor representing a simplified groundwater system was developed to address and answer specific questions regarding contaminant fate and transport in a bioremediation scheme. The system can be used to break down the larger fate and transport questions into smaller, more approachable questions. Once the initial questions are answered, the system can be modified to include additional chemical fates in order to address further fate and transport issues.

1.5 References

Burrows, K.J., Cornish, A., Scott, D., & Higgins, I.J. (1984). Substrate specificities of the soluble and particulate methane monooxygenases of *Methylosinus trichosporium* OB3b. *Journal of General Microbiology, 130,* 3327-3333.

Fox, B.G., Borneman, J.G., Wackett, L.P., & Lipscomb, J.D. (1990). Haloalkene oxidation by the soluble methane monooxygenase from *Methylosinus trichosporium* OB3b: mechanistic and environmental implications. *Biochemistry, 29,* 6419-6427.

Semprini, L., & McCarty, P.L. (1992). Comparison between model simulations and field results for *in situ* biorestoration of chlorinated aliphatics: part 2. cometabolic transformations. *Ground Water, 30,* 37-44.

Travis, C.C. (1992). Toxic waste in groundwater: can it be removed? *The Journal of NIH Research, 4,* 49-51.

Travis, C.C., & Doty, C.B. (1990). Can contaminated aquifers at Superfund sites by remediated? *Environmental Science and Technology, 24,* 1464-1466.

van Loosdrecht, M.C.M., Lyklema, J., Norde, W., & Zehnder, A.J.B. (1990). Influence of interfaces on microbial activity. *Microbiological Reviews, 54,* 75-87.

Westrick, J.J., Mello, J.W., & Thomas, R.F. (1984). The groundwater supply survey. *Journal of the American Water Works Association, 76,* 52-59.

Chapter 2

Modeling Transport Coupled with Substrate Oxidation

2.1 Abstract

A theoretical model representing the fate and transport of a substrate capable of supporting methanotroph growth in a groundwater system is described. The fate considered is bacterial metabolism of the substrate coupled with microbial growth. Previously published models related to this field are reviewed. The model presented herein includes characteristics from several different published models and a different method for describing substrate oxidation. This oxidation is modeled by Michaelis-Menten kinetics. Modified Monod kinetics are used to describe methanotroph growth. It is assumed that the bacteria attached to particles form a monolayer, i.e., substrate diffusion through a biofilm is not considered. A numerical method for solving the arising coupled set of partial differential equations is presented. Analytical solutions for simplified model cases are compared to numerical simulations to show the validity of the numerical solution.

2.2 Introduction

Transport of chemicals in porous media coupled with non-linear reaction and absorption to solids is a complex process. Many researchers have attempted to model the fate of biodegradable compounds in porous media systems such as groundwater (Semprini *et al.*, 1991, 1992; Schafer *et al.*, 1992; Taylor *et al.*, 1991; Wu *et al.*, 1990; Dhawan *et al.*, 1991, 1993; Angley *et al.*, 1992; Molz *et al.*, 1986; Widdowson *et al.*, 1988). Only a few of these models were compared to real systems (Semprini *et al.*, 1991, 1992; Angley *et al.*, 1992). The models that were compared to physical systems were fairly successful in correctly predicting experimental data. However, researchers fit many model parameter values to force the model to correctly predict data; not all parameters were defined before running a simulation. This thesis presents a model that includes non-fitted parameters. Each model parameter is determined by direct measurement or by empirical equations rather than being fit to force simulations to correctly predict data obtained in column experiments.

The model described in this chapter is a simplified one-dimensional transport model. It is based on the advection-dispersion equation, which is modified to include substrate oxidation by bacteria. This oxidation is modeled by Michaelis-Menten kinetics. Cell growth over time is modeled by Monod kinetics. A full description of these kinetic models is contained in Section 2.4.

2.3 Review of Models Previously Published

Several models in the literature discuss transport coupled with substrate and/or contaminant oxidation by bacteria in groundwater (Semprini *et al.*, 1991, 1992;

Schafer *et al.*, 1992; Taylor *et al.*, 1991; Wu *et al.*, 1990; Dhawan *et al.*, 1991, 1993; Angley *et al.*, 1992; Molz, *et al.*, 1986; Widdowson *et al.*, 1988). There are several common features to most models and some differences. All models utilize the advection-dispersion equation for transport and incorporate a sink term for microbial metabolism of substrates, electron acceptors and/or contaminants. The equations for metabolism are generally consistent, using modified forms of Monod kinetics to represent both cellular growth and metabolite oxidation. One model does not include bacterial growth and simplifies the kinetics of uptake to a first-order model (Angley *et al.*, 1992). This was probably done because the researchers were looking at effects of non-equilibrium metabolite sorption to solids in addition to microbial metabolism. Most models include a retardation factor to represent equilibrium sorption of compounds to aquifer solids. It is not common for these models to contain non-equilibrium sorption, though as described above, an exception does exist (Angley *et al.*, 1992). Also uncommon is to include mass transfer resistance to metabolite utilization by bacteria attached to particle surfaces (Semprini *et al.*, 1991; Schafer *et al.*, 1992; Taylor *et al.*, 1991; Wu *et al.*, 1990; Dhawan *et al.*, 1993). Only one group consistently incorporates mass transfer resistances (Molz *et al.*, 1986; Widdowson *et al.*, 1988). A short discussion of the importance of including the boundary layer is found in one of these papers (Widdowson *et al.*, 1988).

2.4 Overview of Michaelis-Menten and Monod Kinetics

Michaelis-Menten substrate utilization kinetics and Monod growth kinetics display similar mathematical characteristics. The Michaelis-Menten equation has the form (Lehninger, 1982):

$$V = \frac{V_{\max} S}{K_m + S} \tag{2-1}$$

where:

V = velocity of reaction $\left(\frac{m_s}{l^3 t}\right)$ (m_s is the mass of substrate)

S = substrate concentration $\left(\frac{m_s}{l^3}\right)$

V_{max} = maximum velocity of reaction $\left(\frac{m_s}{l^3 t}\right)$

K_m = affinity coefficient, or substrate concentration at half the maximum velocity of reaction $\left(\frac{m_s}{l^3}\right)$

The Monod equation for growth kinetics has the form (Monod, 1949):

$$\mu = \frac{\mu_{\max} S}{K_{S_{Monod\,S}} + S} \tag{2-2}$$

where:

μ = specific growth rate of cells ($1/t$)

μ_{max} = maximum specific growth rate ($1/t$)

$K_{S_{Monod\,S}}$ = substrate concentration at half the maximum growth rate $\left(\frac{m}{l^3}\right)$

The Michaelis-Menten model is based on theoretical assumptions about enzymatic processes while the Monod growth equation is empirical. The assumptions

and theoretical basis for the Michaelis-Menten equation are described in Section 2.4.1. Modified Monod equations used in the literature for both substrate utilization and cell growth are presented in Section 2.4.2. A description of the equations used for modeling substrate utilization and cell growth in this thesis is contained in Section 2.5.

2.4.1 Derivation of Michaelis-Menten Kinetics

The Michaelis-Menten model assumes that an enzyme and substrate form an enzyme-substrate complex, which either forms a product and regenerates an enzyme molecule or reforms the original enzyme and substrate molecules. The reactions are:

$$E + S \underset{k_{-1}}{\overset{k_1}{\longleftrightarrow}} ES \qquad (2\text{-}3)$$

$$ES \xrightarrow{k_2} E + P \qquad (2\text{-}4)$$

where:

E = enzyme

S = substrate

P = breakdown product

If we assume pseudo-steady-state conditions, where the concentration of the enzyme substrate complex is approximately constant, then the breakdown and formation of ES are equal. Thus,

$$k_1\left([E_t] - [ES]\right)[S] = k_{-1}[ES] + k_2[ES] \qquad (2\text{-}5)$$

where $[E_t]$ is the total enzyme including free enzyme and enzyme containing the substrate. The pseudo-steady-state assumption holds if the total number of enzyme molecules is much less than the total number of substrate molecules. This is true for most enzymatic reactions. Rearranging the equation, one obtains:

$$[ES] = \frac{[E_t][S]}{[S] + \frac{k_{-1} + k_2}{k_1}} \tag{2-6}$$

The velocity of reaction, V, is equal to k_2*[ES]. Thus,

$$-\frac{d[S]}{dt} = V = \frac{k_2[E_t][S]}{[S] + \frac{k_{-1} + k_2}{k_1}} \tag{2-7}$$

Setting $K_m = (k_{-1}+k_2)/k_1$, and $V_{max} = k_2*[E_t]$, equation 2-1 is derived:

$$V = \frac{V_{max} S}{K_m + S} \tag{2-1}$$

In whole cell experiments, as opposed to pure enzyme experiments, the maximum rate of consumption depends on the cell concentration, assuming that each cell has the same number of active enzymes. The equation is then written:

$$V = \frac{V_{max} S}{K_S + S} \tag{2-8}$$

where V_{max} now represents the maximum velocity found with whole cells and K_s is the substrate concentration at half the maximum velocity in whole cell experiments.

Here, V_{max} is normalized to the total amount of liquid in the reactor. It is common in the literature to report values of V_{max} as the maximum rate of substrate utilization normalized to total cell mass, rather than to liquid volume. In this case, the equation is:

$$V' = \frac{V_{max}' S}{K_S + S} \tag{2-9}$$

The units for V' and V_{max}' in this equation are:

V' = rate of substrate utilization per unit cell mass $\left(\frac{m_s}{t\, m_c}\right)$ (m_s represents substrate mass, m_c represents cell mass)

V_{max}' = maximum rate of substrate utilization per unit cell mass $\left(\frac{m_s}{t\, m_c}\right)$

Note that with these units, V' does not equal -dS/dt. V' must be multiplied by the cell concentration to obtain -dS/dt.

2.4.2 Modified Monod Kinetic Equations Used in Published Models

The environmental engineering literature most commonly uses modified Monod kinetics to model both cell growth and substrate utilization (Widdowson *et al.*, 1988). Substrate utilization is linked to cell growth via a yield coefficient (mass cells produced per mass substrate oxidized). Cell growth and substrate utilization are considered functions of both electron donor (substrate) and electron acceptor (oxygen) concentrations. The typical equations follow (Semprini *et al.*, 1991; McCarty, 1975):

$$\frac{\partial X}{\partial t} = \mu_{\max} \frac{S}{K_{S_{Monod\,S}} + S} \frac{O}{K_{S_{Monod\,O}} + O} X - \mu_{dec} X \qquad (2\text{-}10)$$

$$-\frac{\partial S}{\partial t} = \frac{1}{Y}\left(\frac{\partial X}{\partial t} + \mu_{dec} X\right) \qquad (2\text{-}11)$$

$$-\frac{\partial O}{\partial t} = \frac{F}{Y}\left(\frac{\partial X}{\partial t} + \mu_{dec} X\right) + d_c f_d \mu_{dec} X \frac{O}{K_{S_{Monod\,O}} + O} \qquad (2\text{-}12)$$

where:

X = cell mass concentration $\left(\frac{m_c}{l^3}\right)$

S = substrate concentration $\left(\frac{m_s}{l^3}\right)$

$K_{S_{Monod_S}}$ = substrate half saturation constant $\left(\frac{m}{l^3}\right)$

O = oxygen concentration $\left(\frac{m_s}{l^3}\right)$

$K_{S_{Monod_O}}$ = oxygen half saturation constant $\left(\frac{m}{l^3}\right)$

μ_{dec} = specific decay rate of cells ($1/t$)

Y = cell yield coefficient $\left(\frac{m_c}{m_s}\right)$

F = stoichiometric ratio of substrate to oxygen utilization for cell growth $\left(\frac{m_{oxygen}}{m_{substrate}}\right)$

d_c = cell decay oxygen demand $\left(\frac{m_{oxygen}}{m_{cell}}\right)$

f_d = biodegradable fraction of cells (-)

Several key assumptions are inherent in these equations. These include:

1) Cell yield is not a function of substrate or oxygen concentrations.

2) The stoichiometric ratio of substrate to oxygen utilization, F, is constant.

3) Oxygen is consumed only by cells utilizing the substrate or dead cells for carbon and energy.

Assumption 1 is contradicted by literature data. Researchers have shown that as the methane:oxygen ratio was decreased from 2 to 1 in the feed to a chemostat grown methanotrophic culture, the yield coefficient increased by a factor of 2

(Morinaga *et al.*, 1979). In addition, F increased by a factor of 2 when the cells were switched from oxygen limitation to methane limitation. Finally, in natural systems, a wide variety of bacteria are present. Many naturally occurring bacteria would be capable of aerobically oxidizing carbon matter present in the system. This would negate assumption 3.

It also appears that several papers have confused the concept of cell maintenance energy with cell decay. In the Semprini model (1991) the equations above are used. However, the references in the paper for the value of μ_{dec} are cell maintenance energy coefficients (Heijnen *et al.*, 1981). In papers by Molz *et al.* (1986) and Widdowson *et al.* (1988), the authors use equations similar to 2-10 through 2-12 above. However, they describe μ_{dec} as a maintenance energy term, and then in the paper define the variable as a decay term.

2.5 Proposed Model for Substrate Utilization and Bacterial Growth

There are many difficulties involved in modeling substrate utilization and cell growth, as described in Section 2.4.2. While the models presented in the literature are widely accepted, they generally do not incorporate information about microbial physiology. However, these models are a good first approximation. In order to directly test the applicability of the model I have presented herein, I simplified the physical system in my column experiments. First, I ensured that the oxygen concentration in the liquid phase was much greater than the enzyme affinity coefficient for oxygen (i.e., $[O_2] >> K_{S_{Monod_O}}$). This is described more thoroughly in Chapter 5. By using oxygen concentrations at this level, I can set:

$$\frac{O}{K_{S_{Monod_O}} + O} = 1 \qquad (2\text{-}13)$$

Substrate utilization is modeled by Michaelis-Menten kinetics:

$$\frac{\partial S}{\partial t} = -\frac{V_{max}' XS}{K_S + S} \qquad (2\text{-}14)$$

Cell growth is modeled by the Monod equation with maintenance energy (Pirt, 1965; Heijnen *et al.*, 1981):

$$\frac{\partial X}{\partial t} = (\mu - a)X \qquad \text{for } \mu > a \qquad (2\text{-}15)$$

$$\frac{\partial X}{\partial t} = 0 \qquad \text{for } \mu < a \qquad (2\text{-}16)$$

where:

μ = specific growth rate (1/t)

a = specific maintenance energy rate (1/t)

and μ is defined by equation 2-2:

$$\mu = \frac{\mu_{max} S}{K_{S_{Monod_S}} + S} \qquad (2\text{-}2)$$

Cell decay is not considered in this model.

2.6 Transport

One-dimensional transport of a contaminant in groundwater, without degradation or surface adsorption, can be represented by the advection-dispersion equation:

$$\frac{\partial C_B}{\partial t} = D_L \frac{\partial^2 C_B}{\partial x^2} - U \frac{\partial C_B}{\partial x} \qquad (2\text{-}17)$$

where:

C_B = substrate concentration in the bulk fluid phase $\left(\frac{m}{l^3}\right)$

t = time (t)

D_L = longitudinal dispersion coefficient $\left(\frac{l^2}{t}\right)$

x = distance (l)

U = average linear groundwater velocity $\left(\frac{l}{t}\right)$

2.7 Modeling Transport Combined with Degradation

The model developed herein considers a monolayer of bacteria attached to particle surfaces. Substrate or contaminant diffusion through the biofilm is not considered. Under these conditions, substrate or contaminant molecules moving through a uniform sandy aquifer containing grains coated uniformly with bacteria can: 1) diffuse to the grain/bacterial surface and react with bacterial enzymes; 2) diffuse toward and adhere to the surface; 3) diffuse toward and away from the grain surfaces; or 4) continue moving along the direction of flow. For large grain Peclet numbers, particles' diffusion boundary layers do not cross one another. This should be the case for my laboratory column system, where mean particle diameters are 0.6 - 0.8 mm. Under these conditions, the mass transfer to a particle at a fixed position can be approximated by:

$$N_{substrate} = \frac{D}{\delta}\left(C_B - C_s\right) \qquad (2\text{-}18)$$

where:

$N_{substrate}$ = flux of substrate from the bulk fluid to a particle surface $\left(\frac{m}{l^2 t}\right)$

D = substrate diffusion coefficient $\left(\frac{l^2}{t}\right)$

δ = particle diffusion boundary layer thickness (l)

C_b = bulk concentration $\left(\frac{m}{l^3}\right)$

C_s = substrate concentration near the surface of particles $\left(\frac{m}{l^3}\right)$

The diffusion boundary layer thickness is not easily defined. Therefore, a mass transfer coefficient k_c is often employed to represent the quantity D/δ. This coefficient has the units of length/time. For column experiments done in Chapter 5, empirical relationships are used to estimate k_c.

The substrate flux to particles must equal the amount of substrate oxidized by bacteria attached to particles if no surface absorption is occurring. This is the case for methane. A single-particle-scale can be used to calculate a macroscopic-scale flux in order to identify concentration changes in the bulk liquid due to biological metabolism. The equation follows:

$$\left.\frac{\partial C_B}{\partial t}\right|_{\substack{bacterial \\ metabolism}} = -N_{substrate} \frac{\#sand\ grains}{V_t} \frac{SA}{sand\ grain} \frac{1}{\varepsilon} \qquad (2\text{-}19)$$

where:

$\frac{\#sand\ grains}{V_t}$ = total number of sand grains per total volume $\left(\frac{1}{l^3}\right)$

$\frac{SA}{sand\ grain}$ = surface area of cells exposed to fluid per sand grain (l^2)

ε = fluid volume/total volume, also known as the porosity (-)

Equation 2-19, can be simplified to:

$$\left.\frac{\partial C_B}{\partial t}\right|_{\substack{bacterial \\ metabolism}} = -\alpha\ X\ N_{substrate} = -\alpha\ X\ k_c\left(C_B - C_S\right) \qquad (2\text{-}20)$$

where:

X = cell mass concentration $\left(\frac{m_c}{volume\ fluid}\right)$

α = surface area of cells exposed to fluid per unit mass of cells $\left(\frac{l^2}{m_c}\right)$

I approximate α using the following assumptions:

- a single cell is a sphere 1 μm in diameter,
- one-half the surface of each cell is exposed to fluid,
- a single cell weighs approximately 3×10^{-13} g (based on the weight of an *E.Coli* cell) (Neidhardt *et al.*, 1990).

Bacterial metabolism is modeled by Michaelis-Menten substrate uptake kinetics coupled to Monod growth kinetics. The Michaelis-Menten substrate oxidation kinetics are:

$$\left.\frac{\partial C_s}{\partial t}\right|_{\substack{bacterial \\ metabolism}} = -\frac{V_{max}' X C_s}{K_s + C_s} \qquad (2\text{-}21)$$

Substrate does not accumulate or dissipate over time except by cellular oxidation. Therefore, the change in the bulk substrate concentration must balance the

change in the substrate concentration near the surface of sand grains. Combining equations 2-20 and 2-21, I obtain:

$$\alpha X k_c (C_B - C_S) = \frac{V_{max}' X C_S}{K_S + C_S} \qquad (2\text{-}22)$$

This equation can be solved for the surface concentration in terms of the bulk substrate concentration:

$$C_S = \frac{-(K_S + \frac{V_{max}'}{\alpha k_c} - C_B) + \sqrt{(K_S + \frac{V_{max}'}{\alpha k_c} - C_B)^2 + 4K_S C_B}}{2} \qquad (2\text{-}23)$$

By incorporating equation 2-20 into the advection-dispersion equation, 2-17, I obtain the following overall equation for transport coupled with substrate oxidation by bacteria:

$$\frac{\partial C_B}{\partial t} = D_L \frac{\partial^2 C_B}{\partial x^2} - U \frac{\partial C_B}{\partial x} - \alpha X k_c (C_B - C_S) \qquad (2\text{-}24)$$

where C_S is defined by equation 2-23.

The concentration of cells, X, is a function of time and distance. As described in **Section 2.5**, Monod kinetics with cell maintenance energy are used to define X(x,t). The rate of growth of cells is:

$$\frac{\partial X}{\partial t} = (\mu - a)X = \frac{\mu_{max} X C_S}{K_{S_{Monod\,S}} + C_S} - aX \qquad (2\text{-}25)$$

Equations 2-24 and 2-25 are the governing equations for one-dimensional transport of non-adsorbing substrate molecules coupled with oxidation by growing cells attached to the solid phase of a sandy groundwater system. This set of coupled partial differential equations is solved numerically by the method described in Section 2.8.

The boundary and initial conditions are:

$C_B(0,t)$	=	f(t)	for all t
$\left.\frac{\partial C_B}{\partial x}\right\|_{x=L}$	=	0	for all t
$C_B(x,0)$	=	0	for x > 0
X(x,0)	=	g(x)	for all x

2.8 Numerical Simulation Method

The first step in solving equations 2-23, 2-24 and 2-25 is to break up the space dimension into a set of equi-distant nodes. The initial bulk substrate concentration and cell density are known at all nodes. The next procedure is to move forward one time step and solve for the new bulk substrate concentration at each node. The QUICK (Quadratic Upstream Interpolation for Convective Kinematics) method is used to calculate the first and second derivatives of bulk concentration with respect to distance (Leonard, 1979). This is a fully explicit method; calculations for all concentrations determined at t+Δt are based on the concentrations at time t. The advection term utilizes a four node difference equation, while central differencing is used for the dispersion term. The difference equations are:

$$\left.\frac{\partial^2 C_B}{(\partial x)^2}\right|_x^t = \frac{C_{B_{x+1}}^{\ t} - 2C_{B_x}^{\ t} + C_{B_{x-1}}^{\ t}}{(\Delta x^2)} \qquad (2\text{-}26)$$

$$\left.\frac{\partial C_B}{\partial x}\right|_x^t = \frac{\frac{1}{8}C_{B_{x-2}}^{\ t} - \frac{7}{8}C_{B_{x-1}}^{\ t} + \frac{3}{8}C_{B_x}^{\ t} + \frac{3}{8}C_{B_{x+1}}^{\ t}}{\Delta x} \qquad (2\text{-}27)$$

The substrate concentration near the surface of particles is calculated using equation 2-22. $C_{S_x}^{\ t}$ is calculated using $C_{B_x}^{\ t}$ and X_x^t. The new bulk substrate concentration is:

$$C_{B_x}^{\ t+1} = \left(D_L \frac{C_{B_{x+1}}^{\ t} - 2C_{B_x}^{\ t} + C_{B_{x-1}}^{\ t}}{(\Delta x^2)} - U \frac{\frac{1}{8}C_{B_{x-2}}^{\ t} - \frac{7}{8}C_{B_{x-1}}^{\ t} + \frac{3}{8}C_{B_x}^{\ t} + \frac{3}{8}C_{B_{x+1}}^{\ t}}{\Delta x} - \alpha X k_c \left(C_{B_x}^{\ t} - C_{S_x}^{\ t} \right) \right) \Delta t + C_{B_x}^{\ t} \qquad (2\text{-}28)$$

After calculating the substrate concentrations at each node at time t+Δt, the substrate concentration near particle surfaces and the cell concentration are determined for each node. Equation 2-23 is used to calculate $C_{S_x}^{\ t+1}$.

The concentration of cells at each point in space is determined using equation 2-25. A fourth-order Runge-Kutta method is used for the simulation. Linear interpolation is used to identify the substrate concentration near sand surfaces at times between t and t+Δt. The equations are:

$$X_x^{t+1} = X_x^t + \frac{k_1}{6} + \frac{k_2}{3} + \frac{k_3}{3} + \frac{k_4}{6} \qquad (2\text{-}29)$$

where:

$$k_1 = \Delta t \frac{X_x^t \mu_{\max} C_{S_x}^{\ t}}{K_{S_{Monod}} + C_{S_x}^{\ t}} \qquad (2\text{-}30)$$

$$k_2 = \frac{\Delta t \left(X_x^t + \frac{k_1}{2} \right) \mu_{\max} C_{S_x}^{\ t+\frac{1}{2}}}{K_{S_{Monod}} + C_{S_x}^{\ t+\frac{1}{2}}} \qquad (2\text{-}31)$$

$$k_3 = \frac{\Delta t \left(X_x^t + \frac{k_2}{2} \right) \mu_{\max} C_{S_x}^{\ t+\frac{1}{2}}}{K_{S_{Monod}} + C_{S_x}^{\ t+\frac{1}{2}}} \qquad (2\text{-}32)$$

$$k_4 = \frac{\Delta t \left(X_x^t + k_3 \right) \mu_{\max} C_{S_x}^{\ t+1}}{K_{S_{Monod}} + C_{S_x}^{\ t+1}} \qquad (2\text{-}33)$$

(Press *et al.*, 1989)

The computer program written to solve the numerical equations is contained in Appendix 1.

2.9 Testing the Simulation

In order to test whether the numerical simulation worked properly, it was compared to analytical solutions of simplified model cases. Under certain conditions, the kinetic term for contaminant removal simplifies to either 0 or first order kinetics. These conditions are:

1) The substrate concentration of the oxidizable compound near particle surfaces is much larger than K_S. The enzymatic capabilities of the bacteria are saturated and the bacteria degrade the contaminant at a constant rate: $V_{max}'X$.
2) The substrate concentration is much less than K_S. The term $C_S/(K_S+C_S)$ approaches C_S/K_S. Equation 2-22 becomes:

$$\alpha X k_c (C_B - C_S) = \frac{V_{max}' X C_S}{K_S} \qquad (2\text{-}34)$$

Solving this for C_S, and incorporating C_S back into the flux term, the rate of substrate removal is:

$$\left.\frac{\partial C_B}{\partial t}\right|_{\substack{bacterial \\ metabolism}} = \left(\frac{1}{\frac{1}{\alpha X k_c} + \frac{K_S}{V_{max}' X}} \right) C_B \qquad (2\text{-}35)$$

If I consider time scales much smaller than the minimum doubling time for cells, $\ln(2)/\mu_{max}$, then X remains approximately constant. For this short time scale with respect to cell doubling time, the macroscopic balance for the first case above is:

$$\frac{\partial C_B}{\partial t} = D_L \frac{\partial^2 C_B}{\partial x^2} - U \frac{\partial C_B}{\partial x} - V_{\max}' X \tag{2-36}$$

For case 2, the balance is:

$$\frac{\partial C_B}{\partial t} = D_L \frac{\partial^2 C_B}{\partial x^2} - U \frac{\partial C_B}{\partial x} - \left(\frac{1}{\frac{1}{\alpha k_c} + \frac{K_S}{V_{\max}' X}} \right) C_B \tag{2-37}$$

If I assume the concentration of cells, X, is constant and I set the inlet concentration equal to a constant, C_o, I can solve the steady-state solutions for 2-36 and 2-37. These are:

Case 1:

$$C_B(x) = C_O - \frac{V_{\max}' X x}{U} - \left(\frac{D_L V_{\max}' X}{U^2} \right) \left(e^{-\frac{UL}{D_L}} - e^{\frac{(x-L)U}{D_L}} \right) \tag{2-38}$$

Case 2:

$$C_B(x) = \frac{C_0 \left(e^{\left(\frac{U-v}{2D_L}\right)x} - \frac{U-v}{U+v} e^{\frac{(U+v)x-2vL}{2D_L}} \right)}{1 - \frac{U-v}{U+v} e^{\frac{vL}{D_L}}} \tag{2-39}$$

where:

$$v = U \sqrt{1 + \frac{4 \left(\frac{1}{\frac{1}{\alpha X k_c} + \frac{K_S}{V_{\max}' X}} \right) D_L}{U^2}} \tag{2-40}$$

Another simplified case is considered: the non-steady case including growth with the substrate concentration much greater than the affinity coefficients for substrate utilization and growth. The maintenance energy coefficient is set to 0. The

dispersion coefficient is also set to 0 in order to solve the coupled set of differential equations. These are:

$$\frac{\partial C_B}{\partial t} = -U\frac{\partial C_B}{\partial x} - V_{\max}{}' X \qquad (2\text{-}41)$$

and

$$\frac{dX}{dt} = \mu_{\max} X \qquad (2\text{-}42)$$

The initial condition is different for this case than for the model in order to uphold the assumption that $C_B >> K_{S_{Monod_S}}$ and $C_B >> K_S$. The boundary and initial conditions are:

$C_B(x,0)$	=	C_o	for all x
$C_B(0,t)$	=	C_o	for all t
$X(x,0)$	=	X_o	for all x

Solving 2-42 and incorporating the resulting equation for X into 2-41, I obtain:

$$\frac{\partial C_B}{\partial t} = -U\frac{\partial C_B}{\partial x} - V_{\max}{}' X_o e^{\mu_{\max} t} \qquad (2\text{-}43)$$

The solution to this PDE is:

$$C_B = C_o - \frac{V_{\max}{}' X_o}{\mu_{\max}}\left(e^{\mu_{\max} t} - 1\right) \qquad \text{for } t \le \frac{x}{U} \qquad (2\text{-}44)$$

$$C_B = C_o - \frac{V_{\max}{}' X_o}{\mu_{\max}}\left(e^{\mu_{\max} t} - e^{\mu_{\max}\left(t-\frac{x}{U}\right)}\right) \qquad \text{for } t > \frac{x}{U} \qquad (2\text{-}45)$$

In order to test numerical dispersion in the numerical simulations, one final case is considered: the advection-dispersion equation with no bacterial metabolism of substrate. By setting X_o to 0, the bacterial sink term reduces to 0. In order to uphold the fourth boundary condition listed below only times shorter than the time it takes for

the inlet flow to reach the outlet are considered for this case. The boundary conditions are:

$C_B(x,0)$	=	0	$x > 0$
$C_B(0,t)$	=	C_o	for all t
$X(x,t)$	=	0	for all x,t
$\left.\frac{\partial C_B}{\partial x}\right\|_{x=\infty}$	=	0	for all t

The solution to the advection-dispersion equation for this case is:

$$C(x,t) = \frac{C_0}{2}\left(erfc\left(\frac{x-Ut}{\sqrt{4D_L t}}\right) + e^{\frac{Ux}{D_L}} erfc\left(\frac{x+Ut}{\sqrt{4D_L t}}\right)\right) \qquad (2\text{-}45)$$

2.10 Results

Analytical solutions are compared to numerical simulations in Figures 2.1 through 2.4. Table 2.1 contains parameter values used for numerical simulations. Figure 2.1 shows Cases 1 and 2 (steady-state solutions for C_B much smaller and much larger than the affinity coefficients for substrate utilization). Figures 2.2 and 2.3 show Case 3 (non-steady with C_B much larger than the affinity coefficients for substrate utilization and growth) for times longer and shorter than the time it takes for the entering fluid to reach the column outlet. Figure 2.4 shows Case 4 (the advection-dispersion equation with no bacterial metabolism of substrate).

The results for the numerical simulations directly follow the analytical solutions in all the figures. This shows that the program I designed for the numerical simulation is correctly predicting solutions to limiting cases of the main partial differential equations, equations 2-24 and 2-25. Analytical solutions for a range of limiting cases

were analyzed. Therefore, I can conclude that the program will correctly predict the solution for the entire substrate concentration range. In addition, data in Figure 2.4 show that numerical dispersion for the simulation is negligible compared to physical dispersion.

2.11 Conclusions

The literature is filled with an array of models for coupling oxidation of substrates by bacteria with transport of the substrate in porous media. An attempt was made to decipher the different published models. A new model is defined based on physical characteristics of the natural system. Michaelis-Menten rather than Monod kinetics are used to describe substrate oxidation by bacteria because the Michaelis-Menten equation has a theoretical basis. The Monod equation is empirical. The program written to numerically solve the arising partial differential equations gives results that closely follow analytical solutions to simplified model cases. This program can be utilized to test the theoretical model's predictive capabilities. Comparisons of model predictions to column experiments are presented in Chapter 5. Parameter analyses and model predictions for natural systems are presented in Chapter 6.

Table 2.1. Parameter Values for Simulations Presented in Figures 2.1 - 2.4

Parameter	Units	Figure 2.1 Steady-State $C << K_S$	Figure 2.1 Steady-State $C >> K_s$	Figure 2.2 Non-Steady $C >> K_s$	Figure 2.3 Non-Steady $C >> K_s$	Figure 2.4 Non-Steady Xo=0
C_o	μM	0.1	400	100	100	100
L	dm	10	10	10	10	10
V_{max}'	μmol/hr/μg protein	0.02	0.02	0.02	0.02	0
μ_{max}	1/hr	1.00E-07	1.00E-07	1	0.04	1
D_L	dm^2/hr	0.07	0.07	0.0001	1.00E-07	0.01
k_c	dm/hr	5	5	5	5	5
α	dm^2/μg protein	0.001	0.001	0.001	0.001	0.001
U	dm/hr	10	10	10	0.1	1
K_S	μM	100	0.001	1.00E-06	1.00E-08	5
K_{SMonod}	μM	100	0.001	1.00E-06	1.00E-08	5
X_o	μg protein/ml	10	10	0.1	0.1	0
Δt	hr	0.001	0.001	0.001	0.001	0.001
Δx	dm	0.02	0.02	0.1	0.02	0.02

Figure 2.1. Comparison of Numerical Simulations to Analytical Solutions for Two Limiting Cases: $C << K_s$ and $C >> K_s$*

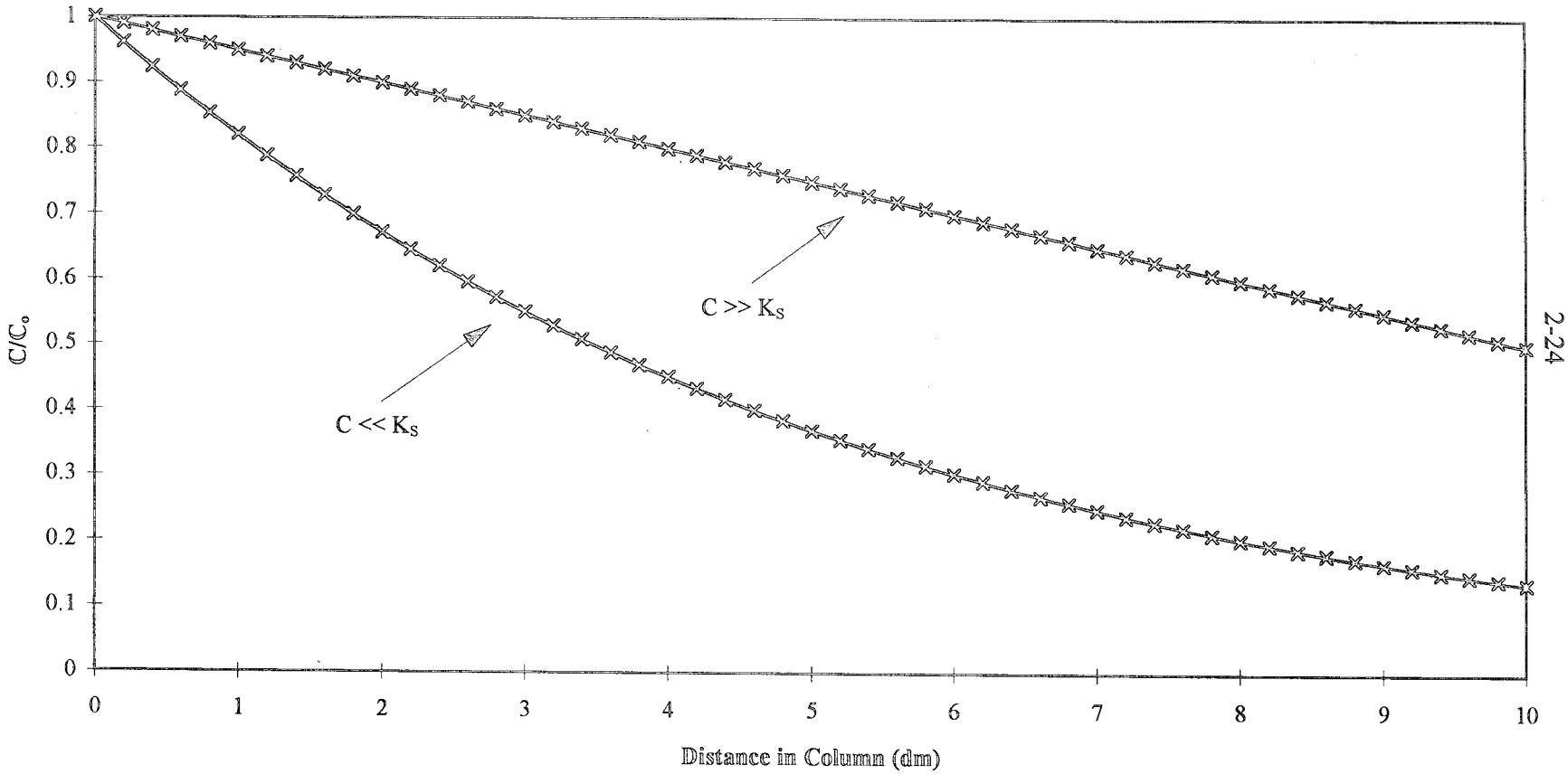

* Lines represent analytical solutions. Symbols represent numerical simulation results. The numerical simulations were allowed to run until steady state was achieved (t=2*Column Length/Pore Water Linear Velocity). Parameter values used for simulations are shown in Table 2.1.

Figure 2.2. Comparison of Numerical Simulation to Analytical Solution for the Non-Steady Case with $C >> K_S$ *

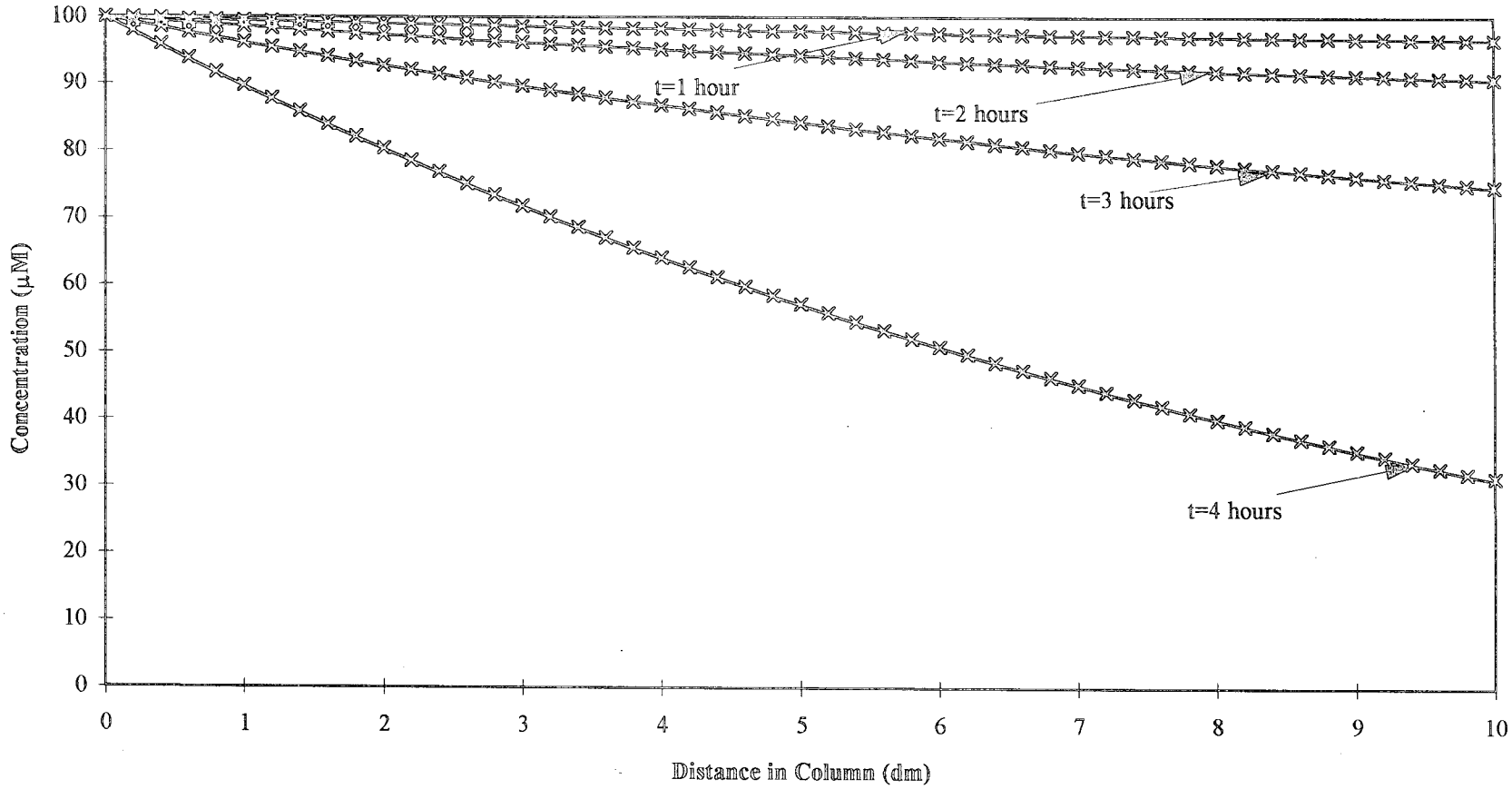

*Dispersion is set to 0 in the analytical solution and 0.0001 in the simulation. The QUICK method is used for the simulation. Lines represent analytical solutions at different times. Symbols represent simulation results. Parameters used for simulations are shown in Table 2.1.

Figure 2.3. Comparison of Numerical Simulation to Analytical Solution for the Non-Steady Case with $C >> K_s$ *

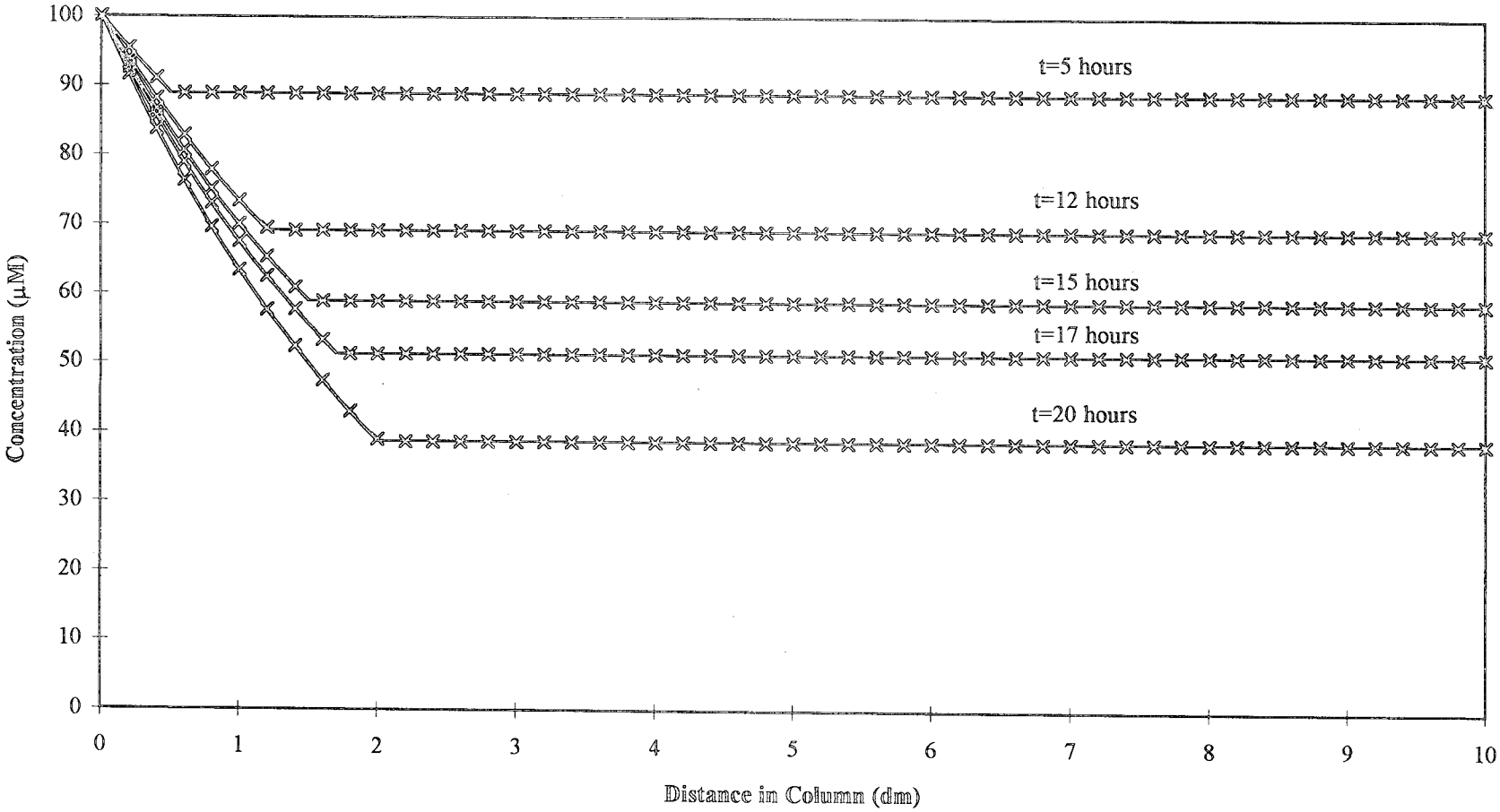

*Dispersion is set to 0 in the analytical solution. The Quick method is used for the simulation, with dispersion set to 1 E-7. Lines represent analytical solutions at different times. Symbols represent simulation results. Parameters used for simulations are shown in Table 2.1.

Figure 2.4. Comparison of Numerical Simulation to Analytical Solution for the Limiting Case: Cell Concentration = 0*

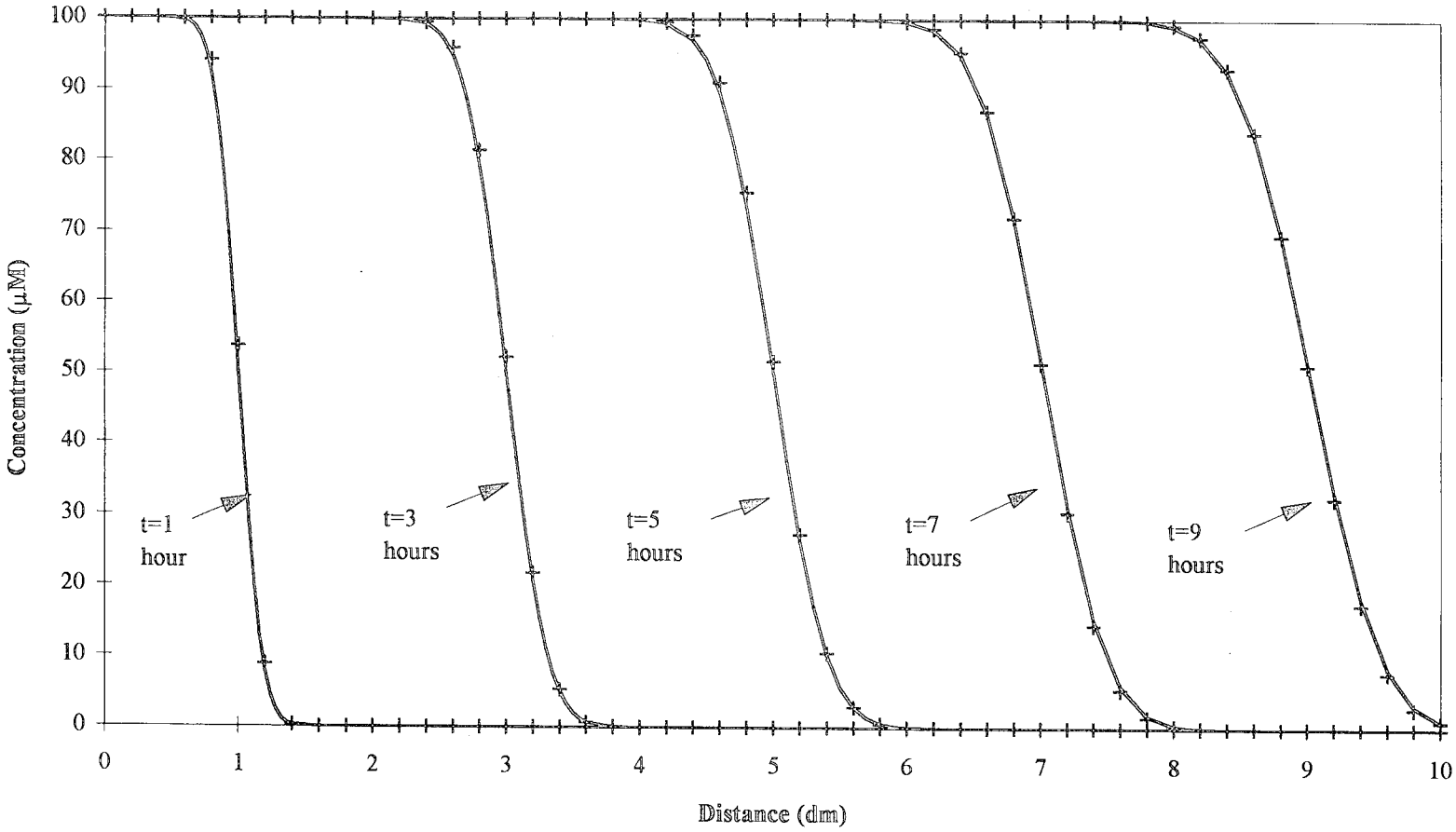

* Longitudinal dispersion was set to 0.01 dm^2/hr (3 x 10^{-4} cm^2/s), Velocity = 1 dm/hr. V_{max}' and X_o were set to 0 for the numerical simulation. Lines represent analytical solutions. Symbols represent numerical simulation results. Parameters used for simulations are shown in Table 2.1.

2.12 References

Angley, J.T., Brusseau, M.L., Miller, W.L., & Delfino, J.J. (1992). Nonequilibrium sorption and aerobic biodegradation of dissolved alkylbenzenes during transport in aquifer material: column experiments and evaluation of a coupled-process model. *Environmental Science and Technology, 26,* 1404-1410.

Dhawan, S., Erickson, L.E., & Fan, L.T. (1993). Model development and simulation of bioremediation in soil beds with aggregates. *Ground Water, 31,* 271-284.

Dhawan, S., Fan, L.T., Erickson, L.E., & Tuitemwong, P. (1991). Modeling, analysis, and simulation of bioremediation of soil aggregates. *Environmental Progress, 10,* 251-260.

Heijnen, J.J., & Roels, J.A. (1981). A macroscopic model describing yield and maintenance relationships in aerobic fermentation precesses. *Biotechnology and Bioengineering, 23,* 739-763.

Lehninger, A.L. (1982). *Principles of Biochemistry.* New York: Worth Publishers.

Leonard, B.P. (1979). A stable and accurate convective modelling procedure based on quadratic upstream interpolation. *Computer Methods in Applied Mechanics and Engineering, 19,* 59-98.

McCarty, P.L. (1975). Stoichiometry of biological reactions. *Progress in Water Technology, 7,* 157-172.

Molz, F.J., Widdowson, M.A., & Benefield, L.D. (1986). Simulation of microbial growth dynamcs coupled to nutrient and oxygen transport in porous media. *Water Resources Research, 22,* 1207-1216.

Morinaga, Y., Yamanaka, S., Takinami, K., & Hirose, Y. (1979). Optimum feeding proportion of methane and oxygen in cultivation of the obligate methane-utilizing bacterium, *Methylomonas flagelata,* in batch culture. *Agricultural and Biological Chemistry, 43,* 2447-2451.

Neidhardt, F.C., Ingraham, J.L., & Schaechter, M. (1990). *Physiology of The Bacterial Cell.* Sunderland: Sinauer Associates, Inc.

Pirt, S.J. (1965). The maintenance energy of bacteria in growing cultures. *Proceedings of the Royal Society of London Series B, 163,* 224-231.

Press, W.H., Flannery, B.P., Teukolsky, S.A., & Vetterling, W.T. (1990). *Numerical Recipes (Fortran Version).* Cambridge: Cambridge University Press.

Schafer, W., & Kinzelback, W. (1992). Stochastic modeling of *in situ* bioremediation in heterogenous aquifers. *Journal of Contaminant Hydrology, 10,* 47-73.

Semprini, L., & McCarty, P.L. (1991). Comparison between model simulations and field results for *in situ* biorestoration of chlorinated aliphatics: part 1. biostimulation of methanotrophic bacteria. *Ground Water, 29,* 365-374.

Semprini, L., & McCarty, P.L. (1992). Comparison between model simulations and field results for *in situ* biorestoration of chlorinated aliphatics: part 2. cometabolic transformations. *Ground Water, 30,* 37-44.

Taylor, S.W., & Jaffe, P.R. (1991). Enhanced *in situ* biodegradation and aquifer permeability reduction. *Journal of Environmental Engineering, 117,* 25-46.

Widdowson, M.A., Molz, F.J., & Benefield, L.D. (1988). A numerical transport model for oxygen and nitrate based respiration linked to substrate and nutrient availability in porous media. *Water Resources Research, 24,* 1553-1565.

Wu, J.C., Fan, L.T., & Erickson, L.E. (1990). Modeling and simulation of bioremediation of contaminated soil. *Environmental Progress, 9,* 47-56.

Chapter 3

Reactor Design Part 1: Methanotroph Attachment to Sand

3.1 Abstract

Several studies have demonstrated that most bacterial activity in natural systems is associated with soils, sediments, and floating particles (van Loosdrecht *et al.*, 1990). In addition, cells in an exponential growth phase tend to adhere to solid surfaces at an increased rate over non-growing cells (van Loosdrecht *et al.*, 1990). For *in situ* bioremediation, these phenomena have important implications. The most commonly discussed procedure for enhancing *in situ* methanotrophic growth for bioremediation involves supplying methane and air to trichloroethylene-contaminated aquifers (**Roberts** *et al.*, 1990). These additions would presumably cause naturally occurring methanotrophs to enter the exponential growth phase. According to past results, these bacteria should adhere to sand and soil particles, rather than float freely in the groundwater. For these reasons, I wished to utilize a methanotroph strain capable of attaching to the column sand for experimental work. To accomplish this task, several strains were studied to ascertain their attachment characteristics. I found that one strain, *Methylomicrobium albus* BG8, attached extensively and strongly to sand particles. Three other strains did not display significant attachment under the laboratory conditions tested. *M. albus* BG8 was further characterized for the kinetics of cell attachment to Ottawa sand. This strain exhibited rapid and extensive initial attachment followed by slow additional attachment.

3.2 Introduction

In order to test the predictive ability of the model presented in Chapter 2, a reactor system was developed. It was designed to represent one-dimensional groundwater flow. Ottawa quartz sand (0.7 mm mean diameter) was used as the porous medium for the reactor because it is homogeneous and well characterized. In addition, information was available concerning its physical and chemical characteristics (**Grant**, 1992). In order to develop the reactor system, a strain capable of remaining attached to the sand in the reactor was needed. Therefore, different methanotroph strains were studied to identify those capable of attaching to the sand, the conditions under which the cells would attach and the strength of the cell adhesion.

3.3 Background on Methanotrophs

Methanotrophs are subdivided into two groups: type I and type II. Phylogenetically, type I methanotrophs fall in the β and γ subdivisions of eubacteria. Type II methanotrophs are in the α–2 subdivision of eubacteria (Bratina *et al.*, 1992). Several phenotypic distinctions exist between type I and type II methanotrophs, as shown in Table 3.1. These bacteria exhibit a broad range of different characteristics. However, there are many more similarities among the strains than differences. All obligate methanotrophs can utilize methane or methanol for carbon and energy. These bacteria are Gram-negative, contain cytochromes *c, a* and *o* or *b*, and grow strictly aerobically. All strains can utilize ammonia for their sole nitrogen source; some can use nitrate and nitrite. In addition, several strains are capable of using complex

nitrogen sources. All methanotrophs have intracytoplasmic membranes, although the two groups have different membrane ultrastructures (Hanson, 1992).

Type II methanotrophs utilize the serine pathway for carbon assimilation. Most Type I methanotrophs assimilate carbon only via the ribulose monophosphate pathway. However, several type I strains have enzymes for the serine cycle (Lidstrom, 1992). Bacteria using the ribulose monophosphate pathway have a slight advantage over cells using the serine pathway because the former pathway is energetically favorable to the latter.

All methanotrophs have the gene for the enzyme particulate methane monooxygenase (pMMO), which is contained in their cell membranes. Some strains are also able to produce a soluble form of the enzyme (sMMO) present in the cytoplasm. The copper-to-biomass ratio in the growth medium has been shown to govern whether sMMO or pMMO is produced in cells that express both MMOs (Stanley *et al.*, 1983). Soluble MMO is formed under low copper-to-biomass ratios, while pMMO is produced under high copper-to-biomass ratios. Both forms of the MMO are known to oxidize TCE (DiSpirito *et al.*, 1992, Koh *et al.*, 1993, Brusseau *et al.*, 1990, Hanson *et al.*, 1990). The sMMO has a broad substrate range including long chain hydrocarbons and aromatic compounds, while the pMMO can oxidize only short chain aliphatic hydrocarbons (Burrows *et al.*, 1984, Higgins *et al.*, 1980). Additional comparisons between the two forms of the MMO are shown in Table 3.2.

3.4 Strains Selected for Study

Two strains from each group were tested for their ability to attach to washed Ottawa sand. *Methylomicrobium albus* BG8 and *Methylomonas* species strain MN were used as type I methanotroph representatives. *Methylocystis parvus* OBBP and *Methylosinus trichosporium* OB3b were the type II methanotroph strains used in the attachment experiments.

3.5 Materials and Methods

3.5.1 Materials

Uniform 1mm diameter Ottawa sand was used for all experiments. Highest purity (>99.99 %) methane was purchased from Matheson Gas Company. Chemicals used for media preparation and sand pretreatment were all reagent grade. Cell growth medium was prepared with distilled-deionized water.

3.5.2 Cell Growth Conditions

Cells were grown to the exponential growth phase in nitrate mineral salts medium supplemented with 10 μM copper sulfate (Whittenbury *et al.*, 1970). Frozen stock cultures were spread plated on agar plates, transferred aseptically to new plates for up to six months, and then transferred to liquid culture. All plates and liquid cultures were incubated at 30°C in a 75% air, 25% methane atmosphere.

3.5.3 Attachment Experiments

After the cultures reached the exponential growth phase, I allowed the growth medium temperature to drop to 22°C. The *Methylomonas* species strain MN culture

was filtered through a paper towel to remove large clumps of cells. Ottawa sand was pretreated to remove organics and iron oxides (Black, 1965). To accomplish this task, thirty percent hydrogen peroxide was added to sand followed by heating at 80°C for one hour. The sand was then rinsed with ddH_2O. This series of steps removed organics from the sand. A mixture of sodium citrate dihydrate and sodium bicarbonate was then added to the sand. This was brought to 80°C and sodium dithionate was added to the mixture. This process removed iron oxides from the sand. After this procedure, the sand was visibly whiter. The iron removal step was completed a total of three times for each batch of sand. This was shown to remove iron below detectable quantities (Grant, 1992).

The washed sand was combined with liquid cultures in a 3:1 (mass:mass) ratio. The sand porosity was 0.36. This created an excess of approximately 25% liquid beyond the sand void volume, i.e., 1.25 void volumes of liquid were present in each sample. Samples in 50 ml plastic centrifuge tubes were rotated using a Cole-Parmer Rototorque at a rate of 4 rpm. Liquid phase cell density was analyzed over time by measuring the liquid OD_{600} on an HP 8452A diode array spectrophotometer. A linear correlation was observed between cell density and the OD_{600} for readings up to 1.0.

Two sets of controls were carried out. The first was a liquid culture sample of each strain with no sand to test for cell attachment to the reaction vessel during the attachment test. The second was pretreated sand added to growth medium with no cells. This control tested for colloids entering the liquid phase from the sand phase, which would cause an increase in the OD_{600} reading of the fluid phase and could affect protein assays used to analyze cell attachment to sand surfaces.

After attachment proceeded for one hour three void volumes of fluid were flushed through the sand. This treatment was termed a filtration cycle. The sand and interstitial fluid were placed back into a rotating tube containing growth medium equivalent to two-thirds of the original void volume of the sand/cell samples. These samples were rotated for 15 minutes at 4 rpm. This treatment was termed a rinse cycle. The sequence of one filtration cycle followed by one rinse cycle was termed a complete wash cycle. Two complete wash cycles plus a final filtration were done on each sample. One additional complete cycle was done for the *M. albus* BG8 strain. A liquid phase sample was collected prior to each filtration cycle. A sand phase sample containing interstitial fluid was collected before and after each filtration cycle.

One strain, *M. albus* BG8, was found to attach well to the Ottawa sand. Therefore, additional tests were carried out to characterize the attachment. Cells grown to the exponential phase in NMS medium with 10 μM copper sulfate were diluted with fresh medium to obtain four different initial cell densities. Pretreated Ottawa sand was combined with cells at each density. Two mixtures were prepared for each density: a 3:1 ratio and a 1:1.4 ratio of sand:cell culture (mass:mass). As described earlier, the 3:1 ratio creates a 25% excess of liquid above the sand. The 1:1.4 ratio provides a 400% excess of liquid. Each sample was rotated at 4 rpm and the liquid phase OD_{600} was analyzed over time to determine the attachment of cells to sand. The two different ratios of sand:cell culture were prepared in order to elucidate the kinetics of cell attachment to Ottawa sand. After one hour, liquid from the samples with the 1:1.4 ratio of sand:cell culture was added to fresh sand to obtain a

3:1 ratio. These samples were allowed to rotate over time and the liquid phase OD_{600} was analyzed.

3.5.4 Protein Assays of Sand and Liquid Samples

In order to determine total cell mass in the collected samples described in the previous section, each sample was assayed for total protein. Two percent sodium dodecyl sulfate (SDS) was added to each sample to obtain a final liquid concentration of one percent SDS. This was done to digest cells and solubilize membrane-associated proteins. The reaction was allowed to continue for a minimum of one hour to ensure complete protein solubilization. The BioRad DC® protein assay was used for each sample. A standard curve was made with bovine serum albumin containing the same percent SDS in each standard to convert data for the samples to actual protein concentrations. Protein concentrations were then converted to approximate cell densities based on an average *Escherichia coli* cell weighing 2.8×10^{-13} g and containing 55% protein by weight (Neidhardt *et al.*, 1990).

3.6 Results and Discussion

Figure 3.1 shows the results of the liquid phase OD_{600} analyses for the four strains. The OD_{600} readings for the control sample that tested for material coming off the sand into the liquid phase were subtracted from all sample readings. The controls for cells attaching to the rotating vessels showed no significant change in the liquid phase OD_{600}, suggesting that cells did not significantly attach to the vessels. *M. trichosporium* OB3b, *Methylomonas* strain MN, and *M. parvus* OBBP displayed no significant decrease in the liquid phase OD_{600} during the one hour attachment time.

With the *M. albus* BG8 sample, a significant decrease in the OD_{600} was observed. Within two minutes, more than 40% of the cells had attached to the sand. This percent increased slowly to approximately 60% by the end of the one hour rotation period.

The protein assays done on the liquid from before adding the cells to the sand and after the cells were allowed to attach to the sand for one hour confirmed the fluid phase OD_{600} results (Figure 3.2). There was no statistically significant difference in the number of cells in liquid before and after attachment for any strains other than *M. albus* BG8. This strain showed a cell number decrease of approximately 50% after one hour of attachment. This correlates well with the 60% decrease found for the liquid phase OD_{600}.

The protein assays performed on collected sand samples also confirmed the previous results (Figure 3.3). The first bar for each cell type represents cells attached to sand plus cells in the interstitial fluid. After a single filtration of the sand with fresh medium, which presumably removes all cells from the interstitial fluid, the total number of cells decreased by more than 75% for the *M. trichosporium* OB3b and *M. parvus* OBBP cultures. A significant proportion, 38%, of *Methylomonas* strain MN cells appeared to remain attached to the sand. These cells tend to form clumps and it is possible that the initial procedure to remove all cell clumps before adding cells to sand was not 100% efficient. If cell clumps attached to sand, the liquid phase OD_{600} would not effectively measure the liquid phase cell density. However, the protein assay results of the liquid phase before and after the cells were exposed to sand suggests that there was no significant proportion of cells attaching to the sand phase.

It is possible that the filtration step did not adequately remove all cells from the interstitial space.

After one complete wash cycle plus one additional filtration, the cells attached to sand dropped below the detection limit of 2×10^7 cells/gram sand for both *M. trichosporium* OB3b and *M. parvus* OBBP cells. *Methylomonas* strain MN cells were not reproducibly detectable after two complete wash cycles plus one additional filtration. The *M. albus* BG8 culture displayed very different characteristics. After two complete wash cycles approximately 60% of the cells remained attached to the sand. Additional wash cycles did not significantly decrease the number of attached cells, suggesting that the cells adhering to the sand particles had attached strongly under the conditions of the experiment.

The results for *M. albus* BG8 attachment to sand under different initial cell densities and different ratios of sand:cell culture are shown in Figure 3.4. Again, a very rapid attachment occurred followed by additional slow attachment kinetics. All the different initial cell densities for each ratio of sand:cell culture displayed similar fractional decreases in the liquid OD_{600}, corresponding to similar fractional attachment of cells to sand. However, the two different sets, 3:1 sand:cell culture and 1:1.4 sand:cell culture, displayed a dissimilar fraction of cells attaching to sand. The set with a higher percent sand had an initial attachment of approximately 60%, while the set with a lower percent sand showed only 30% attachment. At one hour, the higher percent sand samples had an attachment ranging from 75% to 85%, while the attachment of the lower percent sand samples ranged between 50% and 60%. When supernatant from the 1:1.4 sand:cell culture samples was added to new sand to achieve

a 3:1 ratio, there was again an initial decrease in liquid OD_{600} followed by a slower decrease. The initial rate measured as percent decrease per minute was approximately 1/6 the rate of initial attachment for fresh cell culture added to sand. The final percent decrease in liquid OD_{600} for these samples was the same as for the samples with the 3:1 sand:cell culture ratio.

These data suggest that a portion of the *M. albus* BG8 cells are able to rapidly bind to sand. I base this conclusion on the results for the experiment with an initial sand:cell culture ratio of 1:1.4. After the supernatant containing cells was placed in new sand, the fast initial decrease in the fluid phase OD_{600} was not observed. If all cells attached equally well to the sand, an initial rapid drop would have occurred. Another observation is that the attachment results do not show saturation characteristics. A nearly linear increase in total cell attachment with respect to initial liquid phase cell density was observed. A model for cell absorption to sand was not developed because it is beyond the scope of this work. The purpose here was to obtain a qualitative understanding of the absorption characteristics of *M. albus* BG8 cells to sand so that these cells could be understood in the context of cells attached to sand in a bioremediation reactor.

3.7 Conclusions for Cell Attachment

The main conclusion drawn from this work is that under the laboratory growth conditions described herein, only one methanotroph strain, *M. albus* BG8, attaches well to pretreated Ottawa sand. Additional laboratory strains were tested for attachment and none were found to attach well. In short term experiments, a portion

of the *M. albus* BG8 cells appears to attach strongly when exposed to sand at room temperature with moderate mixing in the presence of growth medium without substrate. Based on this knowledge, these cells were chosen for developing a reactor system for bioremediation design. These results also have implications for above ground bioremediation schemes. *M. albus* BG8 cells may be beneficial for use in bioreactors that utilize immobilized cells for remediation. Currently research for most above ground systems has focused on utilizing *M. trichosporium* OB3b. The main reason for this choice is that this strain can produce sMMO which can break down TCE at a faster rate than pMMO under high concentrations of TCE. *M. albus* BG8 does not contain sMMO. However, if higher attached cell densities can be achieved with *M. albus* BG8 cells, they may be more advantageous because an increased cell density may compensate for a lower TCE degradation rate per cell. In addition, it may be possible to genetically engineer *M. albus* BG8 cells to produce sMMO. These genetically engineered microorganisms, with superior attachment characteristics and a faster maximum TCE degradation rate, could be utilized in above ground bioreactors.

The final point of this work is the demonstration that analyzing the fluid phase OD_{600} is a rapid and convenient method to test a strain's ability to attach to solids. If cells are found to attach well to a solid phase, the strength of this adhesion can rapidly be measured by performing protein assays on washed solids as described in the Methods section.

Table 3.1 Characteristics of Type I and Type II Methanotrophs (Hanson, 1992)

Characteristic	Type I	Type II
Genera	*Methylococcus* *Methylomonas* *Methylobacter* *Methylomicrobium*	*Methylosinus* *Methylocystis*
Intracytoplasmic Membrane Ultrastructure	Vesicular disc shaped bundles stacked throughout the cell	Paired membranes extending throughout the cytoplasm or arranged at the cell periphery and running parallel to the cytoplasmic membrane
Cell Shape	Short rods or cocci	Rod or pear shaped
Predominant Monounsaturated Fatty Acid Carbon Chain Lengths	16	18
DNA GC Mole Percent	50-54*	62.5
Resting Stages	*Azotobacter*-like cysts	Exospores and "lipid" cysts
Complete Tricarboxylic Acid (TCA) Cycle	No	Yes
Carbon Assimilation Pathway	Ribulose Monophosphate (RuMP)	Serine Cycle
Able to Fix Nitrogen	No	Yes
Enzymes Present in One Type Only	pyruvate dehydrogenase, hexokinase, 6-phosphogluconate dehydrogenase, glucose 6-phosphate dehydrogenase	α-ketoglutarate dehydrogenase (TCA Cycle)
Carbon Assimilation Enzymes	3-hexulose phosphate synthase (RuMP pathway),	hydroxypyruvate reductase (serine pathway),
Ammonia Assimilation Enzymes	glutamate dehydrogenase, alanine dehydrogenase	glutamine synthetase-glutamine/α-ketoglutarate aminotransferase

* There is one exception, *Methylococcus capsulatus* Bath, which has a DNA GC mole percent ratio of 62%.

Table 3.2 Differences Between the Soluble and Particulate Methane Monooxygenase

Characteristic	Soluble Methane Monooxygenase (sMMO)	Particulate Methane Monooxygenase (pMMO)
Location in the Cell	Cytoplasm	Membranes
Presence in Methanotrophs	Contained in very few strains, mainly type II (Lidstrom, 1992)	Contained in all known Strains (Lidstrom, 1992)
Metal Contained in the Active Site	Iron (Dalton, 1992)	Copper (Nguyen *et al.*, 1994)
Substrate Range	Broad: including substituted aromatics, long chain aliphatic compounds, chlorinated aliphatics (Burrows *et al.*, 1984, Speitel *et al.*, 1993)	Narrow: short chain aliphatic compounds which may be chlorinated (Burrows *et al.*, 1984, DiSpirito *et al.*, 1992)
TCE Degradation Characteristics	High maximum oxidation rate, low affinity	Low maximum oxidation rate, high affinity
Present at High Copper:Biomass Ratios (Stanley *et al.*, 1983)	No	Yes

Figure 3.1 Cell Attachment to Quartz Sand: Loss of Cells from the Liquid Phase to Sand Measured as a Decrease in Fluid OD_{600}

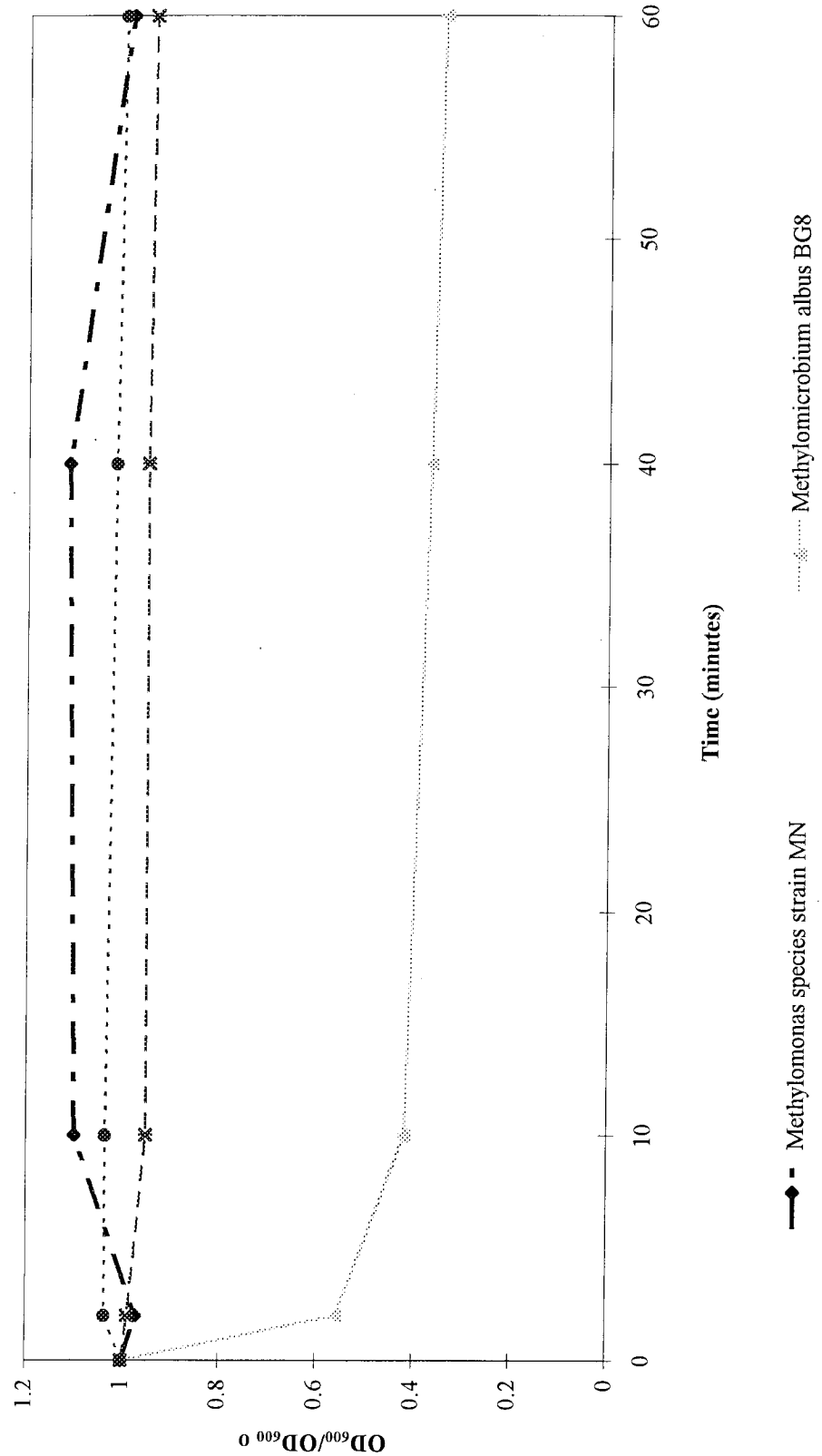

Figure 3.2 Cell Attachment to Sand: Liquid Samples

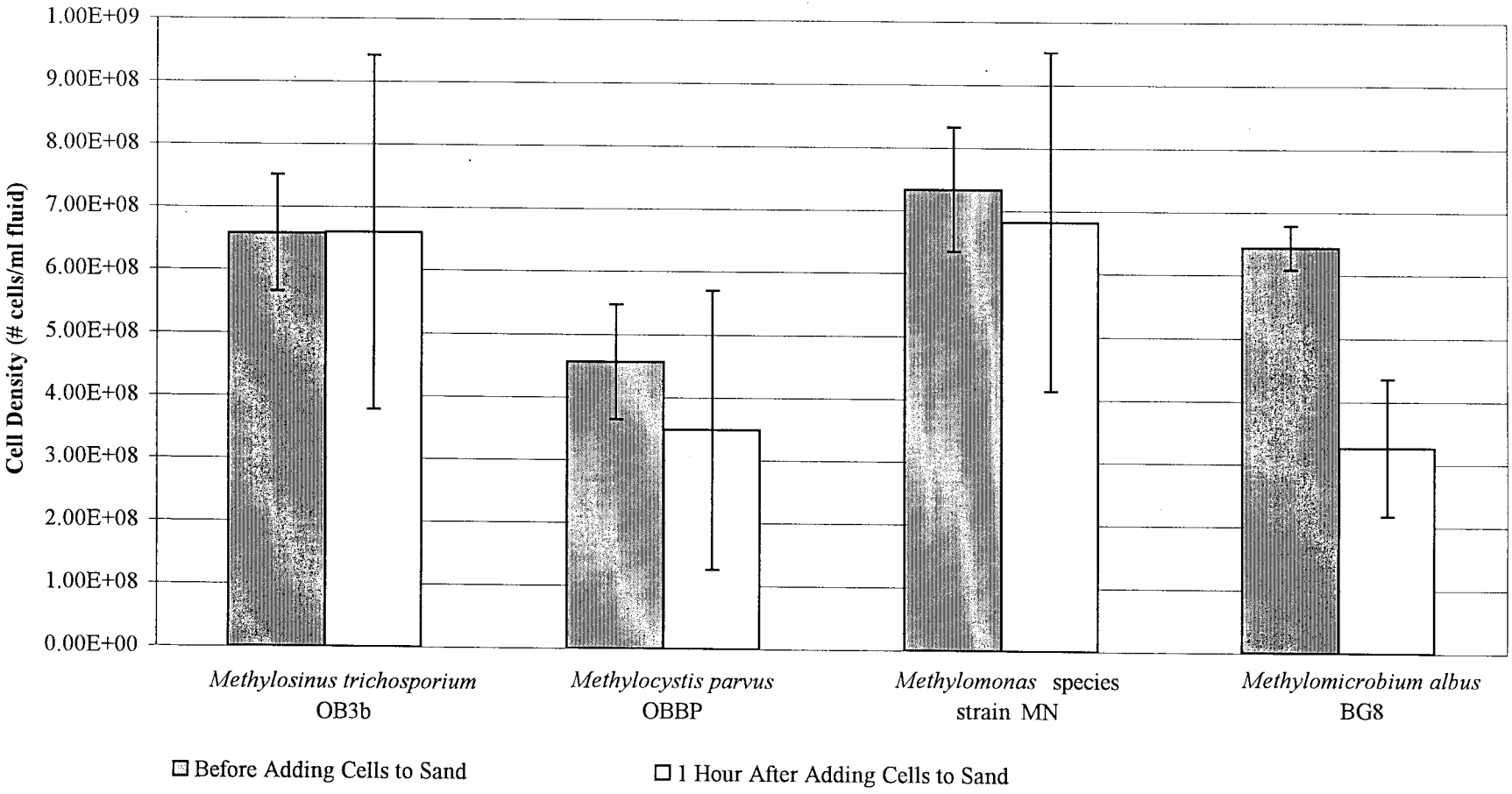

Error bars represent 95% confidence limits based on three replicates of each sample.

Figure 3.3 Cell Attachment to Sand: Sand Samples

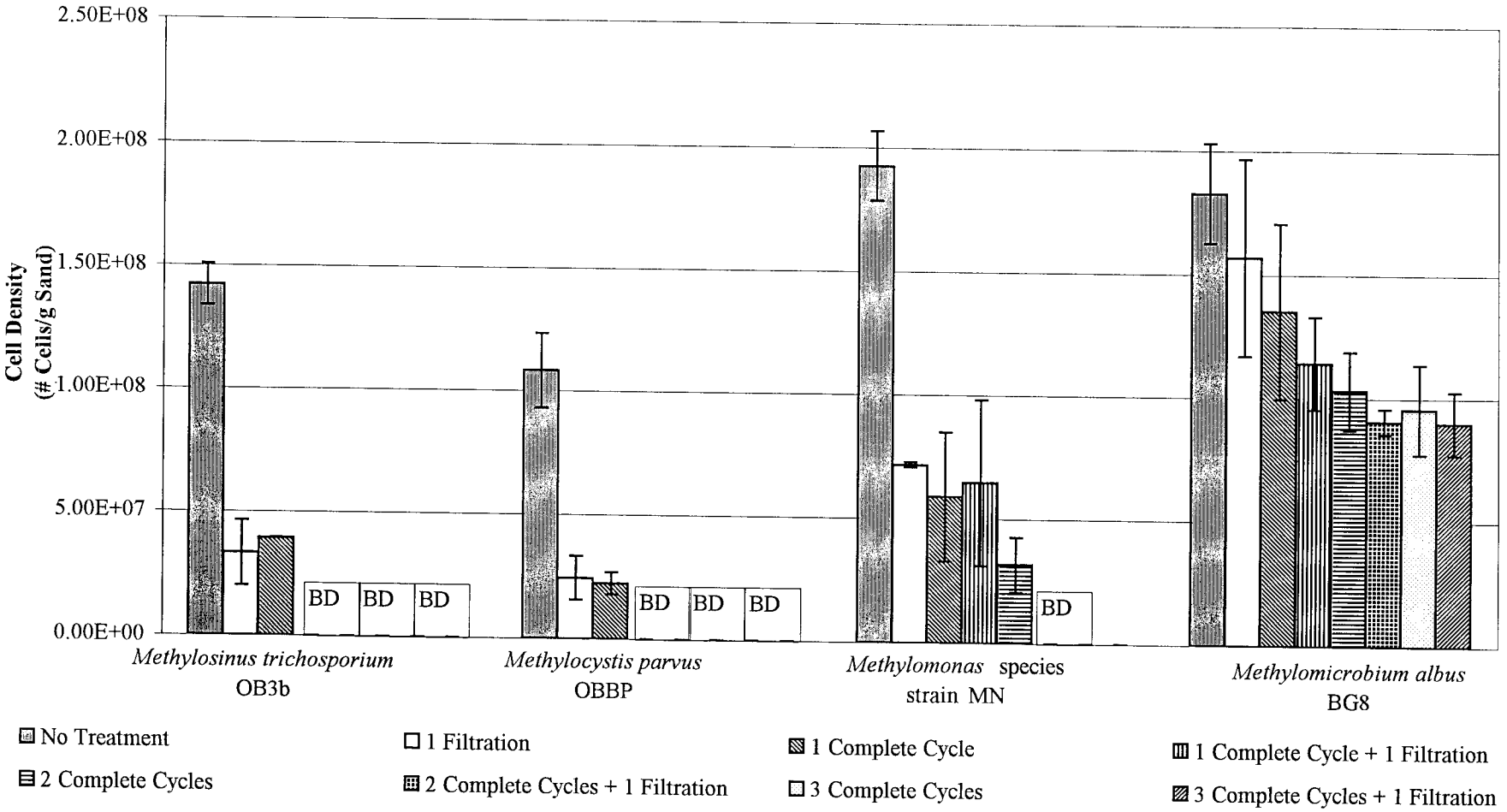

BD=Below the Limit of Detection (2 x 10^7 Cells/g Sand)
Error bars represent 95% confidence limits based on three replicates of each sample.

Figure 3.4. *Methylomycrobium albus* BG8 Attachment to Quartz Sand: Loss of Cells from the Liquid Phase to Sand Measured as a Decrease in Fluid OD_{600}

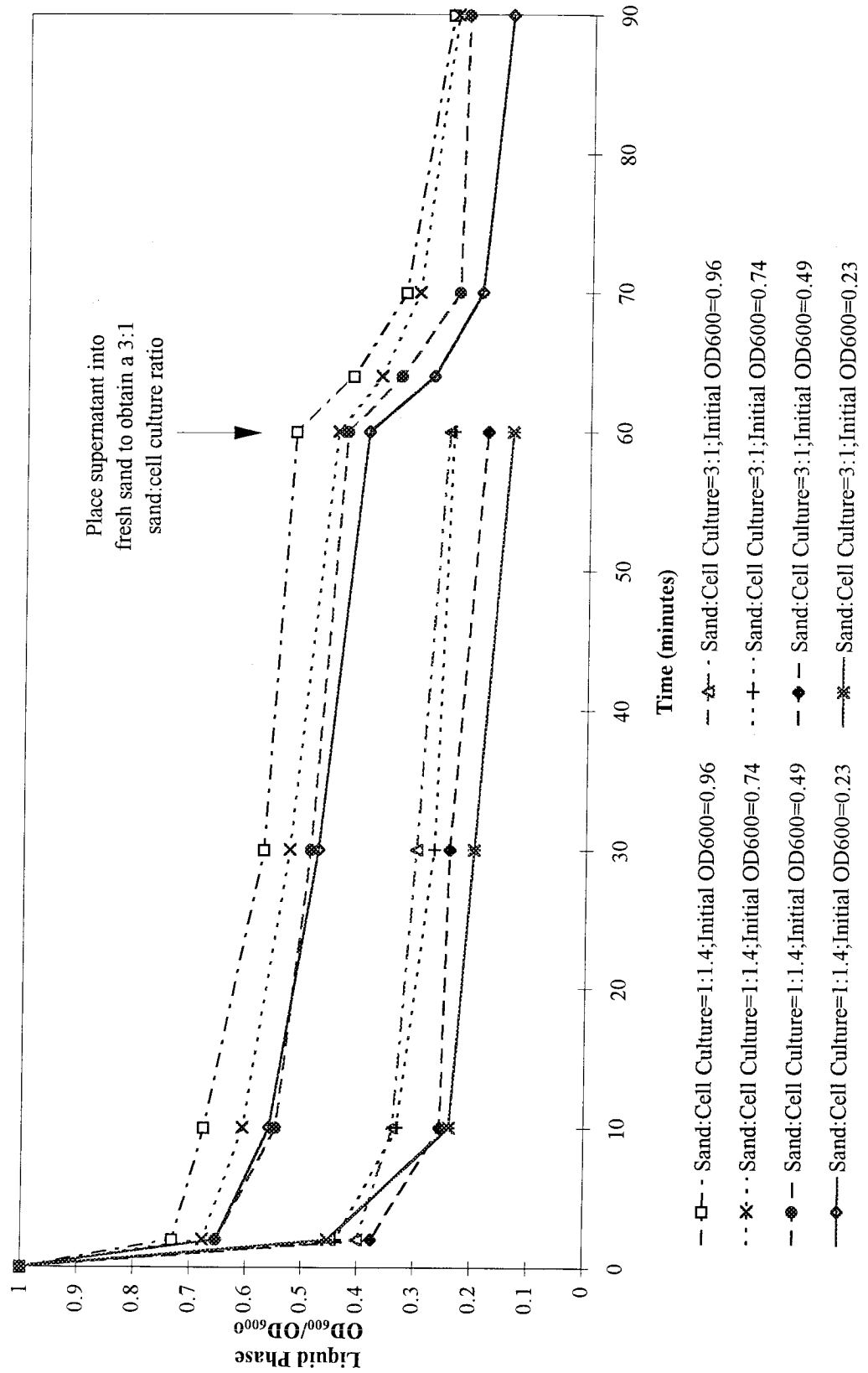

3.8 References

Black, C.A. (1965). *Methods of Soil Analysis Part I.* Madison: American Society of Agronomy, Inc.

Bratina, B.J., Brusseau, G.A., & Hanson, R.S. (1992). The use of 16S rRNA analysis to investigate the phylogeny of methylotrophic bacteria. *International Journal of Systematic Bacteriology, 42,* 645-648.

Brusseau, G.A., Tsien, H., Hanson, R.S., & Wackett, L.P. (1990). Optimization of trichloroethylene oxidation by methanotrophs and the use of a colorimetric assay to detect soluble methane monoxygenase activity. *Biodegradation, 1,* 19-29.

Burrows, K.J., Cornish, A., Scott, D., & Higgins, I.J. (1984). Substrate specificities of the soluble and particulate methane monooxygenases of *Methylosinus trichosporium* OB3b. *Journal of General Microbiology, 130,* 3327-3333.

Dalton, H. (1992). Methane oxidation by methanotrophs. In J.C. Murrell & H. Dalton (Eds.), *Methane and Methanol Utilizers.* (pp. 85-114). New York: Plenum Press.

DiSpirito, A.A., Gulledge, J., Murrell, J.C., Shiemke, A.K., Lidstrom, M.E., & Krema, C.L. (1992). Trichloroethylene oxidation by the membrane associated methane monooxygenase in Type I, Type II, and Type X methanotrophs. *Biodegradation, 2,* 151-164.

Grant, S.C.B. (1992). Detection and Partitioning of Bacteriophage in Fluid/Solid Systems: Application to the Ecology and Mobility of Viruses in the Environment. California Institute of Technology. Ph.D. Thesis.

Hanson, R.S., Netrusov, A.E., & Tsuji, K. (1992). The Obligate Methanotrophs. In A. Balows, H.G. Truper, M. Dworkin, W. Harder, & K. Schleifer (Eds.), *The Prokaryotes.* New York: Springer-Verlag.

Hanson, R.S., Tsien, H.C., Tsuji, K., Brusseau, G.A., & Wackett, L.P. (1990). Biodegradation of low-molecular weight halogenated hydrocarbons by methanotrophic bacteria. *FEMS Microbiology Reviews, 87,* 273-278.

Higgins, I.J., Best, D.J., & Hammond, R.C. (1980). New findings in methane-utilizing bacteria highlight their importance in the bioshpere and their commercial potential. *Nature, 286,* 561-564.

Koh, S., Bowman, J.P., & Sayler, G.S. (1993). Soluble methane monooxygense production and trichloroethylene degradation by a Type I methanotroph, *Methylomonas methanica* 68-1. *Applied and Environmental Microbiology, 59,* 960-967

Lidstrom, M.E. (1992). Aerobic Methylotrophic Bacteria. In A. Balows, H.G. Truper, M. Dworkin, W. Harder, & K. Schleifer (Eds.), *The Prokaryotes.* New York: Springer-Verlag.

Neidhardt, F.C., Ingraham, J.L., Schaechter,M. (1990). *Physiology of The Bacterial Cell.* Sunderland: Sinauer Associates, Inc.

Nguyen, H.T., Shiemke, A.K., Jacobs, S.J., Hales, B.J., Lidstrom, M.E., & Chan, S.I. (1994). The nature of the copper ions in the membranes containing the particulate

methane monoxygenase from *Methylococcus capsulatus* (Bath). *Journal of Biological Chemistry, 269,* 14995-15005.

Roberts, P.V., Hopkins, G.D., Mackay, D.M., & Semprini, L. (1990). A field evaluation of *in situ* biodegradation of chlorinated ethenes: part I, methodology and field site characterization. *Ground Water, 28,* 591-604.

Speitel, G.E., Jr., Thompson, R.C., & Weissman, D. (1993). Biodegradation kinetics of *Methylosinus trichosporium* OB3b at low concentrations of chloroform in the presence and absence of enzyme competition by methane. *Water Research, 27,* 15-24.

Stanley, S.H., Prior, S.D., Leak, D.J., & Dalton, H. (1983). Copper stress underlies the fundamental change in intracellular location of methane monooxygenase in methane oxidizing organisms: studies in batch and continuous cultures. *Biotechnology Letters, 5,* 487-492.

van Loosdrecht, M.C.M., Lyklema, J., Norde, W., & Zehnder, A.J.B. (1990). Influence of interfaces on microbial activity. *Microbiological Reviews, 54,* 75-87.

Whittenbury, R., Phillips, K.C., & Wilkinson, J.F. (1970). Enrichment, isolation and some properties of methane-utilizing bacteria. *Journal of General Microbiology, 61,* 205-218.

Chapter 4

Reactor Design Part 2:
Methane Utilization Kinetic Parameter Determinations

4.1 Abstract

Recent evidence suggests that copper plays a key role in the particulate methane monooxygenase active site (Nguyen *et al.*, 1994). Copper to biomass ratios also determine whether cells produce the soluble or particulate form of the methane monooxygenase (MMO) (Stanley *et al.*, 1983). For these reasons, methane utilization kinetics were determined for *M. albus* BG8 cells grown under both high (15 μM) and low (0.3 μM) copper concentrations. These cells do not produce the soluble MMO (sMMO). Therefore, results obtained for methane utilization kinetic parameters under high and low copper availability represent kinetics of the membrane-bound, or particulate form, of the MMO (pMMO). The results indicate that copper does not have a significant effect on the methane utilization kinetics for *M. albus* BG8 cells. The parameters obtained from these experiments were used to test the model presented in Chapter 2.

4.2 Introduction

Kinetic parameters for methane oxidation by pMMO under low and high copper conditions were ascertained. This was done to identify parameter inputs for the model presented in Chapter 2. I assumed the pMMO enzyme follows Michaelis-Menten kinetics. The model for Michaelis-Menten kinetics assumes that an enzyme and substrate form an enzyme-substrate complex which either forms a product and regenerates an enzyme molecule or reforms the original enzyme and substrate molecules. The kinetic model is presented in Chapter 2.

The kinetic parameters V_{max}' and K_s are obtained by a protocol that involves adding gaseous methane to the headspace of closed serum vials containing live cells. The vials are shaken to equilibrate methane between the gas and liquid phases. Cells metabolize methane present in the liquid phase. The mathematics of describing the fate of methane in this complex system can be simplified if the rate of methane oxidation by cells in liquid is slow enough that the liquid is continuously saturated with methane, i.e., the rate of methane equilibration between the gas and liquid phases is much greater than the rate of methane uptake by cells. The rate of absorption into liquid on a per unit volume fluid basis is defined by:

$$Ra' = k_L a'\left(C^* - C\right) \qquad (4\text{-}1)$$

(Danckwerts, 1970)

where:

Ra' = observed rate of absorption per unit volume fluid $\left(\frac{m}{l^3 t}\right)$

a' = gas-liquid interfacial area per unit volume of fluid $\left(\frac{1}{l}\right)$

k_L = liquid film mass transfer coefficient $\left(\frac{l}{t}\right)$

C^* = concentration of dissolved gas at the gas-liquid interface in equilibrium with gas at the interface $\left(\frac{m}{l^3}\right)$

C = concentration of dissolved gas in the bulk liquid $\left(\frac{m}{l^3}\right)$

The criterion for dissolved gas to be near saturation is:

$$\frac{Ra'}{k_L a' C^*} << 1 \qquad (4\text{-}2)$$

(Danckwerts, 1970)

The numerator in equation 4-2 is the observed rate of absorption per unit volume fluid. When cells in liquid consume methane, the rate of absorption per unit volume is equal to the rate of methane uptake by cells per unit volume fluid. Replacing the numerator in equation 4-2 with the rate of methane uptake, the condition needed to assume gas-liquid partitioning equilibrium becomes:

$$\frac{V' \frac{1}{V_L}(X V_L)}{k_L a' C^*} << 1 \qquad (4\text{-}3)$$

where:

V' = the rate of substrate utilization per unit cell mass $\left(\frac{m_s}{t\, m_c}\right)$

V_L = liquid volume in a sample (l^3)

X = cell mass concentration $\left(\frac{m_c}{l^3}\right)$

A set of experiments was performed to identify k_La' for methane into growth medium under conditions used for kinetics experiments. After this parameter was determined, a cell concentration was estimated which would satisfy equation 4-3 for kinetics experiments. At the end of an experiment, methane oxidation rates were compared to $k_La'C^*$ to check mass transfer limitation of methane uptake by cells.

4.3 Materials and Methods

4.3.1 Materials

Highest purity methane (>99.99%) was obtained from Matheson Gas Company. Chemicals used for medium preparation were all reagent grade. Cell growth medium was prepared with distilled-deionized water (ddH_2O). Twenty ml serum vials were purchased from Pierce. One cm thick butyl rubber stoppers were purchased from Bellco glass. Safety Solve fluid from Research Products International Corporation was used for scintillation fluid. $^{14}CH_4$ was obtained from Dupont (55mCi/mmol).

4.3.2 Cell Growth Conditions

Cells were grown to the mid to late exponential growth phase in nitrate mineral salts (NMS) medium supplemented with zero or 15 μM copper sulfate (Whittenbury *et al.*, 1970). Frozen stock cultures were spread plated on agar plates, transferred aseptically to new plates for up to six months, and then transferred to liquid culture. All plates and liquid cultures were incubated at 30°C in a 75% air, 25% methane atmosphere.

4.3.3 Determining the Mass Transfer Coefficient

Cells were grown to the late exponential phase. The liquid OD_{600} was measured on an Hewlett Packard diode-array spectrophotometer model 8452A to determine the cell density. The cells were concentrated 5- and 10-fold and diluted up to 10-fold. One-half ml of each cell concentration was added to separate 20 ml serum vials. The vials were capped with butyl rubber stoppers and crimp sealed. Two sets of 7 dilutions were made and one set of the 5- and 10-fold concentrated cells was made. One hundred µl pure methane gas was added to each sample of one set of dilutions to achieve an equilibrium liquid concentration of approximately 5 µM methane assuming no mass transfer limitation. Two hundred µl pure methane was added to the second dilution set and the concentrated cells to obtain an equilibrium liquid concentration of approximately 10 µM. The expected equilibrium liquid concentration was calculated using the following equations:

$$c_L = \frac{c_G}{H} \tag{4-4}$$

$$c_G = \frac{\left(c_G\right)_{\substack{pure \\ CH_4}} V_{added}}{V_{Void}} \tag{4-5}$$

$$\left(c_G\right)_{\substack{pure \\ CH_4}} = \frac{P}{RT} \tag{4-6}$$

where:

c_L = equilibrium, non-mass transfer limited, liquid phase methane concentration in a serum vial $\left(\frac{m}{l^3}\right)$

c_G = gas phase methane concentration in a serum vial $\left(\frac{m}{l^3}\right)$

H = dimensionless Henry's constant (29.2) (Duan *et al.*, 1992)

$\left(c_G\right)_{CH_4}^{pure}$ = gas phase methane concentration in the pure methane vial $\left(\frac{m}{l^3}\right)$

V_{added} = volume pure methane added to a serum vial (l^3)

V_{void} = serum vial headspace volume (l^3)

P = pure methane vial pressure (atm)

R = Universal Gas Constant $\left(0.0821 \frac{atm\ liter}{mol\ ^oK}\right)$

T = pure methane vial temperature (^oK)

Combining equations 4-4 through 4-6 gives the following equation for the expected non-mass transfer limited, equilibrium liquid phase methane concentration, c_L, given a specific amount of pure methane added to a vial, V_{added}:

$$c_L = \frac{V_{added}}{V_{void}} \frac{P}{RT} \frac{1}{H} \qquad (4\text{-}7)$$

The main assumptions are: (1) the gas phase can be treated as an ideal gas for calculating the methane concentration in the pure methane source vial, and (2) the amount of methane in liquid in sample vials is negligible compared to the total amount of methane in a vial. The second assumption is based on the liquid concentration equaling less than 4% of the gas concentration (based on a dimensionless Henry's constant of 29.2) and the liquid phase equaling 2.5% of the total vial volume. Based on these data the methane present in liquid represents less than 0.1% of the total methane in a vial.

The total amount of methane transported into the liquid phase is equal to the amount of methane consumed by cells. (No other fate exists for the methane.) This rate of methane uptake was analyzed by assaying the gas phase methane concentrations over time. To accomplish this, 100 µl headspace samples were injected at distinct time points into an Hach-Carle Gas Chromatograph equipped with a flame-ionization detector and an Hayesep 80/100 analytical column purchased from EG&G Engineering. Peak areas were converted to methane concentrations in the gas phase using methane standards analyzed on the GC. Calculated gas phase methane concentrations were used to determine methane uptake rates. Rates for different cell dilutions were compared to one another to determine which samples exhibited mass transfer limited kinetics. Samples which displayed a saturated methane uptake rate, i.e., completely mass transfer limited kinetics, were used to calculate the mass transfer coefficient for the experimental conditions.

4.3.4 Determining the Kinetic Parameters V_{max}' and K_s

4.3.4.1 Experimental Setup - Methane Stock Vials

Radioactive methane was used for all kinetics experiments. A mixture of approximately 1% radioactively labeled methane with 99% cold methane was added to vials containing live cells. To make this mixture, 60 ml serum vials containing ddH_2O were capped with butyl rubber stoppers containing an inserted 25 gauge needle. No air bubbles were in the liquid. The liquid was then displaced with pure cold methane via an additional 25 gauge needle attached to a gassing apparatus. After approximately 50 ml ddH_2O was displaced, the two 25 gauge needles were removed

from the butyl rubber stopper and the vial was crimp sealed. At this point the pressure in the vial was greater than 1 atm. A 25 gauge needle was attached to rubber tubing. The free end of the tubing was placed in a beaker of water to approximately four inches below the water surface. The needle was inserted into the methane serum vial to allow gas to exit until a pressure equilibrium was reached. The tubing was then brought to just below the surface of the water and the gas phase in the serum vial was allowed to equilibrate to atmospheric pressure. The needle was then removed from the vial. Liquid was taken out of this vial via syringe and replaced with an equal volume of headspace from a vial containing radioactively labeled ^{14}C methane gas. The specific activity of this mixture of cold and hot methane was analyzed by placing 100 µl liquid in equilibrium with the mixture into 5 ml scintillation fluid and analyzing the radioactivity.

4.3.4.2 Experimental Setup - Cell Preparation

Cells were grown to the mid exponential phase in the presence of 15 µM added copper and no added copper. The OD_{600} was then analyzed to calculate the cell dilution needed to ensure reaction limited kinetics. A fraction of the cell/medium mixture was filtered through a 0.2 micron filter to remove cells. The collected medium was added to unfiltered cells to obtain the calculated cell dilution. Filtered growth medium was used for diluting cells so they would be exposed to a similar chemical environment as that in which they had grown.

One-half ml diluted cells was added to each of a series of 20 ml serum vials. For cells grown with 15 µM copper, three vials were made for each of three time

points for eight initial methane concentration. The liquid phase initial methane concentrations ranged from one to 75 μM. For cells grown with no added copper, three vials were made for each of three time points for seven initial methane concentrations. The concentration range for this experiment was three to 150 μM methane in liquid. One killed cell control was made for each concentration. All vials were capped with butyl rubber stoppers and crimp sealed. Methane from the stock vial described in Section 4.3.4.1 was added to vials to obtain predetermined liquid concentrations. The amount of methane added to obtain the expected liquid concentration was calculated using equation 4-7.

At one, two, and three hours after methane addition, 100 μl 50% NaOH was added to distinct concentration sets of serum vials to kill cells and halt methane metabolism. This addition also brings the liquid pH to above 11, which dissolves the CO_2 from the headspace by converting it into HCO_3^- in the liquid phase (Rudd *et al.*, 1974). The vials were shaken overnight to ensure complete CO_2 dissolution. Air was flushed through the headspace of each vial for one minute to remove all radioactive methane. A control experiment was done to determine the length of flushing time needed for removing ^{14}C from radioactive methane to levels below 10% of ^{14}C in radioactive products formed during a kinetics experiment. One hundred or 200 μl liquid from each vial was added to five ml scintillation fluid. Radioactivity in the samples was measured with a Packard TriCarb 2000 CA Liquid Scintillation Analyzer. The amount of quenching was determined by adding a known amount of ^{14}C amino acids to fluid from control vials and recounting. The gas phase methane concentration in each control was analyzed via GC. The measured and expected gas phase methane

concentrations were compared to check the reliability of calculating an expected concentration based on the amount of methane added to sample vials.

4.4 Results and Discussion

4.4.1 Mass Transfer Coefficient Determination

The OD_{600} of the 10-fold dilution of cells was 0.33. A separate standard curve of liquid phase OD_{600} vs. protein concentration was made to obtain an approximate protein concentration for each OD_{600} reading. An OD_{600} of 0.33 corresponds to approximately 40 μg protein per ml fluid. Thus, the protein concentration in the orginal undiluted sample was approximately 400 μg protein per ml fluid. Figures 4.1 and 4.2 show methane uptake kinetics for samples with 100 and 200 μl pure methane added to serum vials, respectively (approximately 5 and 10 μM methane in liquid, respectively, if there is no mass transfer limitation). The decrease in gas phase methane concentration is plotted against time for each cell dilution. The control vials showed no methane loss throughout the course of the experiment. Samples with 100 μl added methane showed up to 80% depletion of total methane. The 5x and 10x concentrated samples in the 200 μl added methane set showed greater than 95% methane reduction. This depletion caused a decrease in the methane uptake rate over time, i.e., the second derivative of concentration vs. time does not equal 0. Therefore, linear regressions were performed to determine which data points constituted the initial methane uptake rate, and which points displayed a deviation from the initial rate. This procedure was done for each cell dilution. The points used for the calculation of

initial uptake rates have regression lines shown through them on Figures 4.1 and 4.2. Typically, the rates were linear up to a 45% decrease in methane. The calculated rates, 95% confidence limits, and number of points used to calculate rates are shown in Tables 4.1 and 4.2. Figures 4.3 and 4.4 show the uptake rates versus cell dilution for the 100 and 200 µl added methane data sets, respectively. Data from the linear regressions shown in Figures 4.1 and 4.2 were used to calculate the methane uptake rate per unit volume fluid in a serum vial. The equation used for this calculation follows:

$$MUR = \frac{\Delta c_G}{\Delta t}\frac{V_{void}}{V_{liquid}} \qquad (4\text{-}8)$$

where:

MUR = methane uptake rate $\left(\frac{m}{l^3 t}\right)$

$\frac{\Delta c_G}{\Delta t}$ = change in gas phase methane concentration per unit time, calculated as the linear regression obtained from data in Figures 4.1 and 4.2 $\left(\frac{m}{l^3 t}\right)$

V_{void} = vial void volume (l^3)

V_{liquid} = vial liquid volume (l^3)

With no mass transfer limitation, the methane uptake rate should be linear with cell dilution, i.e., doubling the cell concentration should double the methane uptake rate. The calculated rate for the 0.1x dilution was used to develop a line defining the expected methane uptake given no mass transfer limitation. The rates shown in Figures 4.3 and 4.4 are below the line for predicted rates at the higher cells densities.

Ninety-five percent upper confidence limits for methane uptake rates on the 0.7x dilution and non-diluted (1x) samples in the 100 µl added methane set (Figure 4.3) are below the prediction line. Upper 95% confidence limits for rates for cell dilutions greater than 0.1 in the 200 µl added methane set are all below the line predicting non-mass transfer limited rates. This is shown more clearly in Figure 4.5, which is rescaled to show dilute samples more clearly. These data show that the methane uptake rates are mass transfer limited at the higher cell densities.

In order to estimate k_La' for the system, the methane uptake rate must be maximized, i.e., the plot of methane uptake rate vs. cell dilution should show a saturated methane uptake rate. The data in Figure 4.4 seem to display a saturated uptake rate. However, when these data are plotted on an expanded scale, as shown in Figure 4.6, they display slowed but not saturated methane uptake. Therefore, the data cannot be used to calculate an actual k_La', but can be used to obtain a lower limit on the k_La'. Equation 4-1 is used to calculate the lower limit:

$$k_La'(C^* - C) = Ra' \qquad (4\text{-}1)$$

(Danckwerts, 1970)

Solving for k_La':

$$k_La' = \frac{Ra'}{(C^* - C)} \qquad (4\text{-}9)$$

Ra' is the methane uptake rate by cells per unit volume fluid. Setting the liquid methane concentration to 0 in equation 4-9, I obtain a lower limit for $k_L a'$:

$$\left(k_L a'\right)_{\min} = \left(\frac{Ra'}{C^*}\right)_{\max} \tag{4-10}$$

Ra' is equal to the methane uptake rate, MUR. The calculation for MUR is shown in equation 4-16. The lower limit for mass transfer was estimated with the methane uptake rate in the 10-fold concentrated sample initially containing 200 µl pure methane. The calculated value is:

$$\left(k_L a'\right)_{\min} = \frac{820}{hr} \tag{4-11}$$

This lower limit was used for determining the cell concentration that would give non-mass transfer limited methane uptake in kinetics experiments.

4.4.2 Kinetic Parameter Determination

4.4.2.1 Calculating a Maximum Cell Density for Non-Mass Transfer Limited Kinetics

Previous data suggested the Michaelis-Menten kinetic parameters for methane oxidation by the particulate methane monooxygenase of *M. albus* BG8 were $0.014<V_{max}'<0.050$ (µmol consumed/hour/µg protein) and $7<K_s<30$ (µM) (Semrau, 1995). The rate of methane consumption is defined by:

$$V' = \frac{V_{max}' C}{K_s + C} \qquad (4\text{-}12)$$

where:

V' = rate of substrate utilization per unit cell mass $\left(\frac{m_s}{t\, m_c}\right)$ (m_s represents substrate mass, m_c represents cell mass)

V_{max}' = maximum rate of substrate utilization per unit cell mass $\left(\frac{m_s}{t\, m_c}\right)$

K_S = Michaelis-Menten affinity coefficient $\left(\frac{m}{l^3}\right)$

C = liquid phase methane concentration $\left(\frac{m}{l^3}\right)$

The criterion for non-mass transfer limited kinetics is defined by equation 4-3:

$$\frac{V' \frac{1}{V_L}(X\, V_L)}{k_L\, a' C^*} << 1 \qquad (4\text{-}3)$$

I chose to set the criterion for equation 4-3 to 0.05:

$$\frac{V' \frac{1}{V_L}(X\, V_L)}{(k_L\, a')_{min}\, C^*} < 0.05 \qquad (4\text{-}13)$$

This criterion states that the liquid methane concentration will be at least 95% of the expected equilibrium concentration. Substituting the equation for V' from equation 4-12 into 4-13, I obtain:

$$\frac{\frac{V_{max}' C}{K_s + C} \frac{1}{V_L}(X\, V_L)}{(k_L\, a')_{min} \frac{C}{0.95}} < 0.05 \qquad (4\text{-}14)$$

I calculated a maximum cell concentration which would uphold equation 4-14 for any value of V_{max}', K_s and k_La' that would apply to the experimental setup. This calculation is done by substituting the calculated $(k_La')_{min}$, the minimum value for K_s and C, and the maximum value for V_{max}' into equation 4-14. The values used and maximum protein concentration, X_{max}, are listed below:

$(k_La')_{min}$ = 820/hr

K_s = 7 μM

C = 0 μM

V_{max}' = 0.05 μmol/hr/μg protein.

X_{max} = 6 μg protein/ml.

All kinetics experiments were done with a cell density corresponding to a protein concentration less than 6 μg protein/ml.

4.4.2.2 Cell Densities and Copper Concentrations

The final OD_{600} for cells grown under high copper was 1.3. This corresponds to a protein concentration of approximately 150 μg protein/ml fluid, which was confirmed by direct protein assay. These cells were diluted 50-fold to obtain a cell density corresponding to approximately 3 μg protein/ml.

The low copper experiment was carried out twice. In the first experiment, the final OD_{600} was 0.5, corresponding to approximately 60 μg protein/ml. These cells were diluted 15-fold to obtain 4 μg protein/ml. The actual protein concentration for the undiluted sample determined using the Bio-Rad DC® protein assay was 65 μg/ml. In the second experiment, cells were grown to an OD_{600} of 0.7, corresponding to

approximately 80 μg protein/ml. These cells were diluted 20-fold for kinetic experiments to obtain approximately 4 μg protein/ml. The actual undiluted sample protein concentration was determined to be 73 μg/ml.

The copper concentration in the growth medium containing cells was determined by ICP-MS. For the cells grown with high copper, the concentration was 15 μM. In both experiments with no added copper, the copper concentration was 0.3 μM.

4.4.2.3 Kinetic Parameters

The results for the high copper experiment are shown in Figures 4.7 through 4.10. The data for methane oxidation over time for each initial concentration are shown in Figures 4.7 through 4.9. These figures show the high, median, and low values for total methane oxidation at each time point.

When analyzing oxidation vs. time data, only the points which follow the initial linear rate should be used for a linear regression of the data. Often, data points at later times fall off the initial rate curve. There are many causes for this, including, but not limited to: cell growth causing an increase in enzyme concentration over time, cofactor limitation causing a decrease in enzyme activity, and substrate decrease causing a deviation from the initial concentration and thus a lower rate.

Due to the possible changes in the initial rates over time, the methane oxidation vs. time data were analyzed first for changes in the initial rates. The three hour time points showed deviations from the initial rates for all samples with liquid methane concentrations greater than or equal to 9.2 μM. (See Figures 4.7 through 4.9.) This

included five of the eight concentrations used in the experiment. Therefore, no data for total oxidation during the three hour time period were used in the linear regression analysis.

Linear regressions were performed on all data sets using the one and two hour data points. If a data point fell outside two standard errors from the regression line, the final regression was reanalyzed without this data point. All data not included in the final linear regression are noted in Figures 4.7 through 4.9. The calculated rates, statistical information, and mass transfer limitation analyses are shown in Table 4.3. The mass transfer analyses showed that the methane uptake was not mass transfer limited.

The Michaelis-Menten plot for this experiment is shown in Figure 4.10. The parameters for the Michaelis-Menten prediction curve shown in Figure 4.10 were analyzed using non-linear regression analysis of the data. TableCurve 2D version 3 for IBM was used for all linear and non-linear regression analyses described in this chapter. The kinetic parameters obtained for the high copper case are:

Parameter	Value	Units	Lower 95% Confidence Limit	Upper 95% Confidence Limit
V_{max}	0.030	$\frac{\mu mol}{hr\ \mu g\ protein}$	0.021	0.039
K_s	6.5	μM	5.1	7.9

The 95% confidence limits were calculated using confidence limit data for both protein concentration measurements and kinetic data. The calculated parameters correlate well with those determined previously in the laboratory (Semrau, 1995).

Results for the first low copper experiment are shown in Figures 4.11 through 4.14. Figures 4.11 through 4.13 show the data for methane oxidation over time for each initial concentration. These figures show the high, median, and low values for total methane oxidation at each time point. Data for all time points for all concentrations appeared to follow the initial linear rate. The only data not included in the final linear regression were those falling greater than two standard errors off the regression line when they were included in the regression. Points not included for this reason are noted in Figures 4.11 through 4.13.

The calculated rates, statistical information, and mass transfer limitation analyses are shown in Table 4.4. The mass transfer analyses showed that the methane uptake was not mass transfer limited. The Michaelis-Menten plot of these rate data vs. liquid methane concentration is shown in Figure 4.14. The kinetic parameters for the low copper experiment are:

Parameter	Value	Units	Lower 95% Confidence Limit	Upper 95% Confidence Limit
V_{max}	0.020	$\frac{\mu mol}{hr\ \mu g\ protein}$	0.015	0.025
K_s	8.9	μM	6.9	11

The affinity coefficient, K_s, differed from a previously determined coefficient of 30 μM. (Semrau, 1995) Therefore, this experiment was repeated. The methane oxidation data are shown in Figures 4.15 through 4.17. The data were analyzed as described for the first low copper experiment. The Michaelis-Menten plot is shown in

Figure 4.18. Summary data are shown in Table 4.5. The kinetic parameters follow:

Parameter	Value	Units	Lower 95% Confidence Limit	Upper 95% Confidence Limit
V_{max}'	0.011	$\frac{\mu mol}{hr\ \mu g\ protein}$	0.009	0.012
K_s	9.3	μM	7.5	11

The K_s matched the value found with the first low copper experiment. V_{max}' obtained in this experiment was approximately one-half the value for the initial experiment. This is not a surprising result. The whole cell methane oxidation capacity has been shown to vary by a factor of four to five depending on the health of cells, the phase of growth, and the source of water used for the growth medium (Lidstrom, 1995).

4.5 Conclusions and Summary

The experimental setup described herein allows for analysis of methane utilization kinetic parameters without mass transfer limitation. The kinetic parameters determined for different copper concentrations in the growth medium do not display statistically significant differences. The 95% confidence limits for the V_{max}' values in the high copper and the first low copper experiment overlapped. The 95% confidence limits for the affinity coefficients for all experiments overlap. Thus, it appears that although copper plays a role in the active site of the pMMO enzyme in these experiments, it does not affect the overall methane utilization kinetics in *M. albus* BG8 cells. The values obtained for V_{max}' and K_s in these experiments were used for comparing model predictions to data obtained in column experiments.

Table 4.1. Methane Uptake Rates Raw Data, 100 µl Methane Added to Sample Vials

Cell Dilution	$-(\Delta C_{CH4})_{gas}/(\Delta t)$ (µM/hour) Value	95% confidence limits		Number of Data Points Used to in Evaluation	Methane Uptake Rate (µmol/hr/ml fluid) Value	95% confidence limits		Expected Rate if Consumption is Non-Mass Transfer Limited*
0.1	8.9	7	11	5	0.35	0.27	0.42	0.35
0.2	18	15	21	5	0.69	0.58	0.8	0.7
0.3	24	22	25	5	0.92	0.85	0.99	1
0.4	31	28	35	4	1.2	1.1	1.4	1.4
0.5	35	27	44	4	1.4	1.1	1.7	1.7
0.7	43	39	48	4	1.7	1.5	1.9	2.4
1	57	43	70	3	2.2	1.7	2.7	3.5

Table 4.2. Methane Uptake Rates Raw Data, 200 µl Methane Added to Sample Vials

Cell Dilution	$-(\Delta C_{CH4})_{gas}/(\Delta t)$ (µM/hour) Value	95% confidence limits		Number of Data Points Used in Evaluation	Methane Uptake Rate (µmol/hr/ml fluid) Value	95% confidence limits		Expected Rate if Consumption is Non-Mass Transfer Limited*
0.1	19	17	20	5	0.73	0.67	0.79	0.7
0.2	30	27	32	5	1.2	1.1	1.3	1.5
0.3	41	40	42	5	1.6	1.5	1.6	2.2
0.4	46	45	48	4	1.8	1.8	1.9	2.9
0.5	50	47	53	4	2	1.8	2.1	3.6
0.7	56	52	61	4	2.2	2	2.4	5.1
1	60	55	65	3	2.3	2.2	2.5	7.3
5	160	150	180	5	6.4	5.8	6.9	36
10	230	200	260	5	9	7.6	10	73

* Calculated with 0.1x cell dilution rate, assuming this sample did not exhibit mass transfer limited kinetics

Table 4.3. Methane Uptake Summary and Mass Transfer Limitation Test for the 15 μM added Copper pMMO Kinetic Parameter Analysis

Initial Methane Concentration (μM)	V (Ra') (μmol/(hr-ml fluid)) Value	Standard Error	95% Confidence Limits		$(k_La')_{min}*C^*$ (μmol/(hr-ml fluid))	$Ra'/[(k_La')_{min}*C^*]$
1.8	1.6E-2	3.7E-4	1.5E-2	1.7E-2	1.5	0.011
3.7	3.0E-2	3.5E-4	2.9E-2	3.1E-2	3	0.01
5.5	4.3E-2	1.5E-3	4.0E-2	4.7E-2	4.5	0.01
9.2	5.5E-2	1.4E-3	5.1E-2	5.9E-2	7.5	0.007
18	6.9E-2	1.8E-3	6.4E-2	7.4E-2	15	0.005
37	7.6E-2	1.2E-3	7.3E-2	7.9E-2	30	0.003
55	8.1E-2	1.7E-3	7.7E-2	8.6E-2	45	0.002
73	8.2E-2	2.6E-3	7.5E-2	8.8E-2	60	0.001

Table 4.4. Methane Uptake Summary and Mass Transfer Limitation Test for the First No Added Copper pMMO Kinetic Parameter Analysis

Initial Methane Concentration (μM)	V (Ra') (μmol/(hr-ml fluid)) Value	Standard Error	95% Confidence Limits		$(k_La')_{min}*C^*$ (μmol/(hr-ml fluid))	$Ra'/[(k_La')_{min}*C^*]$
3.7	2.5E-2	7.5E-4	2.3E-2	2.6E-2	3	0.008
7.3	3.8E-2	1.1E-3	3.5E-2	4.1E-2	6	0.006
11	4.8E-2	1.4E-3	4.5E-2	5.1E-2	9	0.005
22	6.2E-2	1.3E-3	5.9E-2	6.5E-2	18	0.003
52	7.6E-2	1.6E-3	7.3E-2	8.0E-2	43	0.002
104	8.1E-2	1.6E-3	7.8E-2	8.5E-2	85	0.001
146	7.7E-2	2.7E-3	7.1E-2	8.4E-2	120	0.0006

Table 4.5. Methane Uptake Summary and Mass Transfer Limitation Test for the Second No Added Copper pMMO Kinetic Parameter Analysis

Initial Methane Concentration (μM)	V (Ra') (μmol/(hr-ml fluid)) Value	Standard Error	95% Confidence Limits		$(k_La')_{min}*C^*$ (μmol/(hr-ml fluid))	$Ra'/[(k_La')_{min}*C^*]$
3.7	1.1E-2	2.8E-4	1.0E-2	1.2E-2	3	0.004
7.3	1.7E-2	1.6E-4	1.7E-2	1.8E-2	6	0.003
11	2.1E-2	7.4E-4	1.9E-2	2.3E-2	9	0.002
22	2.7E-2	7.3E-4	2.5E-2	2.8E-2	18	0.001
51	3.5E-2	1.0E-3	3.2E-2	3.7E-2	42	0.0008
102	3.5E-2	1.2E-3	3.3E-2	3.8E-2	84	0.0004
146	3.6E-2	1.2E-3	3.3E-2	3.9E-2	120	0.0003

Table 4.6. Summary of kinetic parameters for *M. albus* BG8 cells grown under high and low copper

Copper Concentration	V_{max}' (μmol/(hr-μg protein)) Value	Standard Error	95% Confidence Limits		K_s (μM) Value	Standard Error	95% Confidence Limits	
15 μM	0.03	0.0044	0.021	0.039	6.5	0.56	5.1	7.9
0.3 μM #1	0.02	0.0026	0.015	0.025	8.9	0.77	6.9	11
0.3 μM #2	0.011	0.0008	0.009	0.012	9.3	0.7	7.5	11

Figure 4.1. Mass Transfer Analysis: Methane Depletion Over Time for Different Cell Dilutions, 100 µl Pure Methane Added to Sample Vials

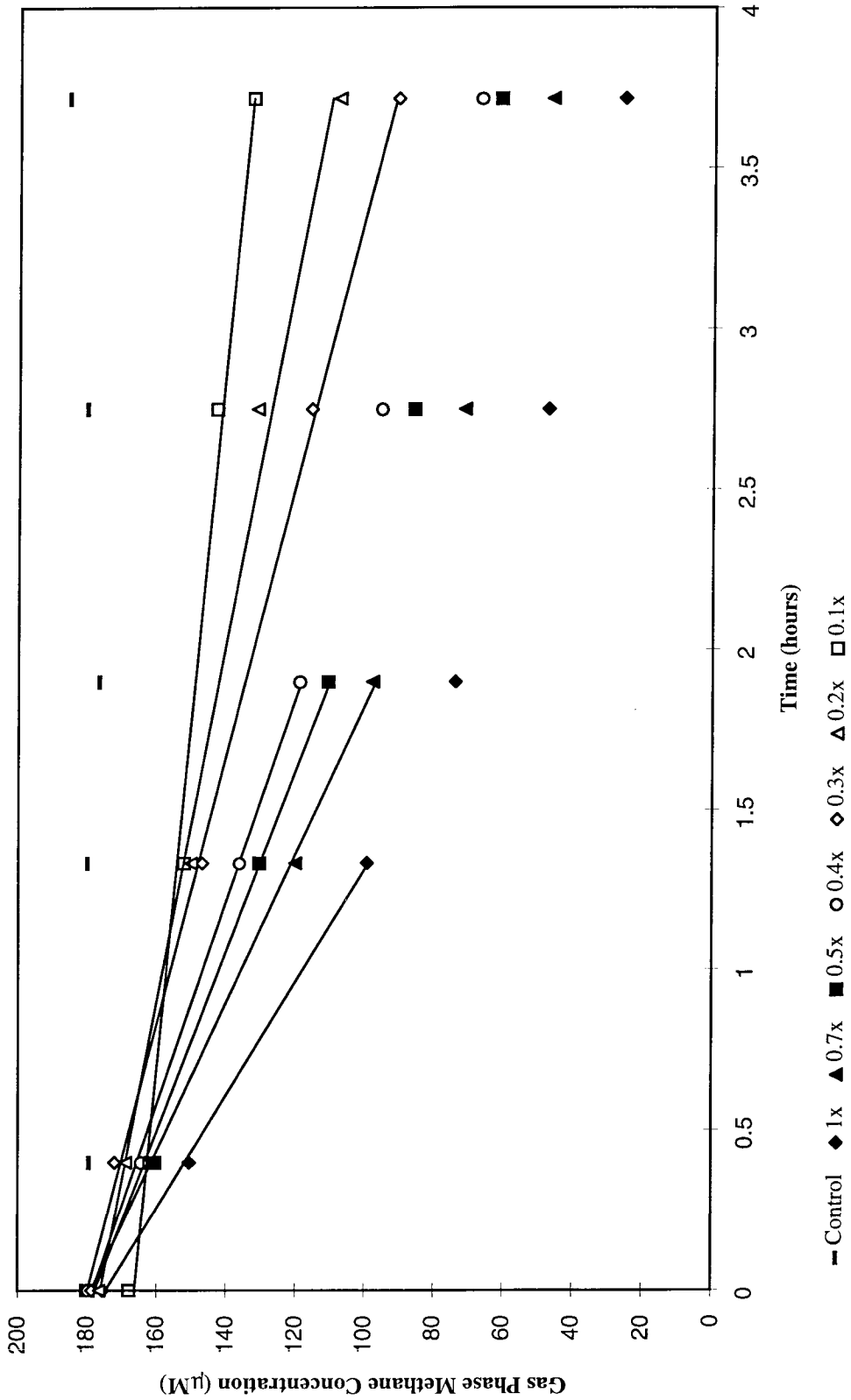

Figure 4.2. Mass Transfer Analysis: Methane Depletion Over Time for Different Cell Dilutions, 200 µl Pure Methane Added to Sample Vials

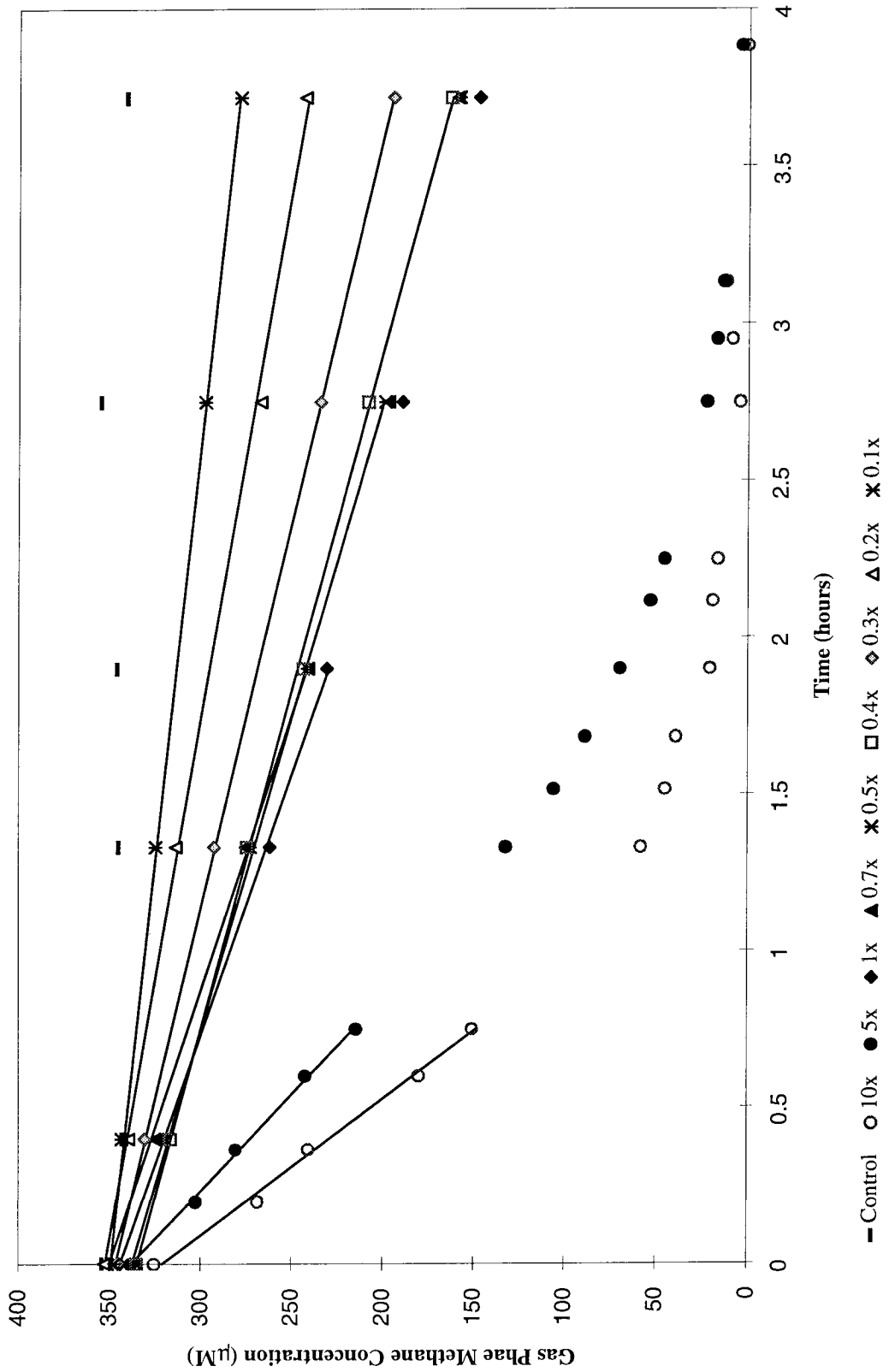

Figure 4.3. Mass Transfer Analysis: Methane Uptake vs. Cell Dilution, 100 µl Pure Methane Added to Sample Vials

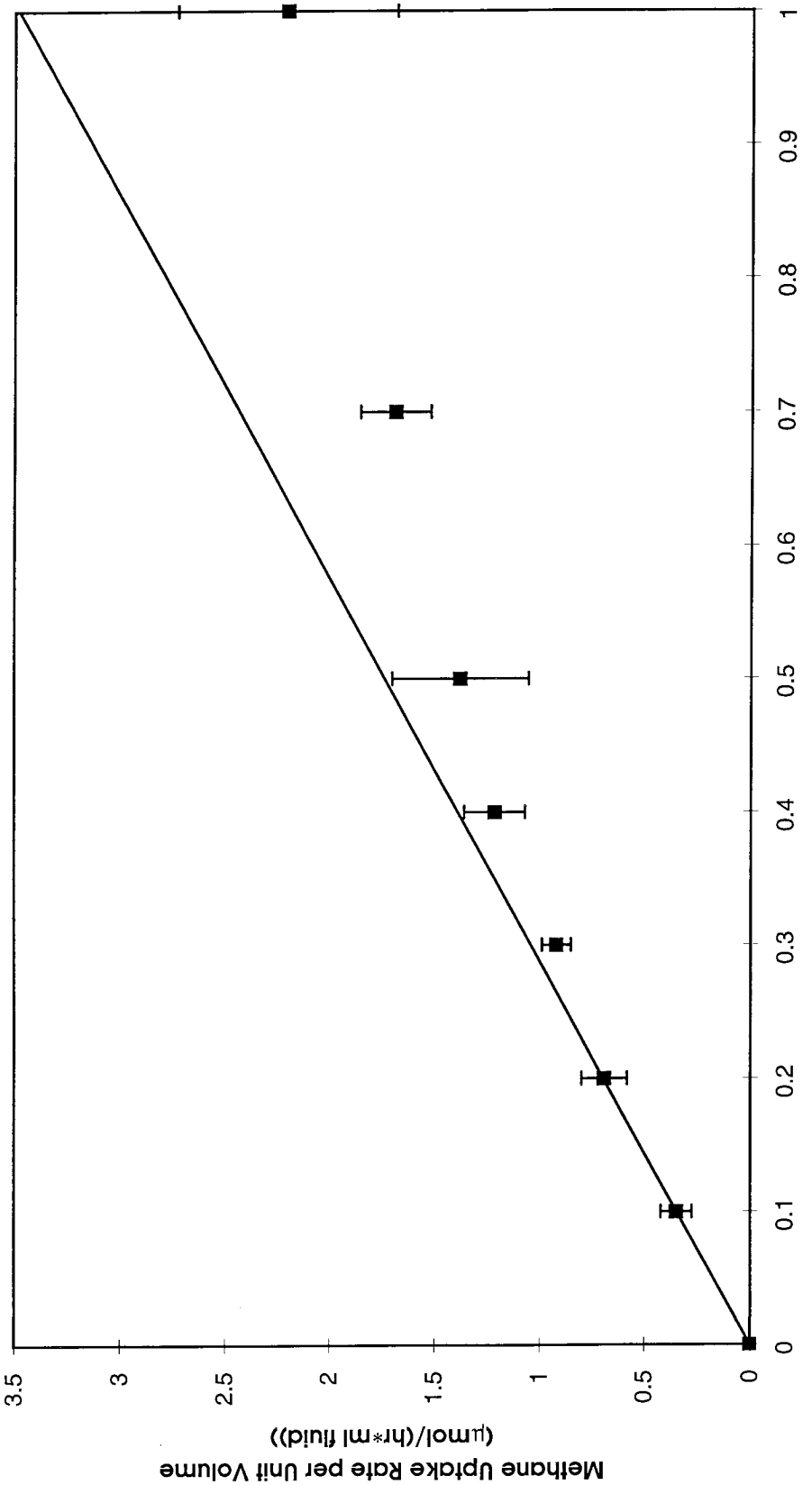

Figure 4.4. Mass Transfer Analysis: Methane Uptake vs. Cell Dilution (< 1) or Concentration (> 1), 200 µl Pure Methane Added to Sample Vials

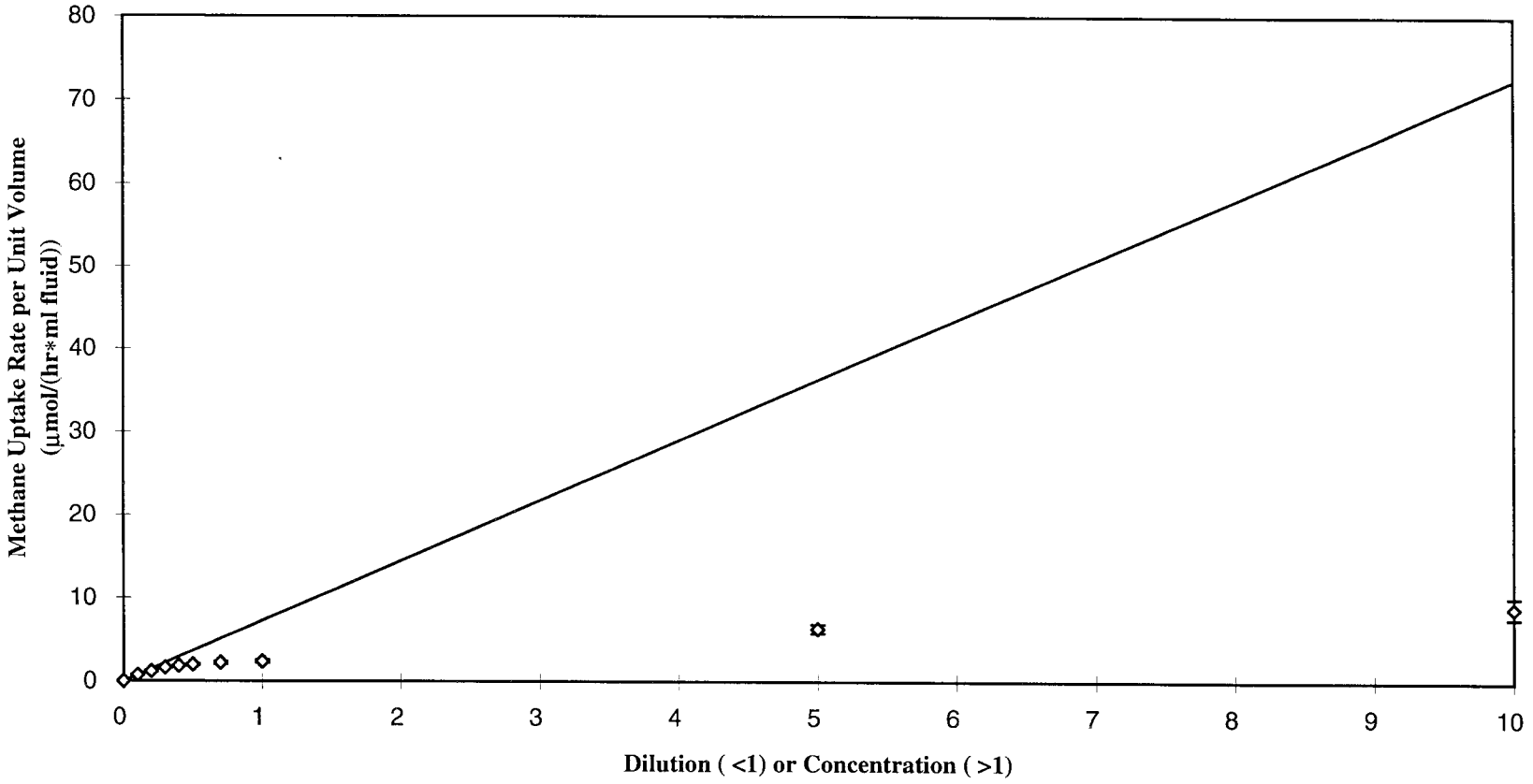

—— Predicted Non-Mass Transfer Limited Rates, Based on 0.1x Dilution

◇ Calculated Rates, error bars represent 95% confidence limits

Figure 4.5. Mass Transfer Analysis: Methane Uptake vs. Cell Dilution, 200 µl Pure Methane Added to Sample Vials

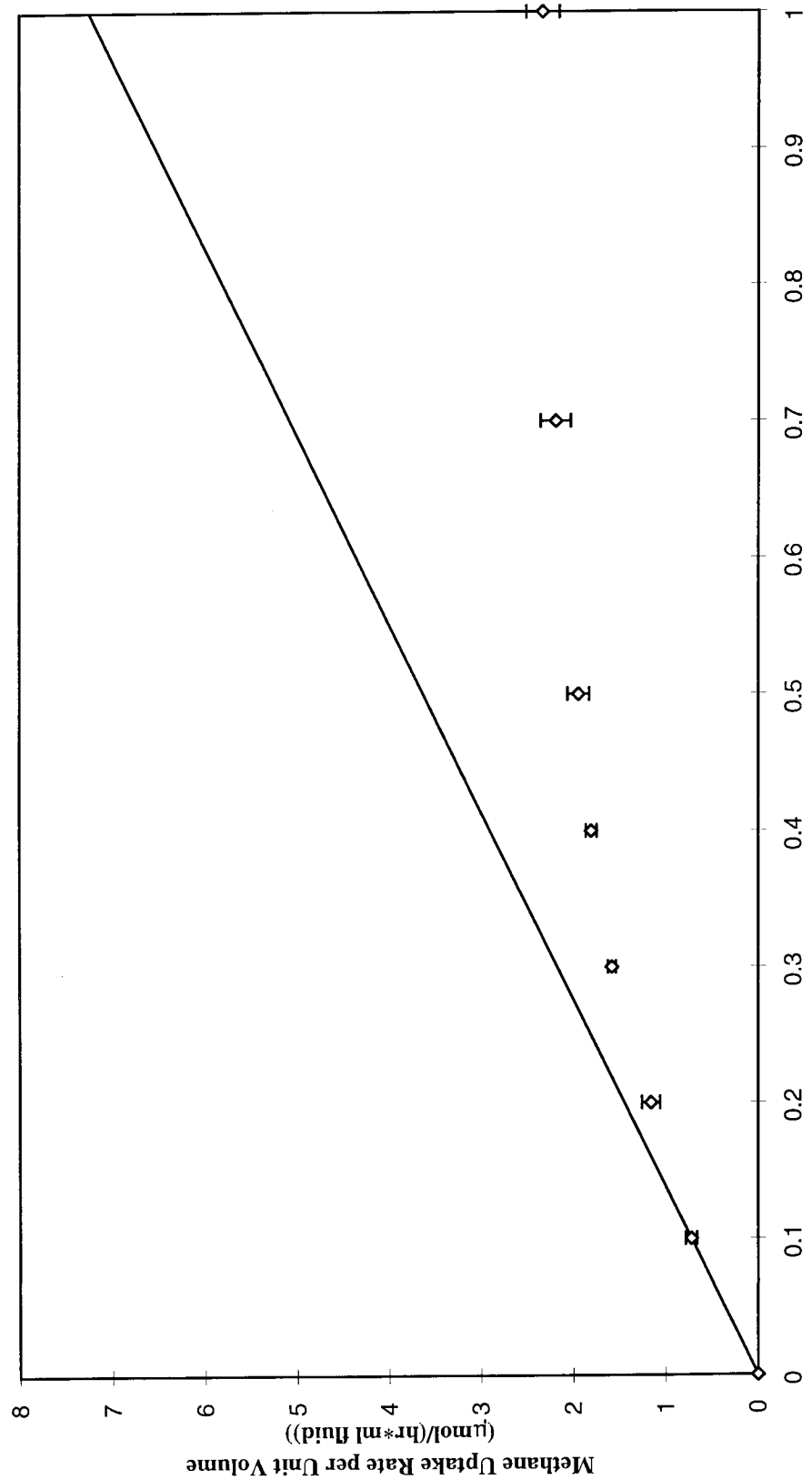

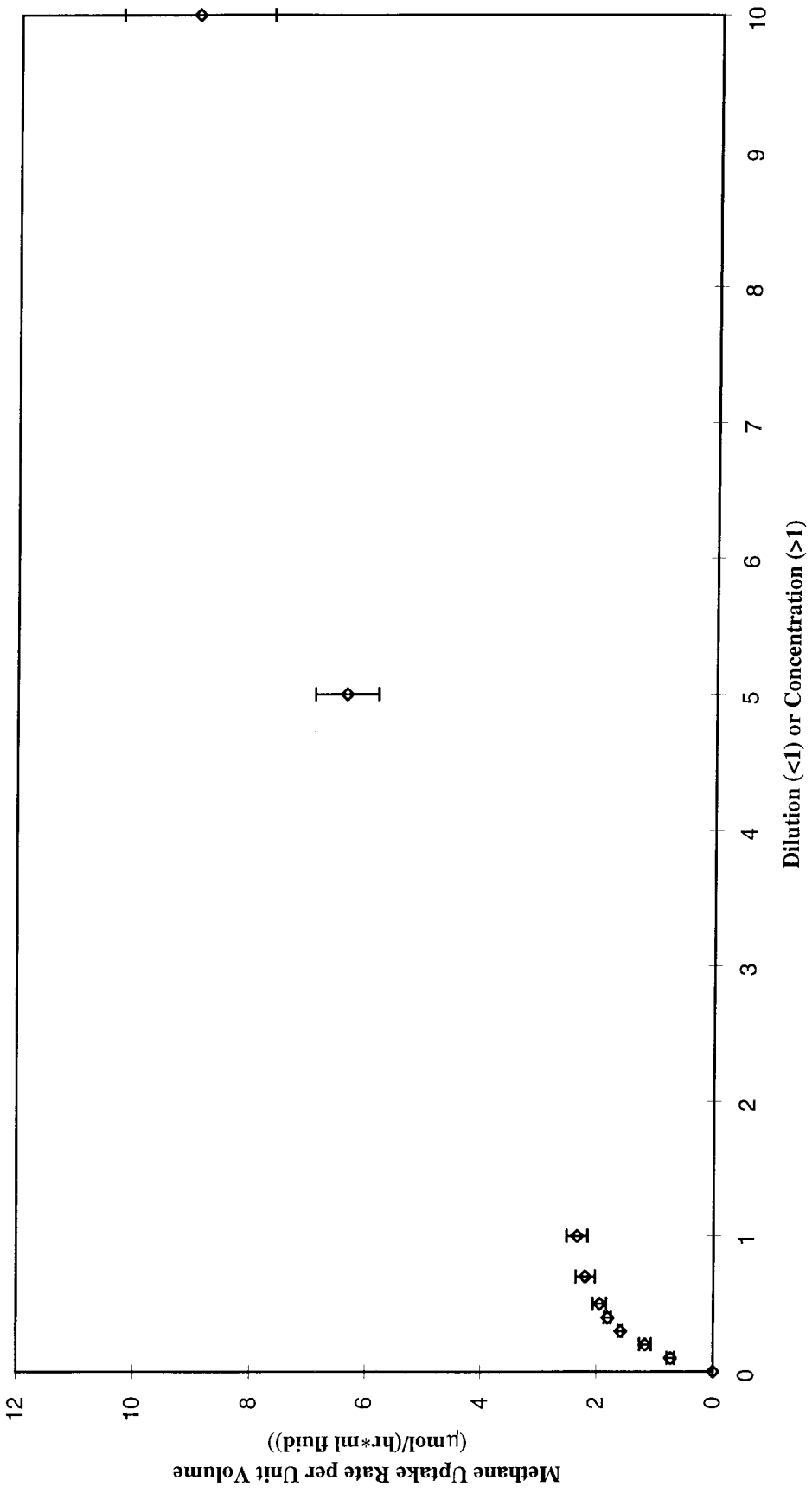

Figure 4.6. Mass Transfer Analysis: Methane Uptake vs. Cell Dilution (<1) or Concentration (>1), 200 μl Pure Methane Added to Sample Vials

Figure 4.7. High Copper Experiment: Methane Oxidation vs. Time for Initial Methane Concentrations of 1.8, 18 and 55 μM, Growth Medium $[Copper]_{total}$=15 μM*

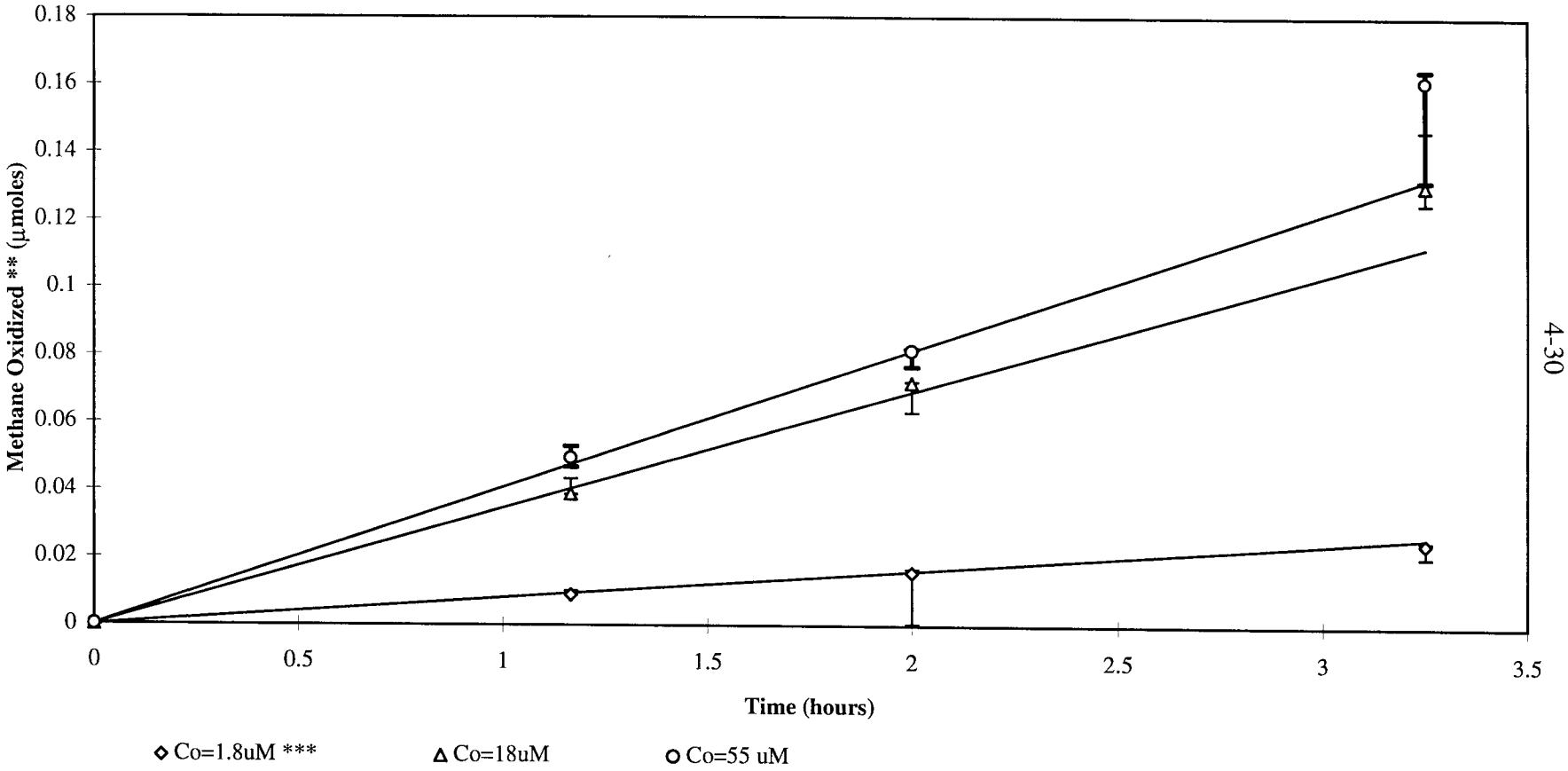

* Median, high and low values shown. 3.25 hour data points were not included in the linear regression analyses.

** Measured as non-volatile ^{14}C products.

*** 2 hour low value was not used in the linear regression analysis.

Figure 4.8. High Copper Experiment: Methane Oxidation vs. Time for Initial Methane Concentrations of 3.7, 9.2 and 73 μM, Growth Medium $[Copper]_{total}$=15 μM*

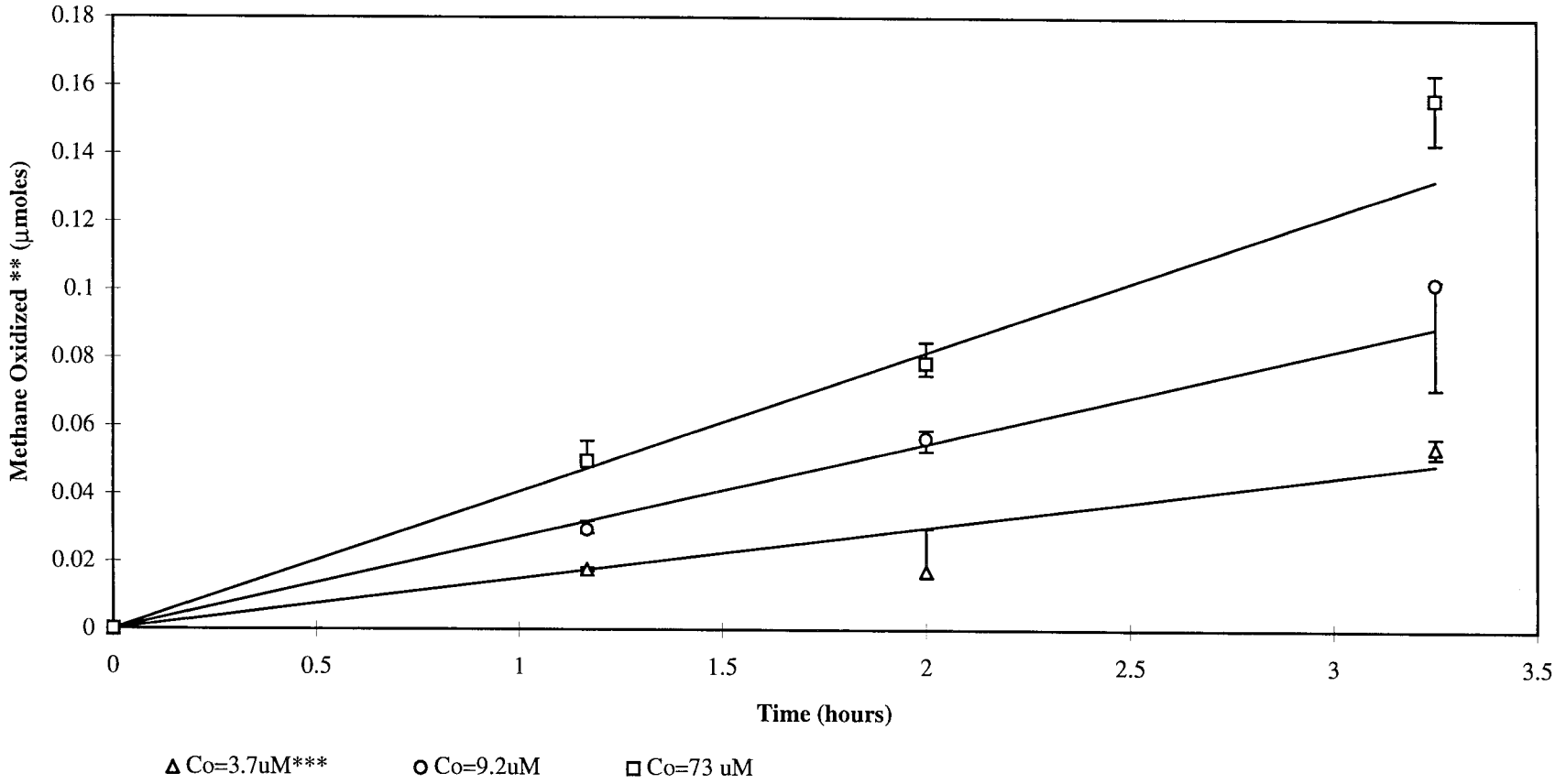

* Median, high and low values shown. 3.25 hour data points were not included in any linear regressions.

** Measured as non-volatile ^{14}C products.

*** 2 lowest values for the 2 hour time point were not included in the linear regression based on statistical analyses.

Figure 4.9. High Copper Experiment: Methane Oxidation vs. Time for Initial Methane Concentrations of 5.5 and 37 μM, Growth Medium $[Copper]_{total}$=15 μM*

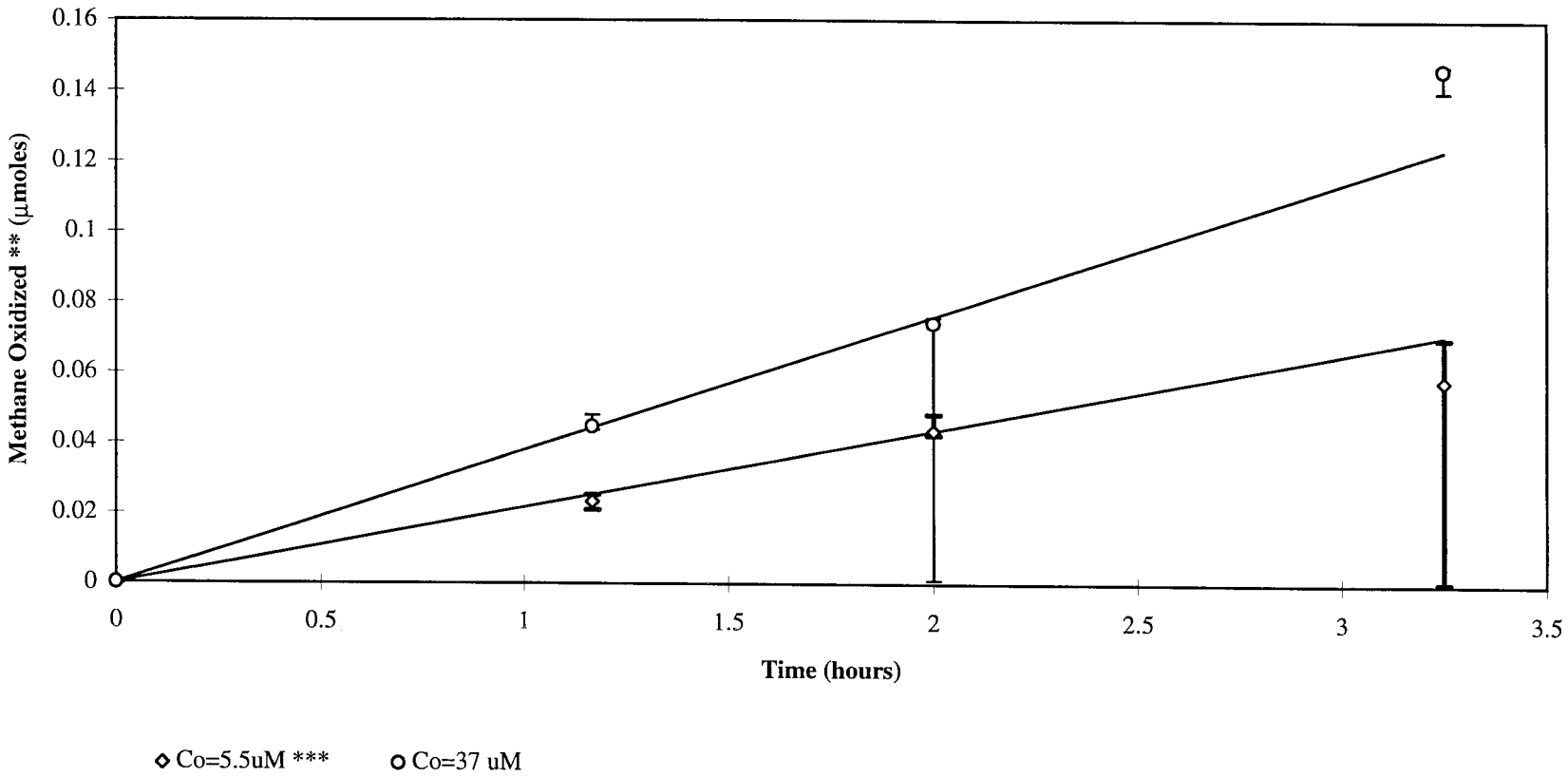

* Median, high and low values shown. 3.25 hour data points were not included in the linear regression analyses.

** Measured as non-volatile ^{14}C products.

*** 2 hour low value was not included in the linear regression analysis.

Figure 4.10. High Copper Experiment: Michaelis-Menten Plot for Methane Consumption by *M. albus* BG8 Grown with 15 μM Copper

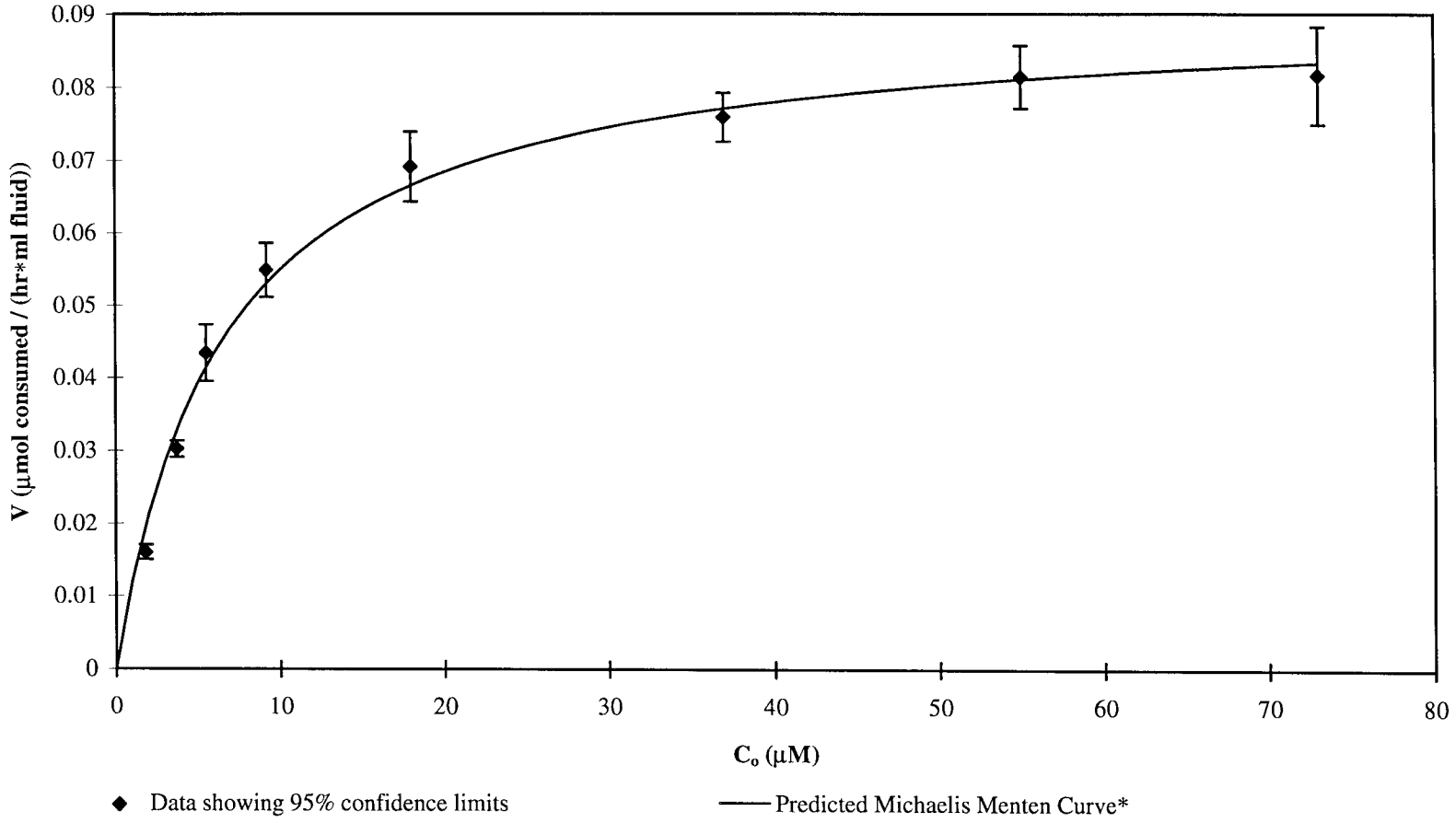

*V_{max}=0.090 μmol/(hr-ml fluid), V_{max}'=0.030 μmol/(hr-μg protein), K_s=6.5μM

95% confidence limits: 0.021 < V_{max}'(μmol/(hr-μg protein)) < 0.039 ; 5.1 < K_s (μM) < 7.9

Figure 4.11. Methane Oxidation vs. Time for Initial Methane Concentrations of 3.7, 22, and 104 μM, $[Copper]_{total}$=0.3μM*

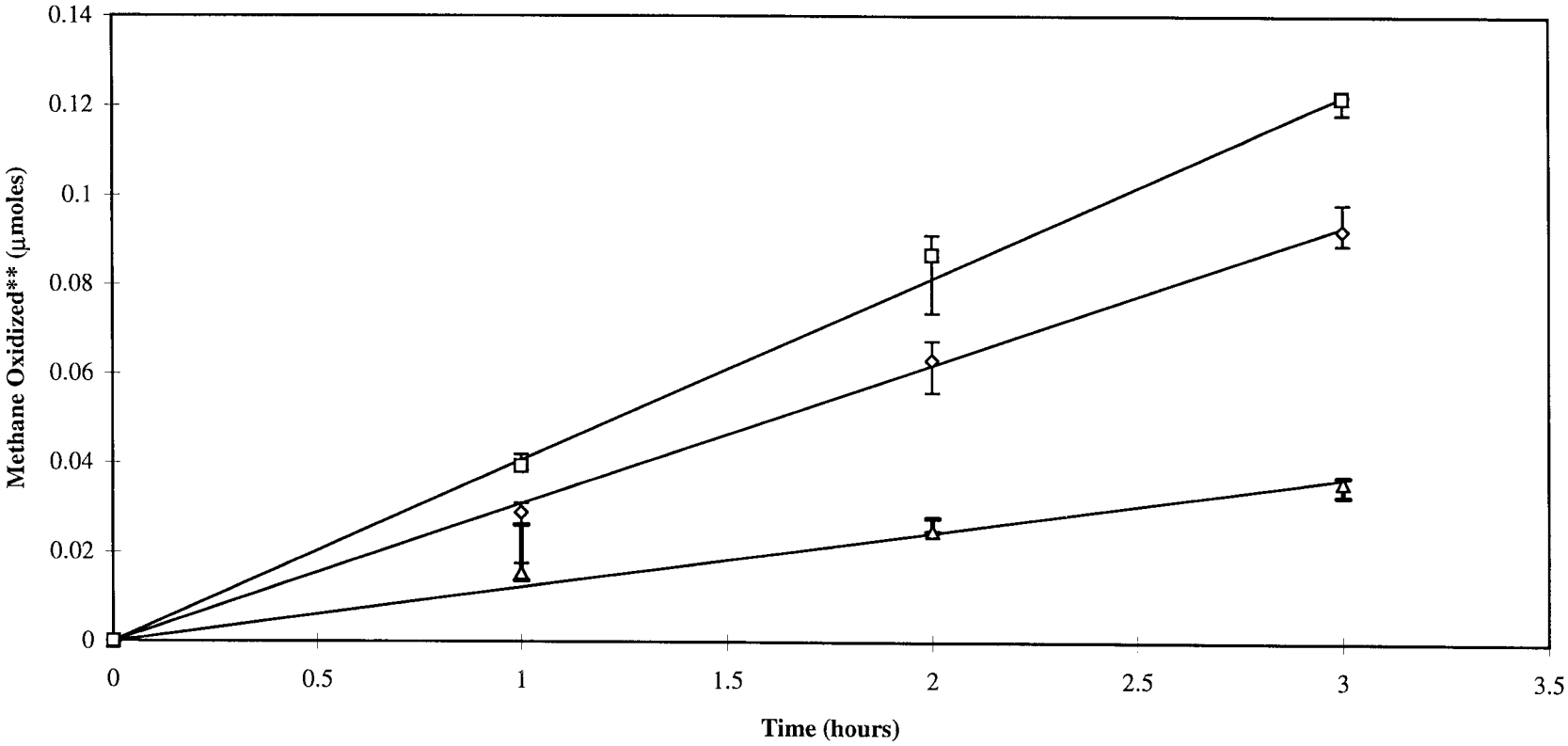

* Median, high and low values shown.

** Measured as non-volatile ^{14}C products.

*** One hour maximum value was not included in the linear regression analysis.

Figure 4.12. Methane Oxidation vs. Time for Initial Methane Concentrations of 7.3 and 146 μM, $[Copper]_{total}$=0.3μM*

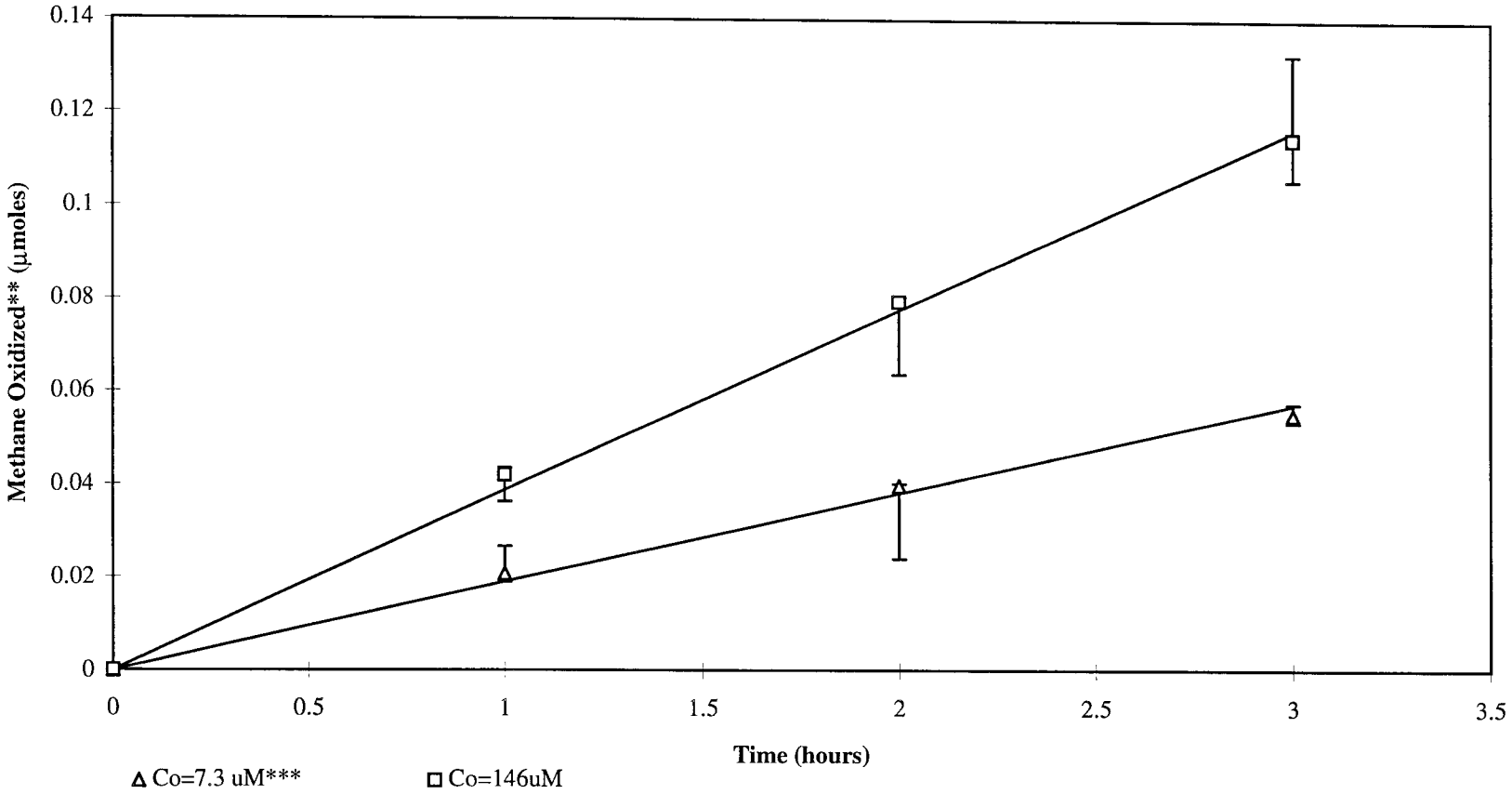

* Median, high and low values shown.

** Measured as non-volatile ^{14}C products.

***Two hour minimum value was not included in the linear regression analysis.

Figure 4.13. Methane Oxidation vs. Time for Initial Methane Concentrations of 11 and 52 μM, $[Copper]_{total}$=0.3μM*

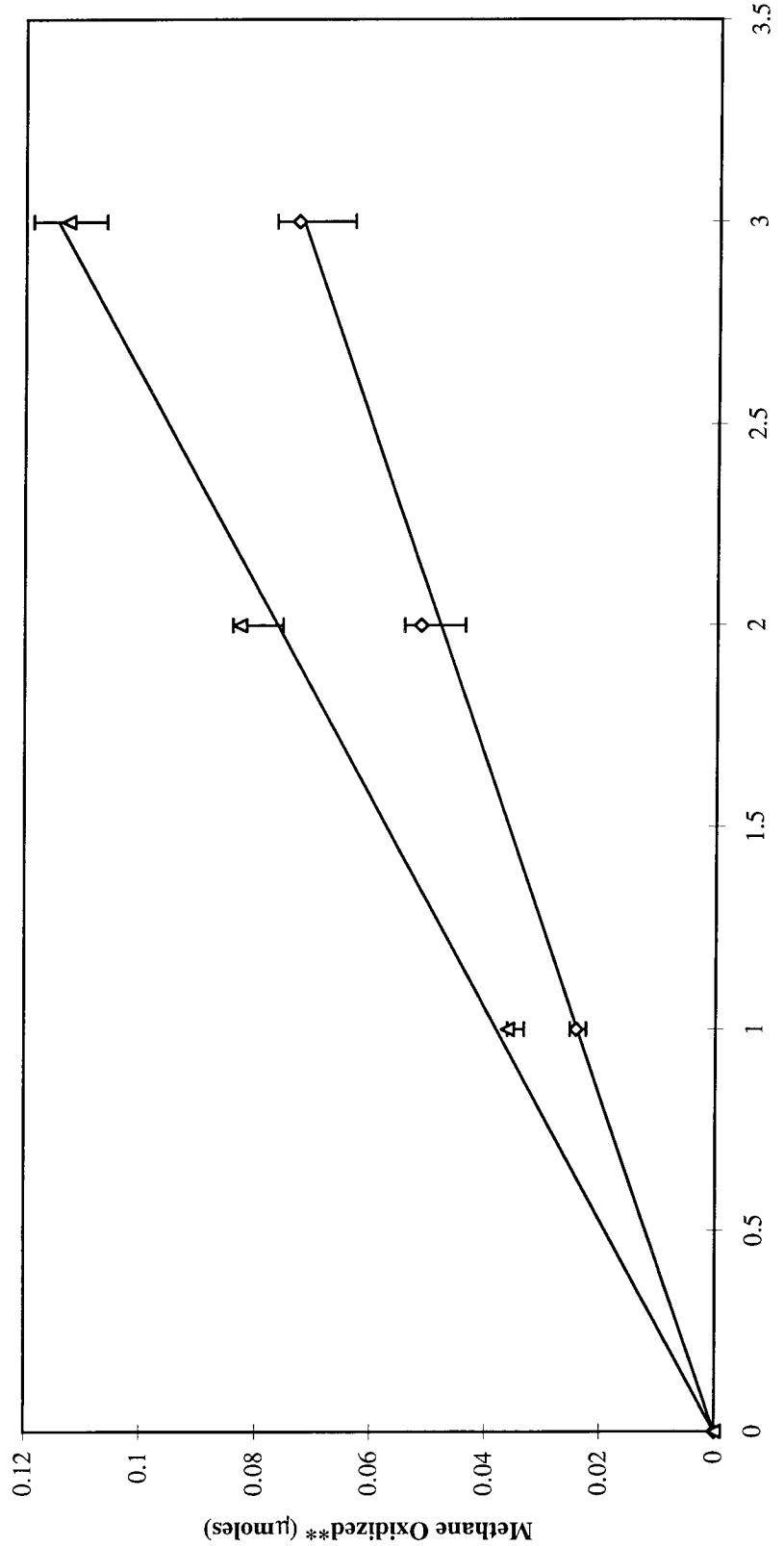

* Median, high and low values shown.

** Measured as non-volatile ^{14}C products.

Figure 4.14. Low Copper Experiment # 1: Michaelis-Menten Plot for Methane Consumption by *M. albus* BG8 Grown with No Added Copper ($[Copper]_{total}$=0.3μM)

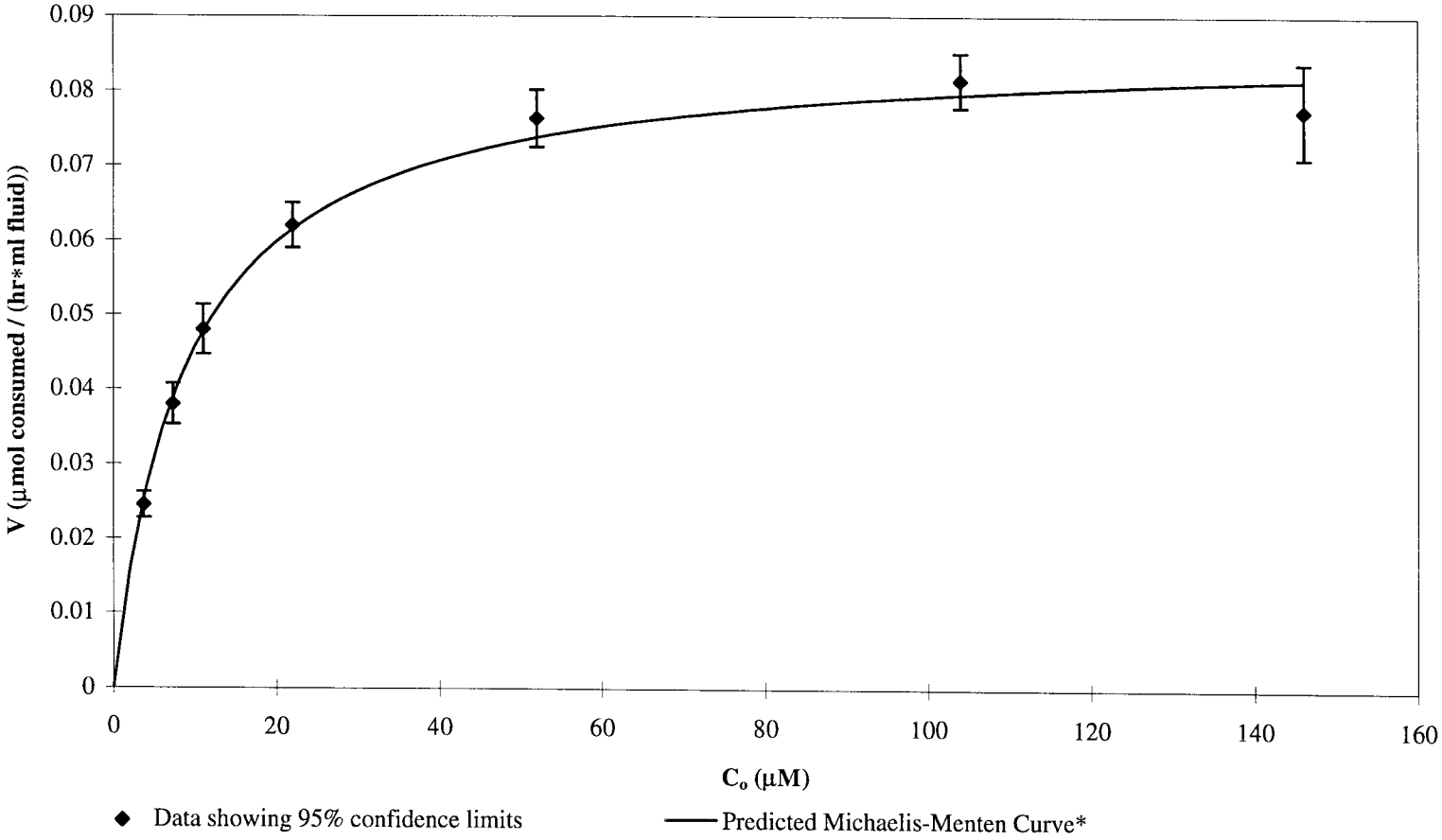

* V_{max}=0.086 μmol/(hr-ml fluid), V_{max}'=0.020 μmol/hr/μg protein, K_s=8.9μM
95% confidence limits: 0.015 < V_{max}' (μmol/(hr-μg protein)) < 0.025; 6.9 < K_s (μM) < 11

Figure 4.15. Low Copper Experiment # 2: Methane Oxidation vs. Time for Initial Methane Concentrations of 3.7, 22 and 146 μM; Growth Medium $[Copper]_{total}$=0.3μM*

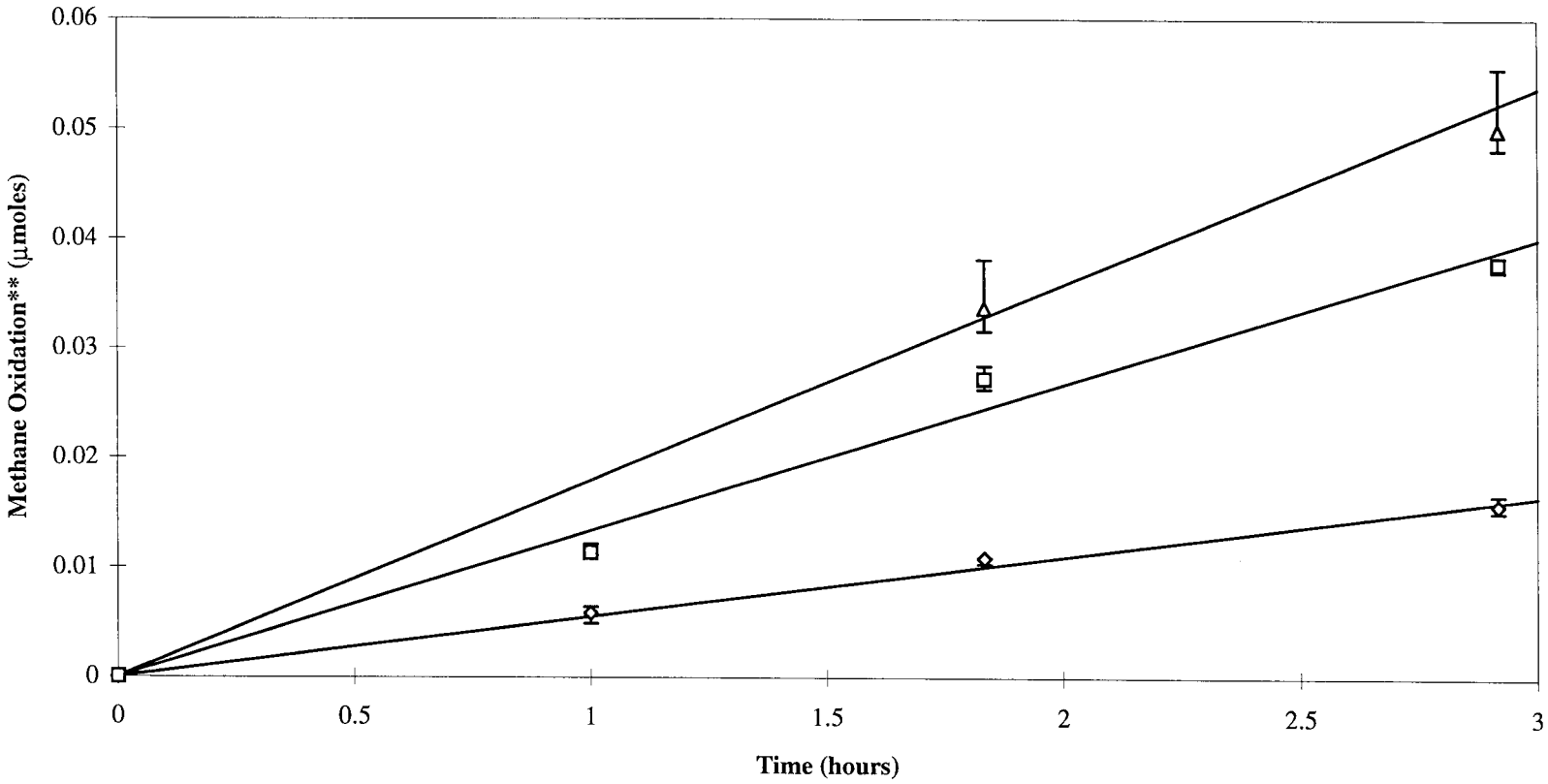

* Median, high and low values shown.

** Measured as non-volatile ^{14}C products.

Figure 4.16. Low Copper Experiment # 2: Methane Oxidation vs. Time for Initial Methane Concentrations of 7.3 and 51 μM; Growth Medium $[Copper]_{total}$=0.3μM*

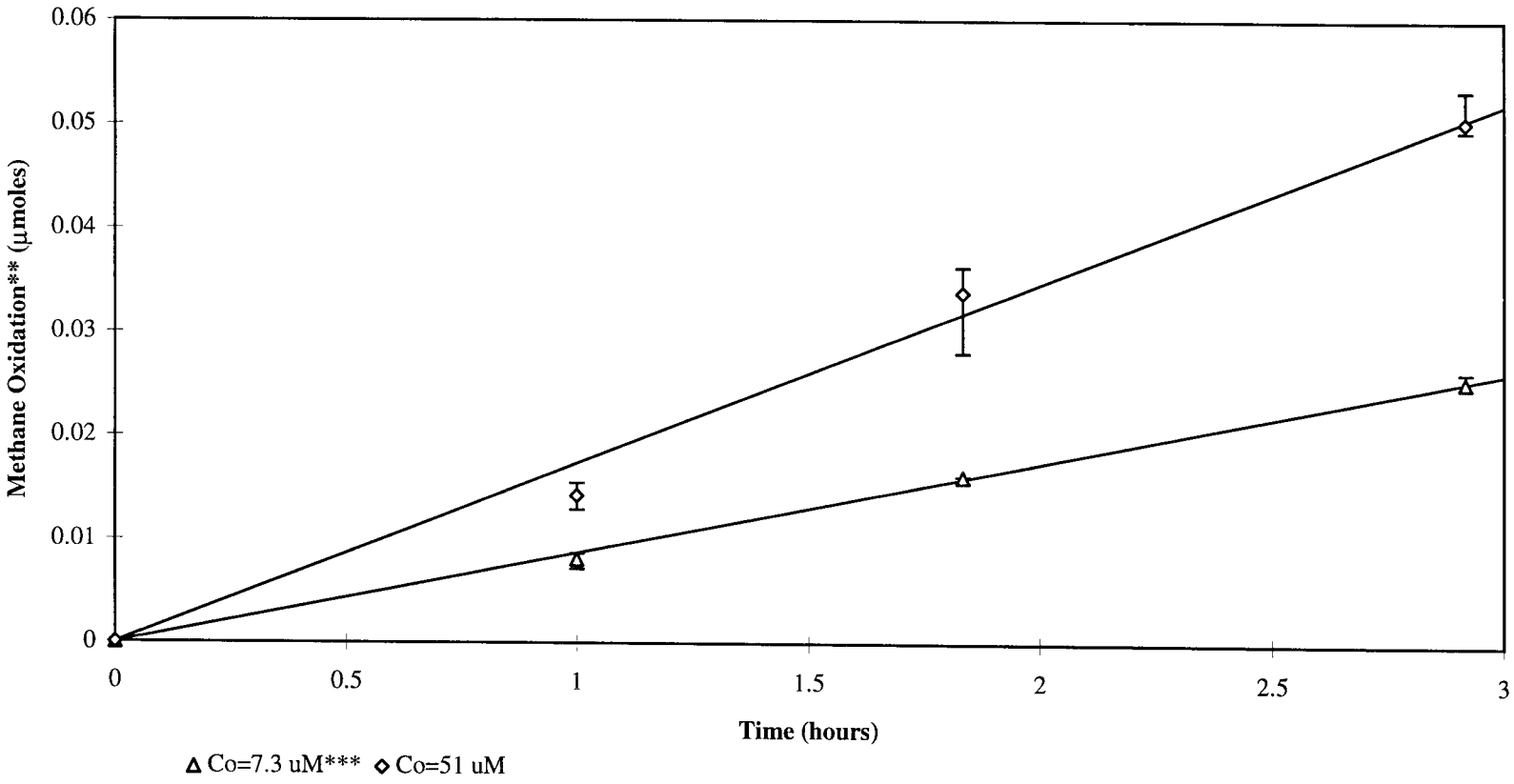

* Median, high and low values shown.

** Measured as non-volatile ^{14}C products.

*** Lowest One hour value was not included in the linear regression.

Figure 4.17. Low Copper Experiment # 2: Methane Oxidation vs. Time for Initial Methane Concentrations of 11 and 102 μM; Growth Medium $[Copper]_{total}$=0.3μM*

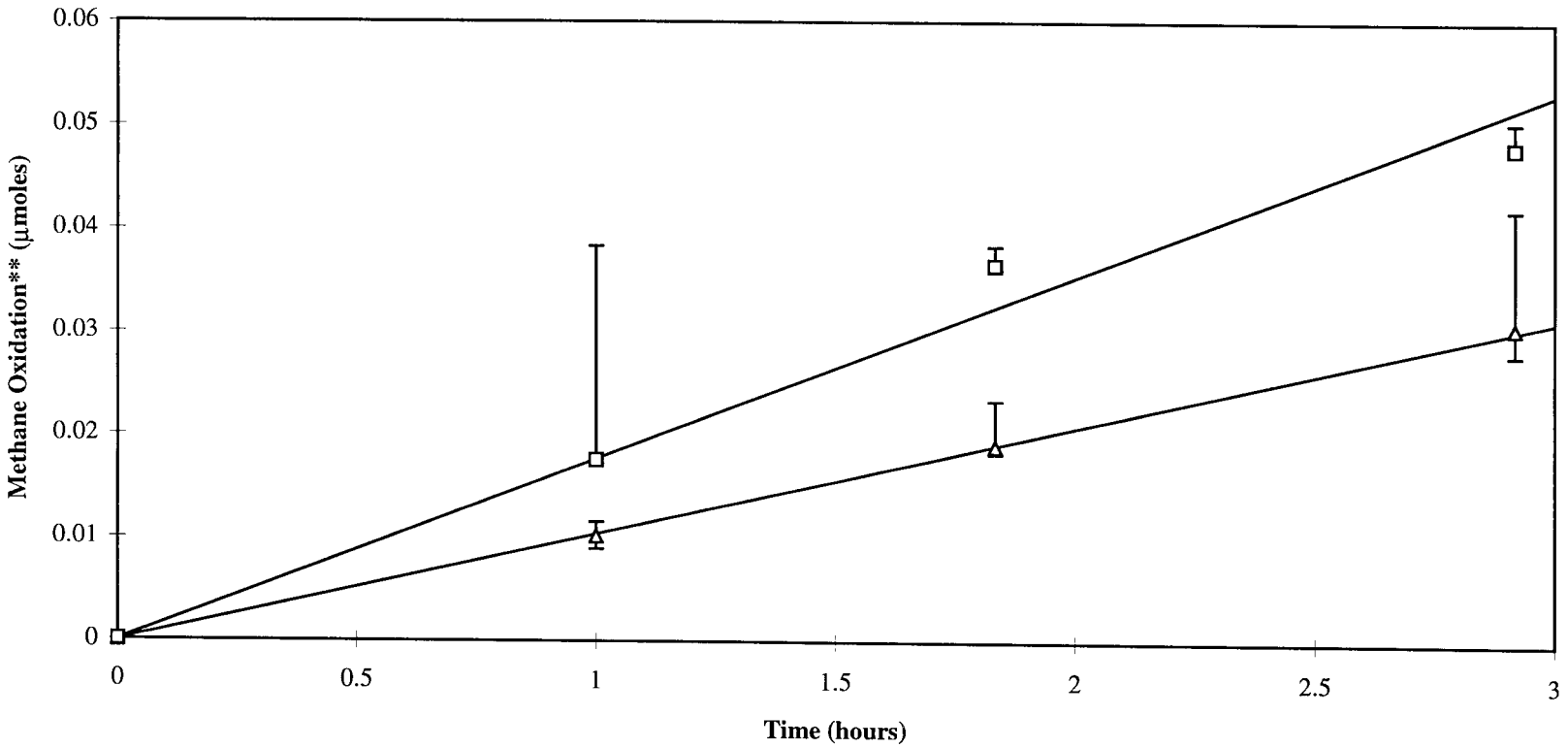

* Median, high and low values shown.

** Measured as non-volatile ^{14}C products.

*** Largest three hour value was not included in the linear regression.

**** Largest one hour value was not included in the linear regression.

Figure 4.18. Low Copper Experiment # 2: Michaelis-Menten Plot for Methane Consumption by *M. albus* BG8 Grown with No Added Copper ([Copper]$_{total}$=0.3μM])

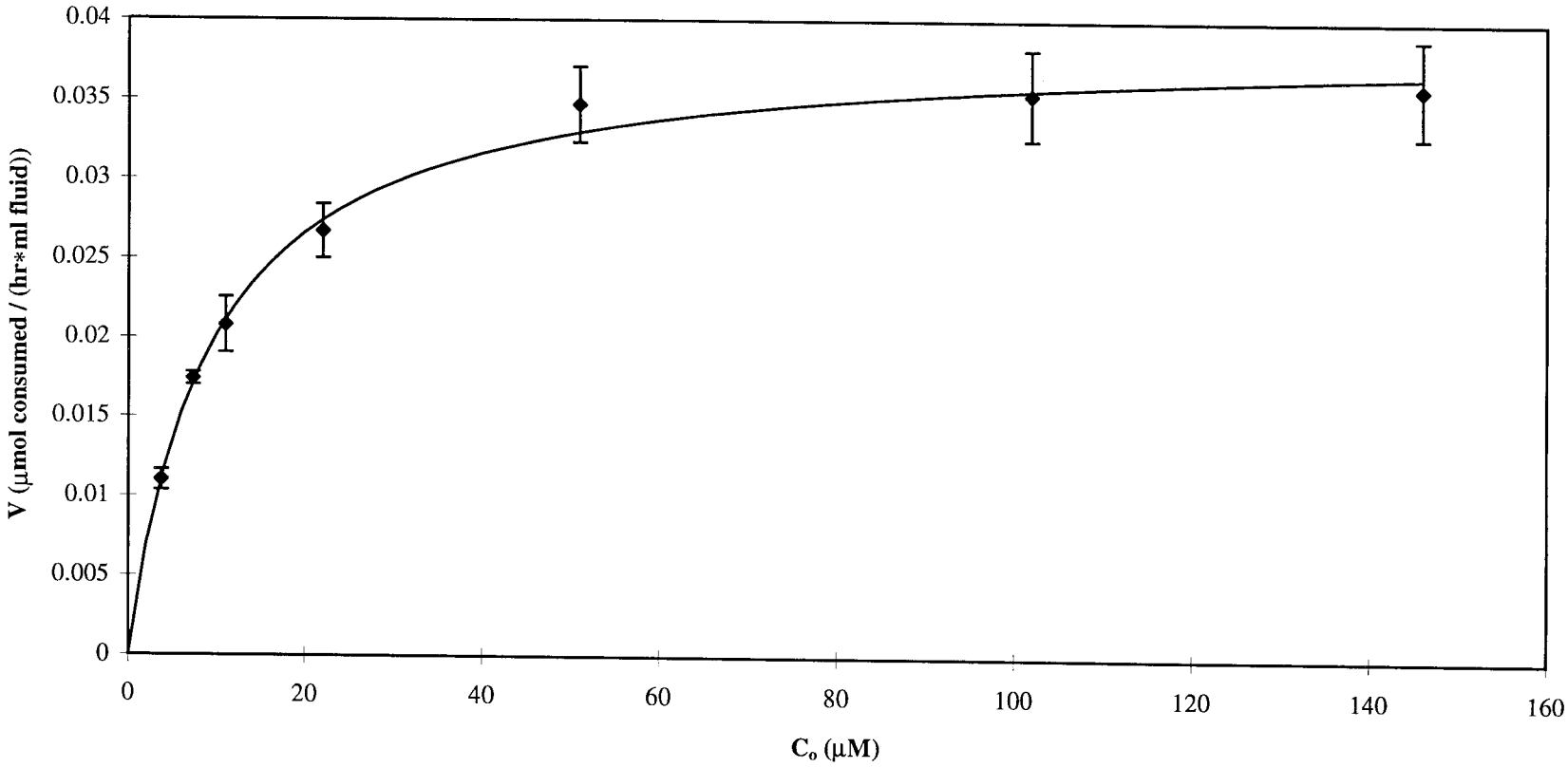

*V_{max}=0.038 μmol/(hr-ml fluid), V_{max}'=0.011 μmol/(hr-μg protein), K_s=9.3μM
95% confidence limits: 0.009 < V_{max}' (μmol/(hr-μg protein)) < 0.012 ; 7.5 < K_s (μM) < 11

4.6 References

Danckwerts, P.V. (1970). *Gas-Liquid Reactions*. New York: McGraw-Hill.

Duan, Z., Moller, N., Greenberg, J., & Weare, J.H. (1992). The prediction of methane solubility in natural waters to high ionic strength from 0 to 250 °C and from 0 to 1600 bar. *Geochimica et Cosmochimica Acta, 56,* 1451-1460.

Nguyen, H.T., Shiemke, A.K., Jacobs, S.J., Hales, B.J., Lidstrom, M.E., & Chan, S.I. (1994). The nature of the copper ions in the membranes containing the particulate methane monoxygenase from *Methylococcus capsulatus* (Bath). *Journal of Biological Chemistry, 269,* 14995-15005.

Rudd, W.M., Hamilton, R.D., & Campbell, N.E.R. (1974). Measurement of microbial oxidation o methane in lake water. *Limnology and Oceanography, 19,* 519-524.

Semrau, J.D. (1995). Kinetic, Biochemical, and Genetic Analysis of the Particulate Methane Monooxygenase. California Institute of Technology. Ph.D. Thesis.

Stanley, S.H., Prior, S.D., Leak, D.J., & Dalton, H. (1983). Copper stress underlies the fundamental change in intracellular location of methane monooxygenase in methane oxidizing organisms: studies in batch and continuous cultures. *Biotechnology Letters, 5,* 487-492.

Whittenbury, R., Phillips, K.C., & Wilkinson, J.F. (1970). Enrichment, isolation and some properties of methane-utilizing bacteria. *Journal of General Microbiology, 61,* 205-218.

Chapter 5

Reactor Design Part 3: Transport Parameter Determinations, Reactor Setup, and Comparison of Model Predictions to Reactor Data

5.1 Abstract

This chapter presents a method for directly evaluating a theoretical model's ability to predict transport of a substrate through an homogeneous porous media system coupled with substrate oxidation by bacteria attached to the porous media. Transport parameters, cell densities measured as protein concentrations, and kinetic parameters of cell growth for experiments were measured and used as inputs for the theoretical model presented in Chapter 2. Kinetic parameters of *Methylomicrobium albus* BG8 cells for methane utilization, presented in Chapter 4, were also used as model inputs. The value for V_{max}' was fit for each experiment and compared to results for this kinetic parameter presented in Chapter 4. The best-fit values for model predictions were 0.008, 0.01, 0.013, and 0.019 μmoles/hr/μg protein for four distinct column experiments, compared to values of 0.011, 0.02, and 0.03 μmoles/hr/μg protein presented in Chapter 4. A fifth column experiment had a lower value, 0.0055 μmoles/hr/μg protein. This experiment had additional anomalies associated with the cell density distribution: the distribution did not match the characteristics of the other four experiments. Two short-term (t_{final} << cell doubling time) and one long-term (t_{final} > cell doubling time) column experiments showed excellent agreement between predicted and measured methane concentrations. An additional long-term experiment showed excellent agreement for one time point and slight deviations between predicted and measured concentrations for two additional time points. The experiment with a low V_{max}' and anomalous cell distribution in the column had similar results for predicted and measured methane concentrations but the fit was not perfect.

5.2 Introduction

A column reactor representing a one-dimensional homogenous sandy aquifer was developed in order to test the predictive ability of the model presented in Chapter 2. *M. albus* BG8 cells, which were shown in Chapter 3 to attach strongly to washed Ottawa sand, were used as the representative methanotroph population in the column reactor. A pure methanotroph strain was used in the reactor in order to simplify the system and decrease the number of variables needed for the model simulation.

Transport parameters for column experiments were either directly evaluated, or calculated by empirical equations, as described in Section 5.3.2. Parameters for cell growth were measured as described in Section 5.3.3. Methane utilization kinetic parameters presented in Chapter 4 were used for model input parameters. Model simulations using these input parameters were then compared to experimental data.

5.3 Materials and Methods

5.3.1 Materials

Highest purity methane (>99.99%) was obtained from Matheson Gas Company. Regular purity oxygen (99.5%) was purchased from Air Liquide. Chemicals used for media preparation were all reagent grade. Cell growth media was prepared with distilled-deionized water (ddH_20). Two ml chromatography vials and red butyl rubber stoppers for these vials were obtained from Wheaton. A one meter long, 2.54 cm inner diameter chromatography column was obtained from Pharmacia. The California Institute of Technology Department of Chemistry glassblower made 10 sampling ports along the length of the column at distances approximately 3 inches

apart. Septa used for Shimadzu GC inlet ports were used for sealing the column ports. Tygon tubing was used to connect the media supply containing methane and oxygen to the peristaltic pump tubing.

5.3.2 Transport Parameter Determinations

The linear velocity for each column experiment was calculated as the fluid volumetric flow rate divided by the void volume per length of column (20 ml/dm). The fluid volumetric flow rate varied for each experiment and was determined by direct measurement.

The mass transfer coefficient, k_c, was determined using the following empirical equation (Wilson *et al.*, 1966):

$$j_D = \frac{1.09}{\varepsilon}(\mathrm{Re}')^{-\frac{2}{3}} \qquad (5\text{-}1)$$

where:

ε = column void fraction (-)

j_D = Chilton-Colburn j-factor (-)

Re' = Reynolds number in terms of the particle diameter, the superficial mass velocity of the fluid, G_o, (mass per unit time per unit cross section of the column without packing) and viscosity of the fluid (-)

This equation is coupled with the following definition of the j-factor (Welty *et al.*, 1984):

$$j_D = \frac{k_c}{U}(Sc)^{\frac{2}{3}} \qquad (5\text{-}2)$$

where:

Sc = Schmidt number ($\mu/(\rho * D_{AB})$)

where:

μ = fluid viscosity (mass/length/time)

ρ = fluid density (mass/length^3)

D_{AB} = diffusivity of component A in component B (length^2/time).

Combining these two equations, I find:

$$k_c = \frac{1.09U}{\varepsilon}\left(\mathrm{Re}' Sc\right)^{-\frac{2}{3}} \qquad (5\text{-}3)$$

This equation is valid for $0.0016 < \mathrm{Re}' < 55$, $950 < Sc < 70{,}600$ and $0.3 < \varepsilon < 0.5$.

The longitudinal dispersion coefficient was determined separately from the column experiments run with cells attached to sand. To calculate an approximate longitudinal dispersion coefficient, a salt tracer experiment was done. Sand was added to ddH_2O and then placed in the column in the same manner as was done for the methane consumption experiments described in Section 5.3.4. At t=0, nitrate mineral salts medium (NMS) was pumped through the column at a volumetric flow rate of 200 ml/hr (linear velocity = 10 dm/hr). The column effluent was collected in a Gilson fractionator. The conductivity, a measure of salt concentration, was assayed for each fraction using a VSI Model 35 conductance meter. The following equation was used to calculate the time at which the collection of a specific liquid fraction was complete:

$$t = \left(fraction\ number\right)\left(\frac{volume}{fraction}\right)\left(\frac{1}{liquid\ \ flow\ rate}\right) \qquad (5\text{-}4)$$

The longitudinal dispersion coefficient for this experiment was analyzed using non-linear regression of the solution to the PDE for a conservative tracer experiencing one-

dimensional flow and dispersion in porous media. The PDE, boundary conditions and initial condition are:

$$\frac{\partial K}{\partial t} = D_L \frac{\partial^2 K}{\partial x^2} - U \frac{\partial K}{\partial x} \tag{5-5}$$

$$K(x,0) = K_i \tag{5-6}$$

$$K(0,t) = K_o \tag{5-7}$$

$$\frac{\partial K}{\partial x}(\infty, t) = 0 \tag{5-8}$$

The solution to equation 5-5 with the boundary conditions given is:

$$K(x,t) = K_i + \frac{(K_o - K_i)}{2}\left(erfc\left(\frac{x - Ut}{\sqrt{4D_L t}}\right) + e^{\frac{Ux}{D_L}} erfc\left(\frac{x + Ut}{\sqrt{4D_L t}}\right)\right) \tag{5-9}$$

where:

K = measured conductivity

K_i = background conductivity of ddH_20

K_o = conductivity of the nitrate mineral salts solution

x = distance in column of the effluent exit (length)

U = fluid linear velocity (length/time)

t = time

D_L = longitudinal dispersion coefficient (length^2/time)

TableCurve 2D version 3 was used for the non-linear regression analysis.

5.3.3 Growth Kinetics: μ_{max} and $K_{S\text{-}Monod}$

The value for $K_{S_{Monod}}$ was assumed to be equal to the affinity coefficient *of M. albus* BG8 cells for methane oxidation. As described in Chapter 4, this affinity

coefficient, K_S, ranged from 6.5 to 9.3 μM. A value of 8 μM was used for all column experiment model predictions presented in this chapter.

The theoretical maximum specific growth rate, μ_{max}, was determined by growing *M. albus* BG8 cells in batch culture. Cells from plates containing NMS with 10 μM added copper were placed in 500 ml side-arm flasks with 100 ml sterile NMS media containing no added copper. The flasks were sealed and the headspace was filled with a 25% methane/75% air mixture. This amount of methane and air ensures that cells will be growing at their maximum specific growth rate. The cells were then grown at 30° C. A Klett colorimeter was used for determining cell density over time. This device uses a non-invasive light scattering technique for measuring cell density.

5.3.4 Medium Preparation and Column Setup

The column reactor setup is shown in Figure 5.14. An 8 liter glass aspirator bottle was used for the methane/NMS supply. Copper was not added to the NMS. Tygon tubing was attached to the aspirator bottle bottom outlet. A two-way valve was connected to this tubing. The valve was closed and the bottle was filled to approximately 6 liters with NMS media. A vacuum was applied to the bottle until the pressure decreased to 0.17 atm. Oxygen was added to the bottle until the pressure was approximately 1 atm. A vacuum was again applied to obtain a bottle pressure of 0.83 atm. Methane was added to the bottle to obtain a final pressure of approximately 1 atm. The liquid was mixed for a minimum of four hours to allow methane and oxygen to equilibrate between the gas and liquid phases.

While methane and oxygen equilibrated in the supply bottle, *M. albus* BG8 cells grown overnight in NMS media containing no additional copper were added to washed Ottawa sand. The cells were allowed to attach for one-half hour. NMS media containing no added copper was placed in the Pharmacia column. After one-half hour of cell attachment, two void volumes of NMS media was filtered through the sand and cells to remove unattached cells. The sand/cell mixture was then added to the Pharmacia column via the column outlet end and allowed to settle, i.e., the sand first filled the area closest to the column inlet and then filled the column through to the outlet end. No air bubbles were present in the system. After the column was filled with sand, the column was tapped with a metal object to settle the sand. After complete packing occurred, the Pharmacia outlet was placed on top of the sand.

While the cells were allowed to attach to sand, the medium/methane/oxygen supply bottle was connected to two intermediary bottles (one 1 liter and one 1/2 liter aspirator bottle) via Tygon tubing and the medium was allowed to fill these bottles. Caution was taken to prevent turbulent flow through these bottles because this would cause methane and oxygen loss at the outlet. A minimum of 500 ml liquid was discarded from the tubing connected to the bottom outlet of the last aspirator bottle. This was done to ensure that any loss of methane caused by the procedure would not affect the column methane supply.

A two-way valve was placed at the end of the tubing for outlet flow from the 1 liter aspirator bottle. This allowed for closing off the liquid supply. The free end of the valve was connected to a 14 gauge needle. This needle was connected to size 13 peristaltic tubing contained in a Cole-Parmer peristaltic pump. The free end of this

tubing was connected to another 13 gauge needle which was connected to a three-way valve. One outlet of this valve served as a fluid ejection point. The other opening was connected via Tygon tubing to a three-way valve which was connected to the Pharmacia column inlet. This three-way valve served as a sampling port for the column inlet concentration (defined as port 0). A Shimadzu GC septum fit snugly into one of the valve openings. This allowed direct analysis of the inlet liquid by syringe.

A minimum of 50 ml liquid was allowed to exit the ejection port prior to the column entrance. The valve was then turned to begin supplying NMS media containing oxygen and methane to the column. The maximum time taken between adding cells to sand and commencing column flow was one hour. After commencing column flow the outlet fluid was collected to determine the flow rate. The outlet samples were also used to ascertain cell detachment from sand in the column. The liquid was placed in a Neubauer cell counting chamber for this purpose. The cell detection limit is 4×10^5 cells/ml.

5.3.5 Column Sampling Procedure: Methane Analysis

In order to analyze methane concentrations for column experiments, I developed methods for sampling liquid in the column. Liquid phase methane concentrations were measured down to 5 μM methane by sampling 1 μl liquid directly from sampling ports along the length of the column. The maximum quantity of sample liquid that could be injected into the GC column was approximately 1 μl. Therefore, in order to lower the limit of detection, I developed a procedure for analyzing liquid samples indirectly. Five ml liquid samples were collected from sampling ports via

syringe. The liquid was obtained by closing the column outlet valve and allowing fluid to enter the syringe, i.e., the port of collection became the column outlet for the duration of filling a syringe. This took approximately two minutes. The last collected ml was ejected from the syringe as waste. One ml fluid was then placed into each of three 2 ml chromatography vials. Immediately after placing fluid into a chromatography vial, the vial was sealed with a butyl rubber stopper. These vials were vigorously shaken to speed the process of methane transport from the liquid phase to the headspace. One hundred µl headspace was then injected into an Hach-Carle GC using a gastight A-2 Dynatech syringe. This syringe sampling procedure was used for each sampling port which had a GC reading less than 100 (GC Range set to 10) for the 1 µl liquid samples.

A control experiment was done to ascertain the time needed for equilibrating methane between the gas and liquid phases in the 2 ml chromatography vials, and to determine the method's accuracy for calculating the column liquid methane concentration. This control also served to test methane loss from the column.

The experiment was performed in the following manner. Liquid containing methane (approximately 10 - 500 µM methane) was pumped through a sand-packed column without cells at flow rates ranging from 100 to 350 ml/hour (approximately .5 - 2 void volumes per hour). One µl liquid samples from different ports were analyzed by GC to determine the liquid methane concentration.

Following this step, 5 ml liquid was collected from column ports via syringe by the method described above. One µl liquid samples from the syringe were analyzed by GC to check if any methane leakage occurred during sample collection. One set of

three 2 ml chromatography vials containing 1 ml liquid from this syringe was made. Additional sets of three chromatography vials containing liquid and methane from the column were collected via syringe. Each set of three chromatography vials was analyzed for methane at one distinct time point. The time points ranged from t=0 to t=2 days from the time of sample collection. Samples were analyzed by injecting 100 µl headspace into the GC.

GC readings for samples assayed at different times were compared to one another to determine the length of time needed for methane equilibration between the gas and liquid phases and to test methane leakage from the vials. The GC readings were also converted to concentration of methane present in liquid before methane equilibrated between the gas and liquid phases. This calculated methane concentration was compared to the concentration found for the 1 µl liquid samples taken directly from sampling ports to ascertain this method's reliability for calculating methane concentrations. The methane concentrations found for different sampling ports in a single experiment were compared to one another to determine if methane leaked significantly through column ports.

5.3.6 Column Sampling Procedure: Cell Density Analysis

After completing the liquid methane analysis for a column experiment, flow to the column was halted. The top and bottom of the column were dismantled. Sand from the column was divided into fractions representing sections between sampling ports. These sand fractions were assayed for total protein, a representation of total cell numbers. Four 5 g sand samples containing approximately 4.1 g sand and 0.9 g

media were made for each sand fraction. Two percent sodium dodecyl sulfate (SDS) was added to each sample to obtain a final liquid concentration of one percent SDS. This was done to digest cells and solubilize membrane-associated proteins. The reaction was allowed to continue for a minimum of one hour to ensure complete protein solubilization. Protein concentrations were assayed twice for each sample using The BioRad DC ® protein assay. A standard curve was made with bovine serum albumin containing the same percent SDS in each standard to convert data for the samples to actual protein concentrations.

5.3.7 Model Simulation Procedure

The measured values for column length, affinity coefficient for methane, maximum specific growth rate, specific maintenance rate, longitudinal dispersion coefficient, linear velocity, mass transfer coefficient, and sand surface area per unit volume fluid were input to the model. In addition, the inlet methane concentration was input using the assumption that the change in the measured inlet concentration over time was linear. This was done because there were slight changes in the inlet methane concentrations. The following equation was used:

$$C(0,t) = C_o + \text{slope}*t \qquad (5\text{-}10)$$

where:

$C(0,t)$ = methane concentration at x=0 at time t (mass/length^3)

C_o = methane concentration at x=0 at time t=0 (mass/length^3)

slope = change in inlet methane concentration with respect to time (mass/length^3/time)

t = time

C_o and slope were determined by fitting a line to the measured methane concentrations at x=0 for two distinct time points. However, methane was analyzed only at one time point for the short term column experiments. Therefore, the average of the slopes found for the long term column experiments was used as the slope for the short term experiments.

The protein concentrations used as inputs for model simulations were evaluated by estimating initial concentrations which would match the measured final concentration at t_{final}, the end of an experiment. Input protein concentrations for the model were appropriately modified to obtain a protein concentration at t_{final} within the 95% confidence limits of the analyzed protein concentrations. After determining protein concentrations for model inputs the value for V_{max}' was fit to the data. A fit was done for this parameter because the data in Chapter 4 show that this parameter varies by a factor of three for cells grown under similar conditions.

5.4 Results and Discussion

5.4.1 Longitudinal Dispersion Coefficient

Results for the experiment done to determine D_L are shown in Figure 5.1. Non-linear regression analysis produced a best-fit value for D_L of 0.12 dm^2/hr with 95% confidence limits of 0.1 dm^2/hr $< D_L <$ 0.14 dm^2/hr. This was determined only for a flow rate of 200 ml/hr (10 dm/hr). The column experiments were done at volumetric flow rates ranging from 170 ml/hr to 250 ml/hr. Therefore, the estimated value for D_L may not be within the 95% confidence limit listed above for each

experiment. However, the sensitivity analysis for the longitudinal dispersion coefficient presented in Chapter 6 shows that this coefficient does not have a significant effect on the model predictions for the range of flow rates and bacterial densities in column experiments presented in this thesis. Therefore, the estimated value of D_L for a flow rate of 200 ml/hr is used as the longitudinal dispersion coefficient for all experiments.

5.4.2 Maintenance Energy

The specific maintenance rate was not directly evaluated for *M. albus* BG8 cells. Literature data for chemostat-grown methanotrophs were used to estimate this parameter. Drozd *et al.* (1978) reported a maintenance energy coefficient of 1.2 mmol methane/gram cell/hr and a yield coefficient of 13 gram cell/mol methane for *Methylococcus* sp. (NCIB 11083). This gives a calculated specific maintenance rate of 0.016/hr. Sheehan and Johnson (1971) published data on yields and growth rates of a mixed methane oxidizing culture grown in a chemostat. The slope for the plot of 1/yield vs. 1/dilution rate gives an estimate of the maintenance energy. The intercept is the theoretical maximum yield (Pirt, 1965). Using this analysis for methane limited cultures from the Sheehan and Johnson data, I calculated a maintenance energy coefficient of 2.2 ± 7.3 mmol methane/gram cell/hr. The yield coefficient was calculated to be 11 ± 4 gram cell/mol methane. This equates to a specific maintenance rate of 0.024/hr. Nagai *et al.* (1973) published a value for the maintenance energy coefficient of 1.9 mmol methane/gram cell/hr for a methane grown psuedomonad that was an obligate methylotroph. The yield coefficient was 16 gram cell/mol methane.

This gives a specific maintenance rate of 0.03/hr. Based on these data, the specific maintenance rate used for model simulations was 0.02/hr. This value is typical for bacteria growing on one-carbon compounds (Rokem *et al.*, 1978; Heijnen *et al.*, 1981).

5.4.3 Maximum Specific Growth Rate: μ_{max}

Results for determining the maximum specific growth rate for *M. albus* BG8 cells grown at 30° C are shown in Figure 5.2. The Klett readings (a measure of cell density) are plotted against time for three different samples. This is a semi-log plot. The linear region of each sample represents Klett readings for cells during their exponential growth phase. This is the region used for calculating μ_{max}. Data points used for the linear regression analysis have linear regression results plotted through them. The equation used for calculating μ_{max} follows (Pirt, 1975):

$$\mu_{max_{app}} = \mu_{max} - a \qquad (5\text{-}11)$$

where:

$\mu_{max_{app}}$ = the apparent maximum specific growth rate (1/time)

μ_{max} = the maximum specific growth rate assuming maintenance energy requirements = 0 (1/time)

a = specific maintenance rate (1/time)

The $\mu_{max_{app}}$ values calculated by linear regression of the data in Figure 5.2 are 0.077/hr, 0.063/hr and 0.053/hr, corresponding to doubling times of 9, 11 and 13 hours, respectively. Incorporating the specific maintenance rate above, 0.02/hr, into equation 5-11 yields μ_{max} values of 0.097/hr, 0.083/hr, and 0.073/hr. A statistical

analysis was not performed on these data because it would be inappropriate: the maximum growth rate of cells may change due to slight variations in the growth media. The μ_{max} value used for all model simulations was 0.08/hr.

5.4.4 Controls: Methane Leakage, Sampling Assays

Control experiments for testing the column sampling procedure were done a total of five times at five different input methane concentrations. The concentrations ranged from approximately 10 to 500 μM methane. This range was chosen because it includes the entire concentration range used in column experiments and detectable by the 1 μl liquid sampling assay. Results are shown in Figures 5.3 through 5.7.

The first control, shown in Figure 5.3, was done at an inlet methane concentration of approximately 500 μM methane. The inlet flow was 350 ml/hr. Both the inlet methane concentration and flow rate were at least twice the values used for most column experiments done with bacteria. The methane concentrations analyzed at ports 0, 5, and 7 show no significant decrease throughout the column; thus it appears that methane does not escape from the column by leakage through sampling ports.

The data for headspace samples of chromatography vials containing 1 ml liquid from the column collected via a 5 ml syringe depict another point. The vials sampled at two hours give the same results as the vials sampled at 20 hours. There is no significant difference in methane concentrations between samples assayed at different times. This suggests two things. First, the methane is in equilibrium between the gas

and liquid phases within 2 hours and second, methane does not leak significantly from the vials over a 20 hour period.

One additional point is noteworthy in this experiment. The average calculated methane concentration in the vials prior to methane equilibration between the gas and liquid phases is 13% less than the methane concentration in liquid in the column. This suggests that methane is lost somewhere between filling the 5 ml syringe with liquid from the column and sealing the vials containing 1 ml liquid from the syringe.

In order to identify where methane loss occurred, a second experiment was done. The first experiment was repeated with the following change: after filling a 5 ml syringe, 1 µl syringe liquid was assayed for the methane concentration. This procedure allowed me to determine whether methane was leaking from the syringe as the syringe filled with liquid. The results for this experiment are shown in Figure 5.4.

In addition to adding a new sampling procedure, I changed the inlet methane concentration and flow rate to begin to cover a range of concentrations and flow rates. The inlet methane concentration was approximately 200 µM, with a flow rate of 200 ml/hr. These are typical values for column experiments done with bacteria.

Again, there was no apparent methane loss throughout the column, as evidenced by the similar methane concentrations found for ports 0, 3, and 8. Liquid from the 5 ml syringe was directly assayed at ports 3 and 8. The concentrations found overlapped the data for direct column liquid measurements. This suggests that methane loss is not occurring while the syringe fills with liquid. However, an interesting result was found. In this experiment, there was a 4% increase in the calculated liquid methane concentration for vials compared to direct liquid

measurements. This increase was not statistically significant. Based on this result, I could not make any conclusions about which step brought about methane losses. In addition, the result suggested that a certain amount of random sampling error occurs in the sampling process.

Two conclusions I draw from this experiment are that the 2 ml vials do not have significant methane loss up to 41 hours, and that vigorously shaking these vials causes complete methane equilibration. I base these conclusions on the data for the calculated methane concentrations for vials sampled at 0, 20, and 41 hours after sample preparation. The concentrations fell within the same range for all time points.

The next three control experiments, shown in Figures 5.5 through 5.7, are similar to the previous one. The main differences are inlet methane concentrations and flow rates. I repeated this experiment three more times in order to determine whether I would obtain the same result for the entire range of methane concentrations detectable by direct liquid measurement. The inlet methane concentrations for the three experiments were approximately 45, 10, and 7 μM methane. The flow rates for each concentration were 230, 150, and 130 ml/hr, respectively. In each of these experiments I found a decrease in calculated methane concentrations for the vial samples compared to direct liquid measurements. The decrease ranged from 7% to 24%. However, direct measurement of syringe liquid gave the same result as direct measurement of column liquid for all three experiments, suggesting that methane loss occurred between ejecting 1 ml liquid into 2 ml vials and sealing the vials.

Based on all these results I concluded that the syringe sampling procedure was acceptable for obtaining methane concentrations below the detection limit for direct

liquid analysis. The procedure allowed me to detect methane down to approximately 0.5 μM methane. However, whenever I used this procedure for methane analysis, I made a conservative assumption that the calculated methane concentration could be off by up to 50%.

5.4.5 Comparison of Reactor Data to Model Predictions

Five column experiments were done. The results are presented in Figures 5.8 through 5.12. Tables 5.1 through 5.6 show the model parameters used for simulations of the column experiments. Tables 5.2 through 5.6 show the results for protein assays done on sand fractions for each column experiment. The first two experiments shown were done over time periods less than two hours. Methane concentrations throughout the column were analyzed at only one time point. In the following three experiments fluid was pumped through the column for up to fifteen hours, and methane concentrations were analyzed two or three distinct times during the duration of the experiment.

5.4.5.1 Short Term Column Experiments, Limited Growth

The first two experiments were done to ascertain the pattern of cell attachment in the column when flow commenced. In order to determine this initial distribution pattern, I ran these experiments for less than two hours. Results for the protein determinations at t_{final} are shown in Tables 5.2 and 5.3. For the experiment shown in Figure 5.8, the protein concentrations ranged from 48 ± 8 μg protein/ml fluid at the column inlet increasing up to 66 ± 16 μg protein/ml fluid at the column outlet (corresponding to approximately 3.1×10^8 cells attached/ml void volume near the inlet

and 4.3×10^8 cells attached/ml void volume near the column outlet based on a single *E. Coli* cell containing 1.5×10^{-13} g protein (Neidhardt *et al.*, 1990)). The sand added to the column contained 70 μg protein/ml void volume.

The decrease in cell density in the column vs. the amount of cells present in sand added to the column suggests that cells are detaching from the sand as it is added to the column and/or during the experiment. The latter assumption is negated by the results for cell concentrations in the column effluent. I never detected cells in this fluid. The detection limit was 4×10^5 cells/ml. The former assumption of cell detachment as sand is added to the column is supported by observations I made during the addition of sand to the column. I was able see a change in the clarity of the liquid above settled sand as I added sand to the column. My assumption is that as I added sand, some cells detached and resided in the liquid above the sand. As I added additional sand to the column, the cells which had detached earlier attached to sand added at a later time. This would account for the increase in cell density with distance in the column.

Results for the model simulation, shown in Figure 5.8, show good agreement with data obtained for methane concentrations throughout the column during the experiment. The simulation value used for V_{max}' was 0.01 μmoles methane consumed/hr/μg protein. This value is near the range of V_{max}' values found in Chapter 4: $0.012 < V_{max}' < 0.03$ μmoles/hr/μg protein.

Results for the second short duration column experiment are comparable to the first experiment. NMS/methane flow to the reactor proceeded for 1 hour, at which time the flow was stopped and sand fractions were collected for cell attachment

analyses. Again, protein concentrations increased from the column inlet to the column outlet. The increase was much greater in this experiment: the cell density near the column outlet, 30 ± 16 μg/ml, was three times the cell density near the column inlet, 11 ± 26 μg/ml. The uncertainty for these samples was also higher. The sand added to the column had a cell density of 25 ± 20 μg/ml. The column methane analysis and model prediction results, shown in Figure 5.9, have excellent agreement. The V_{max}' value used for the model simulation was 0.019 μmoles consumed/hr/μg protein. This value is within the range of values determined for *M. albus* BG8 cells.

5.4.5.2 Column Experiments Run for Times on the Order of Maximum Cell Doubling Times

The maximum cell doubling time used for model simulation inputs was 12 hours. Three column experiments were done for periods on the order of 10 hours. The first experiment, shown in Figure 5.10, had good agreement between measured and predicted methane concentrations. The parameters used for the simulation are shown in Tables 5.1 and 5.4. The best-fit value for V_{max}' was 0.008 μmoles methane/hour/μg protein. This is slightly below the range for the three values reported in Chapter 4. Table 5.4 summarizes the protein concentrations used as model inputs, the concentrations output by the model at t_{final}, and the assayed protein concentrations measured at the end of the experiment (t_{final}). The protein concentrations for sand from port 6 to the column outlet were not assayed because the measured methane concentrations were negligible in this portion of the column. The protein concentrations used as model inputs followed the trend seen with the short term

column experiments: protein concentrations increasing from nearest the inlet up to the column outlet. This increase for the portion of the column where protein concentrations were assayed was 30 μg/ml up to 75 μg/ml. The model protein concentrations at t_{final} were within 1.5 standard deviations of the measured protein concentrations.

The next column experiment, shown in Figure 5.11, had slightly different results. The model inputs for the simulation are shown in Tables 5.1 and 5.5. The best-fit value for V_{max}' was 0.0055 μmoles/hr/μg protein, one-half the minimum value presented in Chapter 4 for *M. albus* BG8 cells.

The model predictions for protein concentrations at t_{final} are all within one standard deviation of the assayed concentrations. However, the only way to obtain these values was to use input concentrations which increased and then decreased with distance. The inputs began at 25 μg/ml, rose to 45 μg/ml half-way up the column and decreased back to 25 μg/ml at the column outlet. This is contrary to the results obtained for the two short term experiments and the first long term experiment where I found that protein concentrations only increased with increasing distance. Model simulations for methane concentrations, shown in Figure 5.11, follow the general trends for the measured data. However, as with the protein concentration analyses, there are obvious deviations. At t = 4 hours, data are below model predictions for two points in the column. At t = 14 hours, data are above model predictions for two points in the column.

Methane concentrations were analyzed at three distinct time points for the final experiment, shown in Figure 5.12. The model inputs for the simulation are shown in

Tables 5.1 and 5.6. The best-fit value for V_{max}' was 0.013 μmoles/hr/μg protein, which is within the range of values presented in Chapter 4.

The model predictions for protein concentrations at t_{final}, shown in Table 5.6, are all within one standard deviation of the assayed concentrations. The input values for initial protein concentrations used for simulations increase with increasing distance in the column, as described for the short term column experiments and the first long term column experiment. The simulation inputs began at 20 μg/ml from port 0 to port 1 and rose to 45 μg/ml near the column outlet.

Model simulations correctly predict most of the measured data. At t = 1 hour, the simulation curve falls directly on all measured methane concentrations. At t = 8 hours, the simulation deviates from the data near the column inlet. This is also the case at t = 15 hours. However, I believe these deviations are not significant given the complex nature of the system. The model is correctly predicting the methane utilization rates as well as the increased methane oxidation by cells due to growth over time. It is possible that the deviations are due to errors in the input parameters for the maximum specific growth rate coupled with errors in the initial cell densities.

An important point to note for all model simulations for the column experiments is that the inclusion of mass transfer resistance between the bulk fluid and particle surfaces created minimal differences in methane oxidation that would have occurred if the model had not included this mass transfer resistance. This is shown in Figure 5.13. This figure is the same as Figure 5.12 with the addition of model simulations excluding mass transfer resistance from the bulk fluid to particle surfaces. These added simulations deviate from the predictions for the model including mass

transfer resistances only as the methane concentration approaches the affinity coefficient, K_S, of *M. albus* BG8 cells for methane. This phenomenon is addressed in more detail in Chapter 6.

5.5 Conclusions

The column reactor used for testing the predictive model was found to have no measurable methane loss from column sampling ports. The sampling procedure developed to lower the methane detection limit was acceptable for detecting methane down to approximately 0.5 μM methane.

Based on the two experiments done for short time periods, I concluded that cell densities in the column increased with increasing distance from the column inlet. I believe this was caused by the method of sand/cell addition to the column reactor. The protein concentrations used for model inputs at t = 0 display this characteristic for all experiments that had V_{max}' values consistent with those found in Chapter 4.

Overall, the theoretical model is correctly predicting methane utilization rates. The model predictions follow not only the methane oxidation at initial time points but also the characteristic increase of methane oxidation over time, presumably caused by cell growth. There are some deviations from predicted and measured methane concentrations. This is to be expected due to the complex nature of a biological system. It is possible that some bacteria were detaching from the sand and reattaching at points further down the column. However, this was not a measurable phenomena; bacteria were not detected in the column effluent above the detection limit of 4×10^5 cells/ml (corresponding to approximately 0.06 μg protein/ml). Based on the results

presented in Chapter 3 for *M. albus* BG8 attachment to sand, I did not expect cell detachment to occur. This possibility cannot be disproved, but is beyond the scope of this work. In addition, bacteria in natural systems will be less likely than laboratory strains to detach from solid surfaces due to the presence of cell capsules which are lost in laboratory-grown cultures.

The results presented in this chapter support the hypothesis that the model presented in Chapter 2 can correctly predict substrate transport coupled with both substrate oxidation by bacteria and bacterial growth. The model can be used to gain insight to the length of time needed for inducing growth of naturally occurring methanotroph populations to levels that will provide measurable oxidation of contaminants such as trichloroethylene. In addition, the model can be used to ascertain the importance of including the mass transfer resistance for substrate transport from the bulk liquid to particle surfaces. This is described more fully in Chapter 6.

Table 5.1. Model Parameters for Figures 5.8 through 5.12

Parameter	Figure 5.8	Figure 5.9	Figure 5.10	Figure 5.11	Figure 5.12	Value Basis
C_o at t=0 (μM)	225	230	140	115	132	M
Change in Inlet Concentration (μM/hr)	-1	-1	1	-1	-1.5	M
Column Length (dm)	6	6	8.6	8.6	8.6	M
V_{max}' (μmol/hr/μg protein)	0.01	0.019	0.008	0.0055	0.013	F-M*
K_s (mM)	8	8	8	8	8	M**
μ_{max} (1/hr)	0.08	0.08	0.08	0.08	0.08	M
Specific Maintenance Rate: a (1/hr)	0.02	0.02	0.02	0.02	0.02	L^1
Velocity (dm/hr)	7.8	10	13	7.6	13	M
D_L (dm^2/hr)	0.12	0.12	0.12	0.12	0.12	M
Mass Transfer Coefficient: k_c (dm/hr)	1.3	1.4	1.5	1.3	1.5	C
Cell Surface Area per Mass of Cells: α (dm^2/μg protein)	0.001	0.001	0.001	0.001	0.001	L^2
Δx (dm)	0.02	0.02	0.02	0.02	0.02	D
Δt (hr)	0.001	0.001	0.001	0.001	0.001	D

M=Measured
F-M=fitted within the range of measured values
L^1=literature value (Drozd *et al*., 1978)
L^2=literature value (Neidhardt *et al*., 1990)
C=calculated using an empirical equation
D=defined
* See Chapter 4: the range of values was 0.011 - 0.03 μmol/hr/μg protein
** See Chapter 4: the range of values was 6.5 - 9.3 μM

Table 5.2. Cell Density in the Column Reactor Measured as Protein Concentration: Assayed Concentrations and Model Inputs for Figure 5.8

Column Sampling Port	Model Protein Concentration at t=0 (μg/ml)	Model Pro. Conc. at End of Expt. t=1 hour (μg/ml)	Assayed Protein Concentration (Average of 8 Samples) (μg/ml)	Standard Deviation of Assayed Protein Concentration (μg/ml)
0-1	45	48	48	4
1-2	45	48	49	3.6
2-3	45	47	41	4.7
3-4	60	62	63	8.3
4-5	65	66	66	8.9
5-6	65	65	67	8.8
6-7	65	65	66	8.2
7-8	65	65	ND	ND

ND - Not Determined

Table 5.3. Cell Density in the Column Reactor Measured as Protein Concentration: Assayed Concentrations and Model Inputs for Figure 5.9

Column Sampling Port	Model Protein Concentration at t=0 (μg/ml)	Model Pro. Conc. at End of Expt. t=1 hour (μg/ml)	Assayed Protein Concentration (Average of 8 Samples) (μg/ml)	Standard Deviation of Assayed Protein Concentration (μg/ml)
0-1	10	11	11	13
1-2	15	16	15	9
2-3	15	16	17	9
3-4	15	16	15	4
4-5	20	21	20	5
5-6	30	31	30	12
6-7	30	31	30	8
7-8	30	30	ND	ND

ND - Not Determined

Table 5.4. Cell Density in the Column Reactor Measured as Protein Concentration: Assayed Concentrations and Model Inputs for Figure 5.10

Column Sampling Port	Model Protein Concentration at t=0 (μg/ml)	Model Pro. Conc. at End of Expt. t=9 hour (μg/ml)	Assayed Protein Concentration (Average of 8 Samples) (μg/ml)	Standard Deviation of Assayed Protein Concentration (μg/ml)
0-1	30	49	53	8
1-2	30	48	42	11
2-3	30	48	36	9
3-4	55	85	79	41
4-5	65	91	74	13
5-6	75	83	108	55
6-7	75	75	ND	ND
7-8	85	85	ND	ND
8-9	85	85	ND	ND
9-10	85	85	ND	ND

ND - Not Determined

Table 5.5. Cell Density in the Column Reactor Measured as Protein Concentration: Assayed Concentrations and Model Inputs for Figure 5.11

Column Sampling Port	Model Protein Concentration at t=0 (μg/ml)	Model Pro. Conc. at End of Expt. t=14 hour (μg/ml)	Assayed Protein Concentration (Average of 8 Samples) (μg/ml)	Standard Deviation of Assayed Protein Concentration (μg/ml)
0-1	25	52	53	7.6
1-2	25	50	53	11
2-3	25	48	53	13
3-4	30	50	52	9.5
4-5	38	51	56	13
5-6	45	50	60	13
6-7	35	36	35	4.2
7-8	25	25	25	11
8-9	25	25	16	4.6
9-10	25	25	25	2.5

Table 5.6. Cell Density in the Column Reactor Measured as Protein Concentration: Assayed Concentrations and Model Inputs for Figure 5.12

Column Sampling Port	Model Protein Concentration at t=0 (μg/ml)	Model Pro. Conc. at End of Expt. t=14 hour (μg/ml)	Assayed Protein Concentration (Average of 8 Samples) (μg/ml)	Standard Deviation of Assayed Protein Concentration (μg/ml)
0-1	20	44	37	7.6
1-2	20	42	36	11
2-3	30	56	62	13
3-4	40	55	61	9.5
4-5	40	45	58	13
5-6	40	40	38	13
6-7	40	40	41	4.2
7-8	45	45	36	11
8-9	45	45	ND	ND
9-10	45	45	ND	ND

ND - Not Determined

Figure 5.1. Conductivity of Fluid Exiting Column vs. Time, Linear Velocity = 10 dm/hr

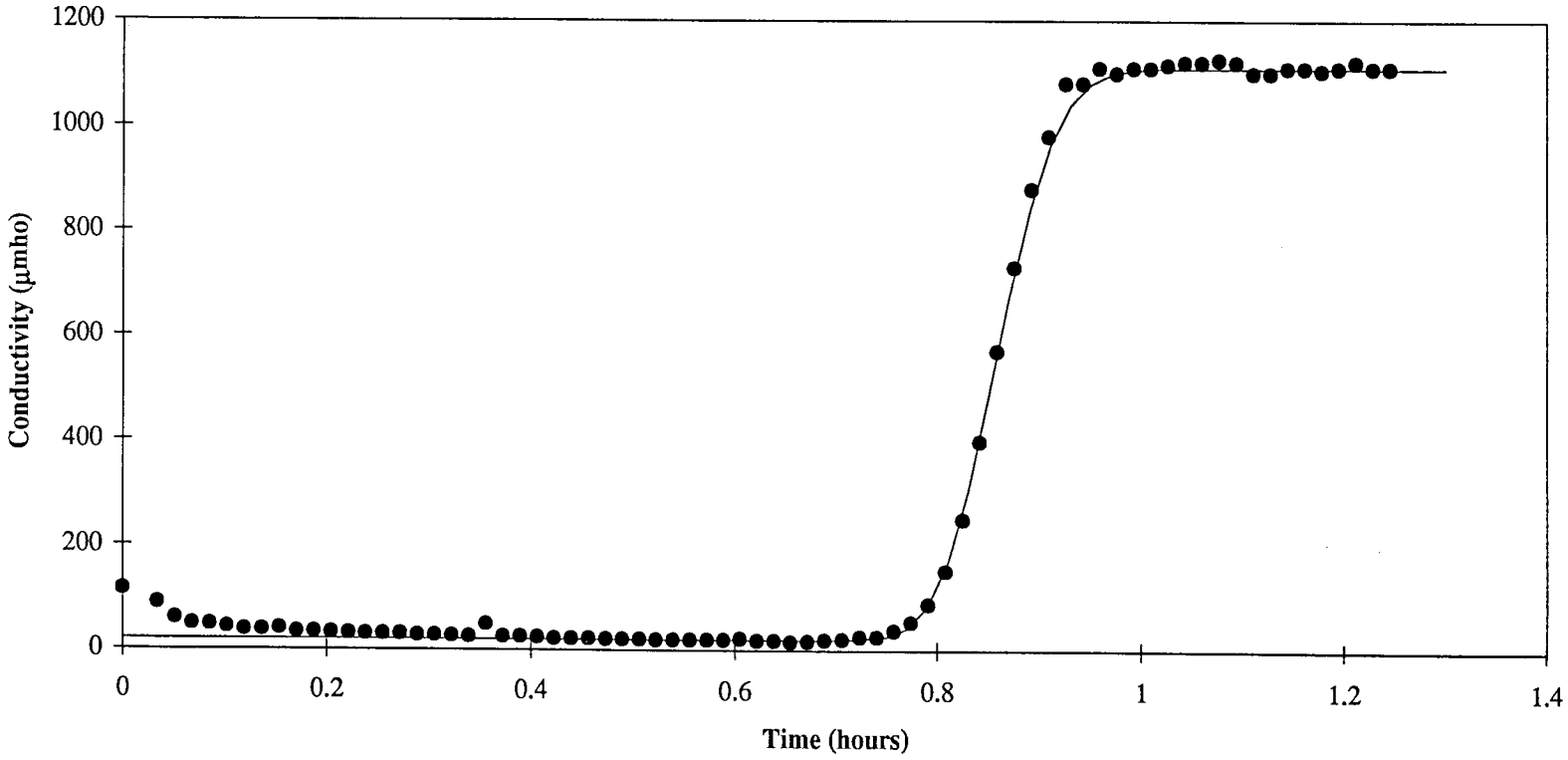

Symbols represent data, solid line is the predicted curve with D_L=0.12 dm^2/hr.

Figure 5.2. *M. albus* BG8 Growth Curve: Cell Density Measured as Klett Units vs. Time*

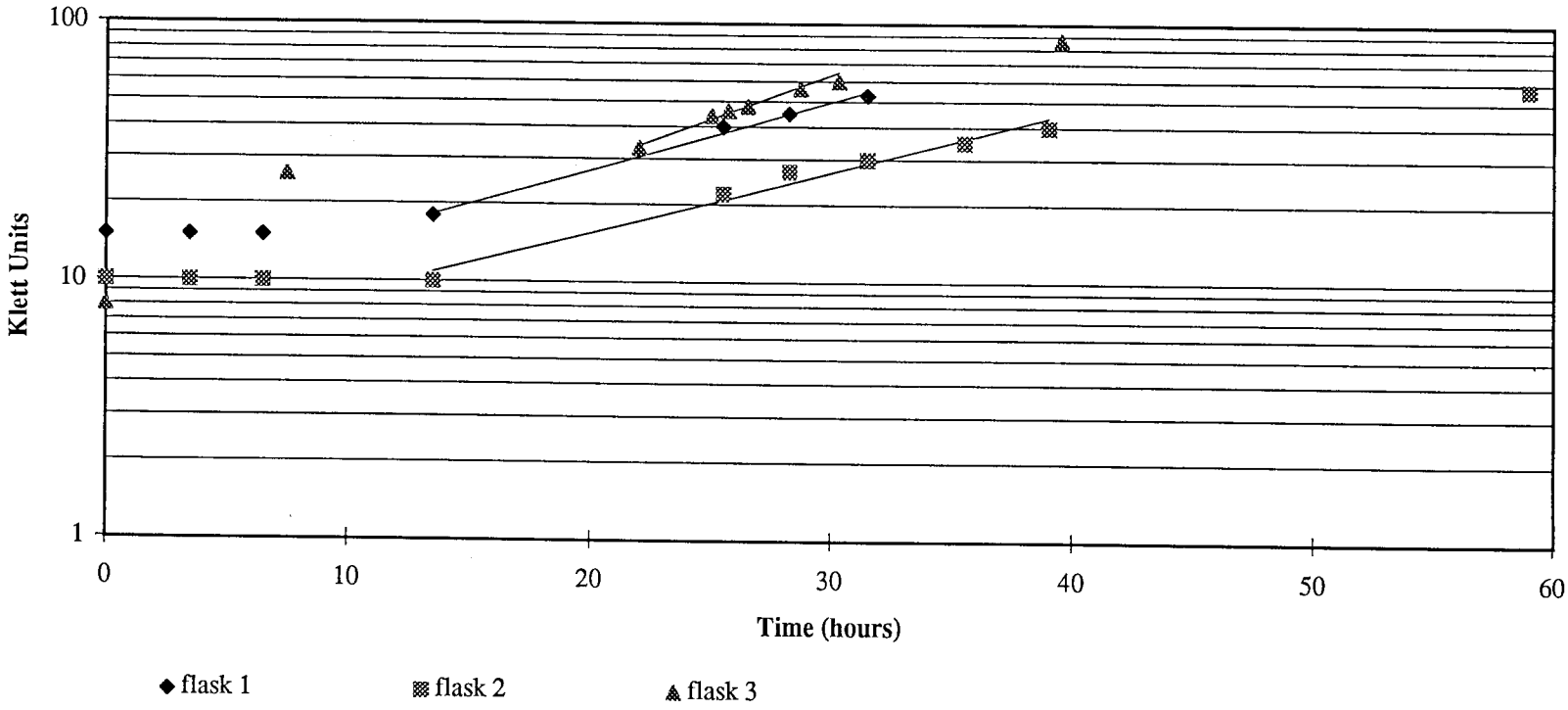

* Symbols represent Data. Lines represent linear regressions of the data intercepted by lines. Calculated doubling times are: flask 1: t_d=11 hours, flask 2: t_d=13 hours, flask 3: t_d=9 hours. All samples were grown at 30°C in NMS media with no added copper.

Figure 5.3. Comparison of Methane Concentrations in Column Liquid and Liquid in 2 ml Vials Containing 1 ml Column Liquid, $[CH_4]_0 \cong 500$ μM*

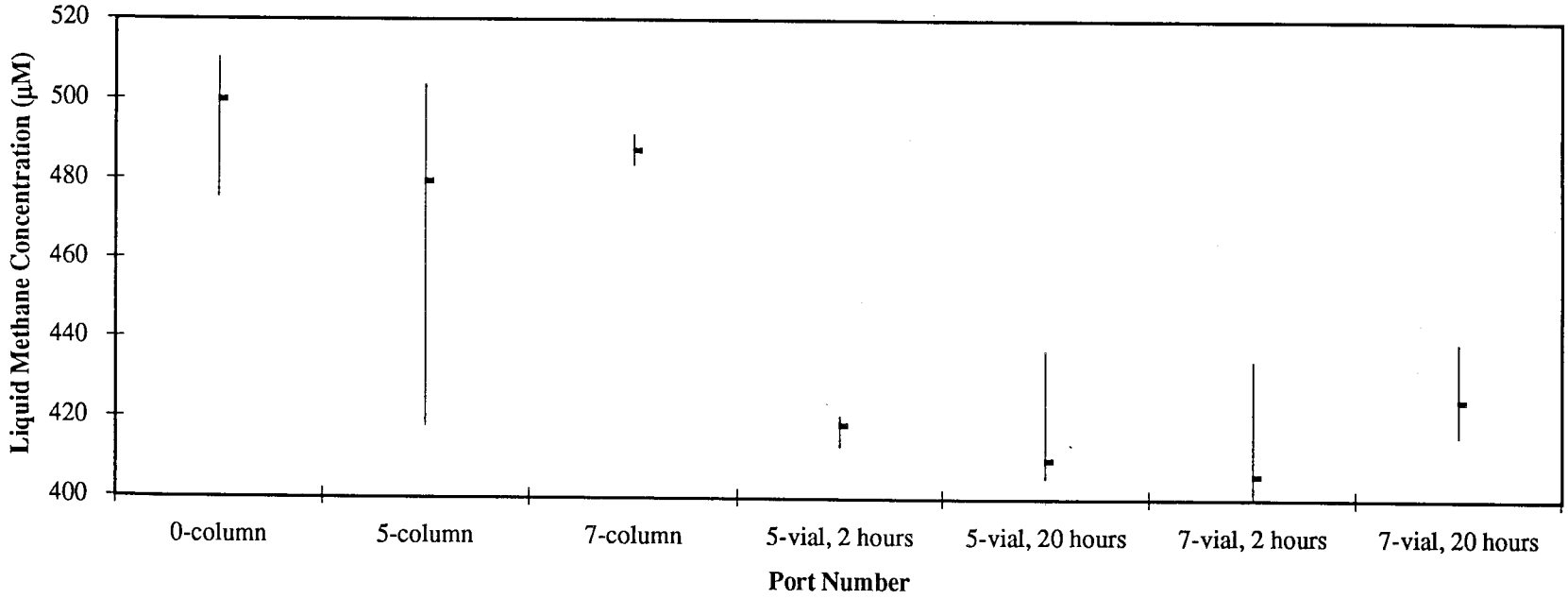

*Data shown are median, high and low values. Column flow rate = 350 ml/hour. Column data are based on analyses of 1 μl liquid samples collected directly from sampling ports. Vial sample data represent headspace analyses of 2 ml chromatography vials containing 1 ml liquid collected via syringe. Concentration data for these samples are the liquid concentrations prior to methane equilibration between the gas and liquid phases. The time shown is the time between making and analyzing a sample. There is a 13% decrease in the average liquid methane concentration for vial samples compared to the average for column samples.

Figure 5.4. Comparison of Methane Concentrations in Column Liquid, Liquid in 5 ml Sampling Syringes, and Liquid in 2 ml Vials Containing 1 ml Liquid from Sampling Syringes, $[CH_4]_o \equiv 195$ μM*

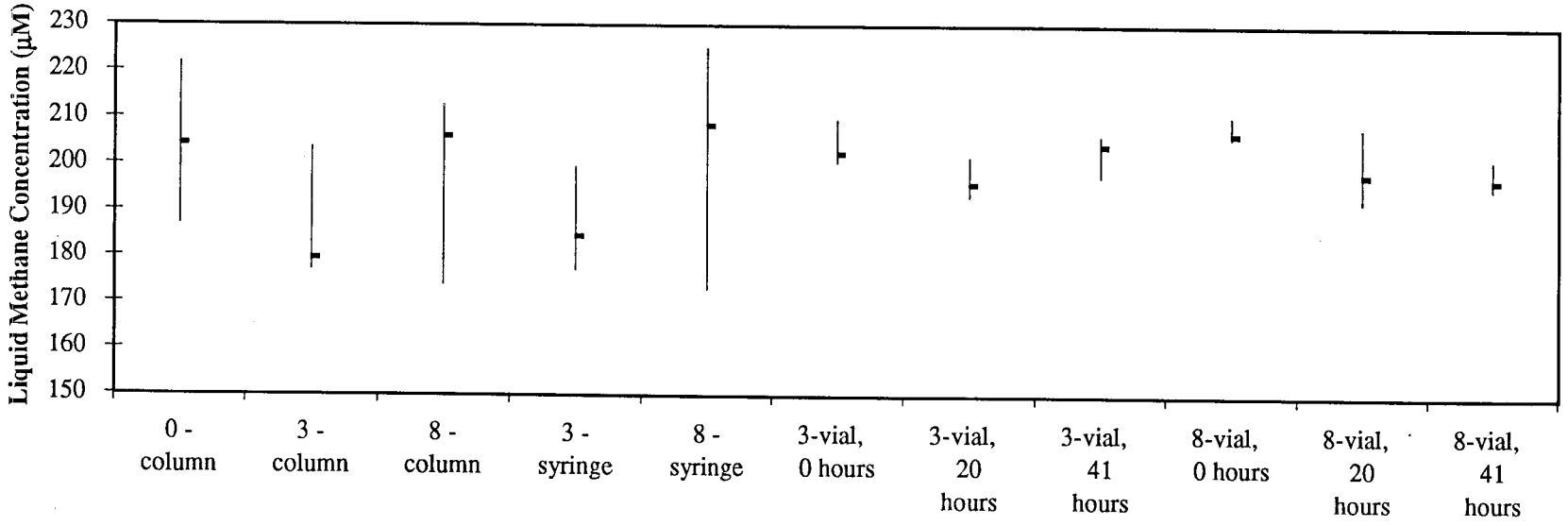

*Data shown are median, high and low values. Column flow rate = 200 ml/hour. Column and syringe sample data are based on 1 μl liquid samples collected directly from the indicated source. Vial sample data represent headspace analyses of 2 ml chromatography vials containing 1 ml column liquid collected via syringe. Concentration data for these samples are the liquid concentrations prior to methane equilibration between the gas and liquid phases. The time shown is the time between making and analyzing a sample. There is a 4% increase in the average liquid methane concentration for vial samples compared to the average for column samples.

Figure 5.5. Comparison of Methane Concentrations in Column Liquid, Liquid in 5 ml Sampling Syringes, and Liquid in 2 ml Vials Containing 1 ml Liquid from Sampling Syringes, $[CH_4]_o \cong 45$ µM*

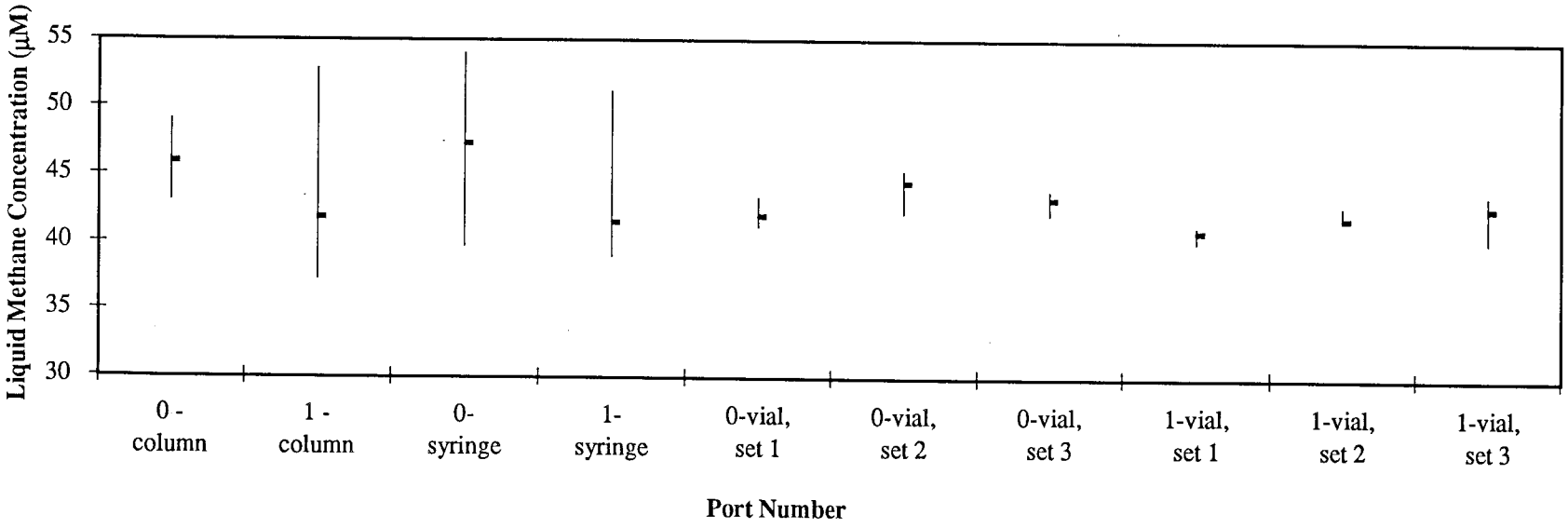

*Data shown are median, high and low values. Column flow rate = 230 ml/hr. Column and syringe sample data are based on 1 µl liquid samples collected directly from the indicated source. Vial sample data represent headspace analyses from 2 ml chromatography vials containing 1 ml column liquid collected via syringe. Concentration data for these samples are the liquid concentrations prior to methane equilibration between the gas and liquid phases. The three data sets for vials are three different samplings with the 5 ml syringe. All vials were sampled within one hour from the time liquid was extracted from the column. There is a 7% decrease in the average liquid methane concentration for vial samples compared to the average for column samples.

Figure 5.6. Comparison of Methane Concentrations in Column Liquid, Liquid in 5 ml Sampling Syringes, and Liquid in 2 ml Vials Containing 1 ml Liquid from Sampling Syringes, $[CH_4]_o \equiv 10$ µM*

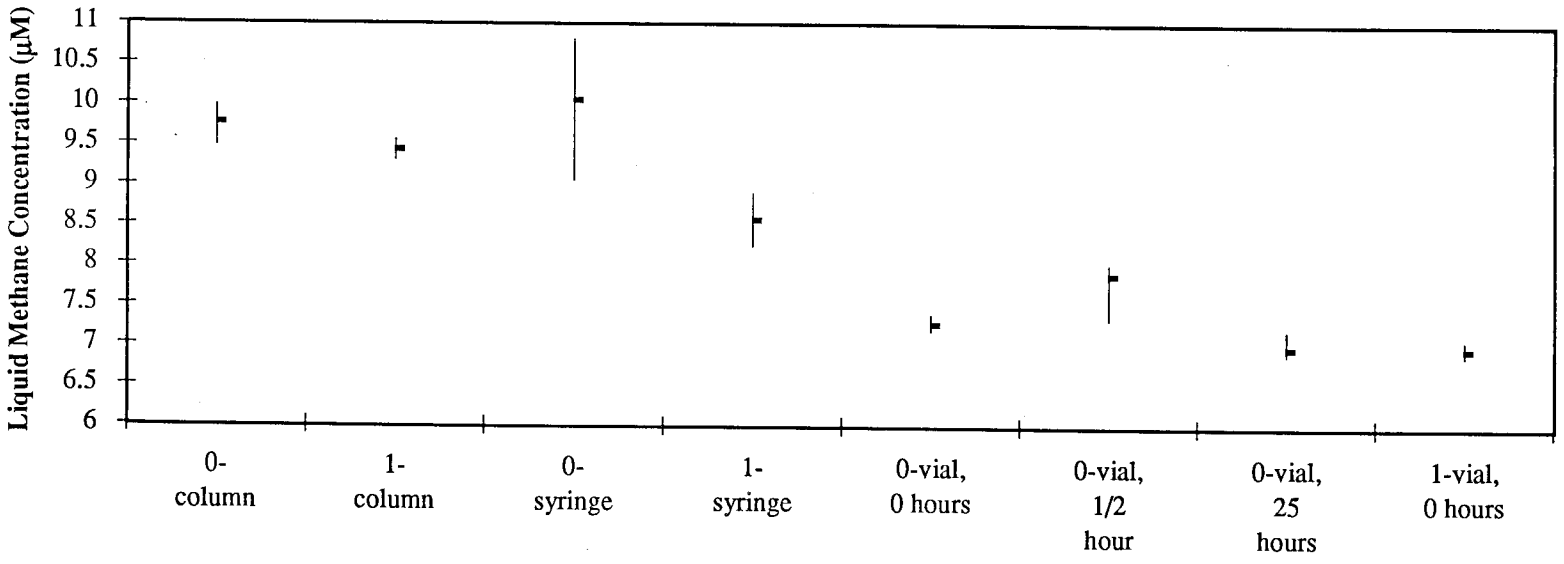

*Data shown are median, high and low values. Column flow rate = 150 ml/hr. Column and syyringe sample data are based on 1 µl liquid samples collected directly from the indicated source. Vial sample data represent headspace analyses of 2 ml chromatography vials containing 1 ml column liquid collected via syringe. Concentration data for these samples are the liquid concentrations prior to methane equilibration between the gas and liquid phases. The time shown is the time between making and analyzing a sample. There is a 24% decrease in the average liquid methane concentration for vial samples compared to the average for column samples.

Figure 5.7. Comparison of Methane Concentrations in Column Liquid, Liquid in 5 ml Sampling Syringes, and Liquid in 2 ml Vials Containing 1 ml Liquid from Sampling Syringes, $[CH_4]_o \cong 7$ µM*

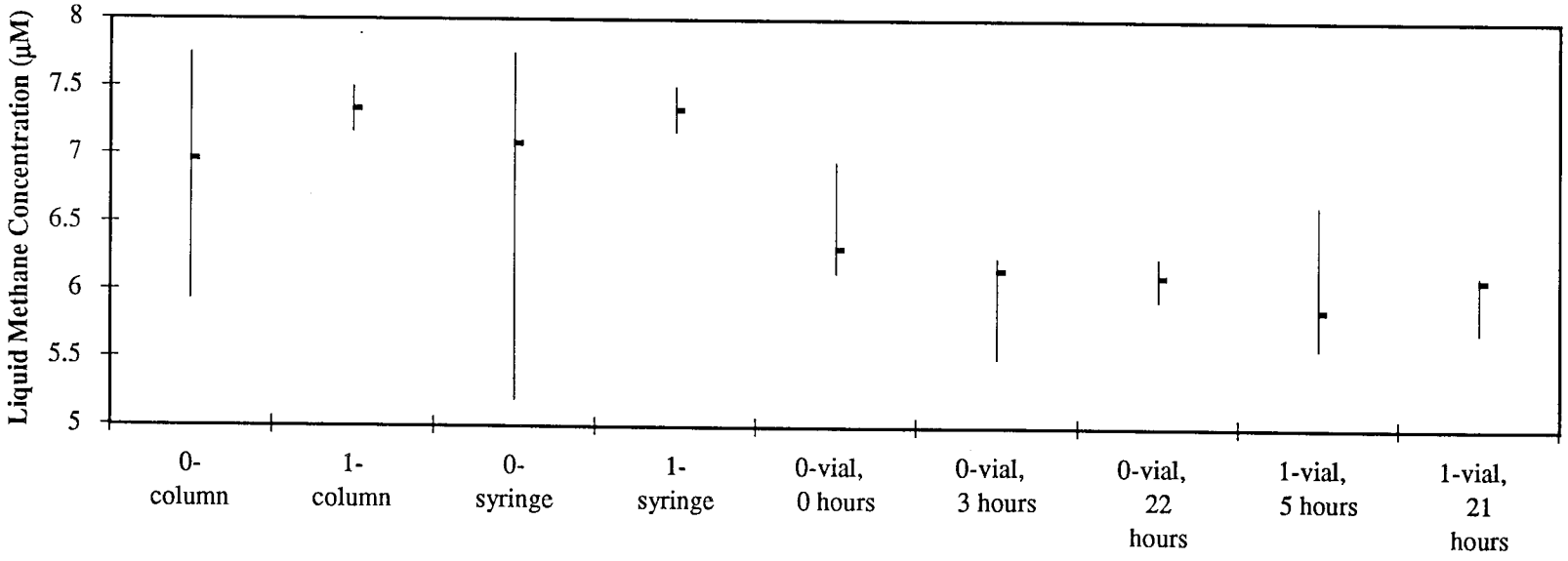

* Data shown are median, high, and low values. Column flow rate = 130 ml/hr. Column and syringe sample data are based on 1 µl liquid samples collected directly from the indicated source. Vial sample data represent headspace analyses of 2 ml chromatography vials containing 1 ml column liquid collected via syringe. Concentration data for these samples are the liquid concentrations prior to methane equilibration between the gas and liquid phases. The time shown is the time between making and analyzing a sample. There is a 13% decrease in the average liquid methane concentration for vial samples compared to the average for column samples.

Figure 5.8. Comparison of Column Data to a Model Simulation: Methane Concentrations Analyzed at t = 1 Hour After Commencement of Inlet Flow to Column Reactor*

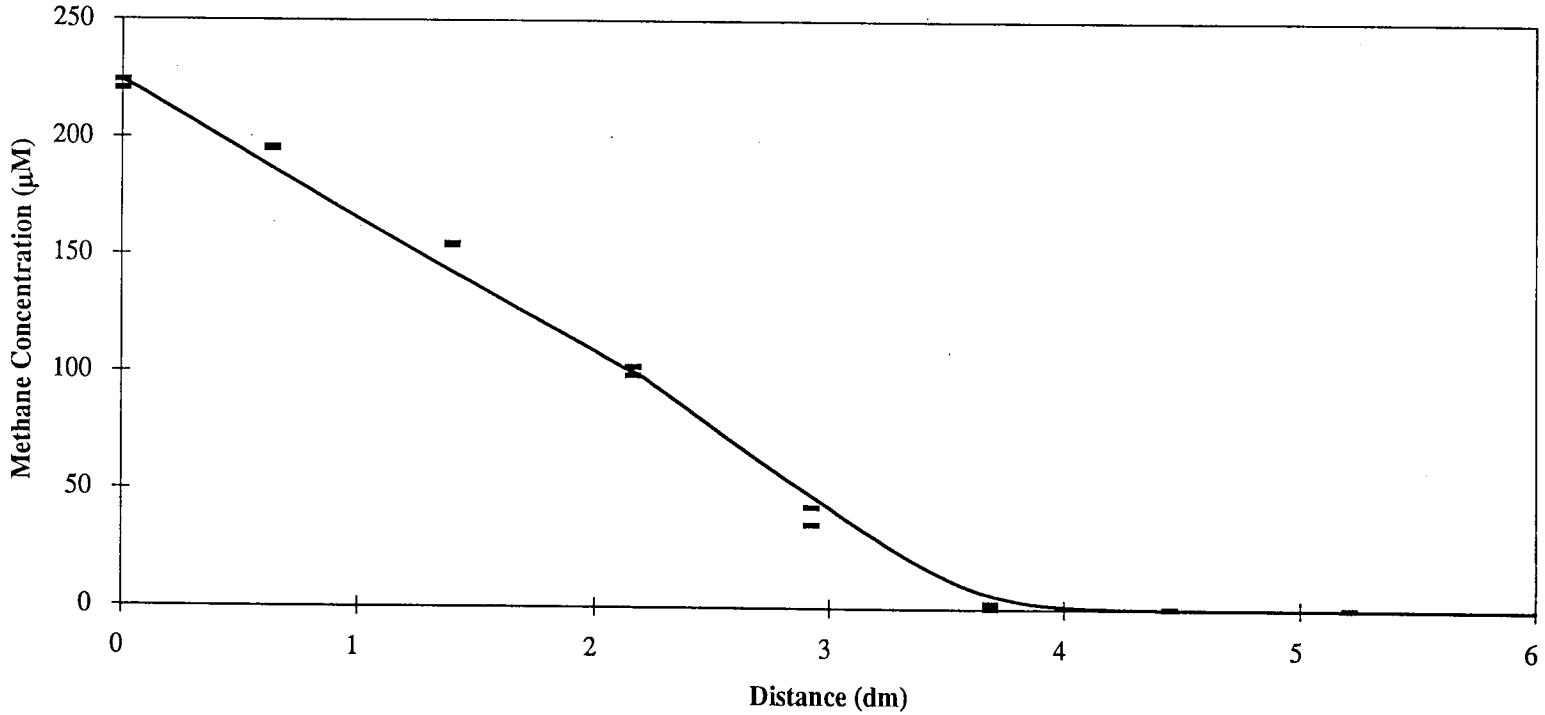

* Two samples were analyzed for $[CH_4]$ at each column sampling port. Dashes represent data. The line represents model predictions. All parameters used for model predictions are shown in Tables 5.1 and 5.2.

Figure 5.9. Comparison of Column Data to Model Predictions: Methane Concentrations Analyzed at t = 1 Hour After Commencement of Inlet Column Flow*

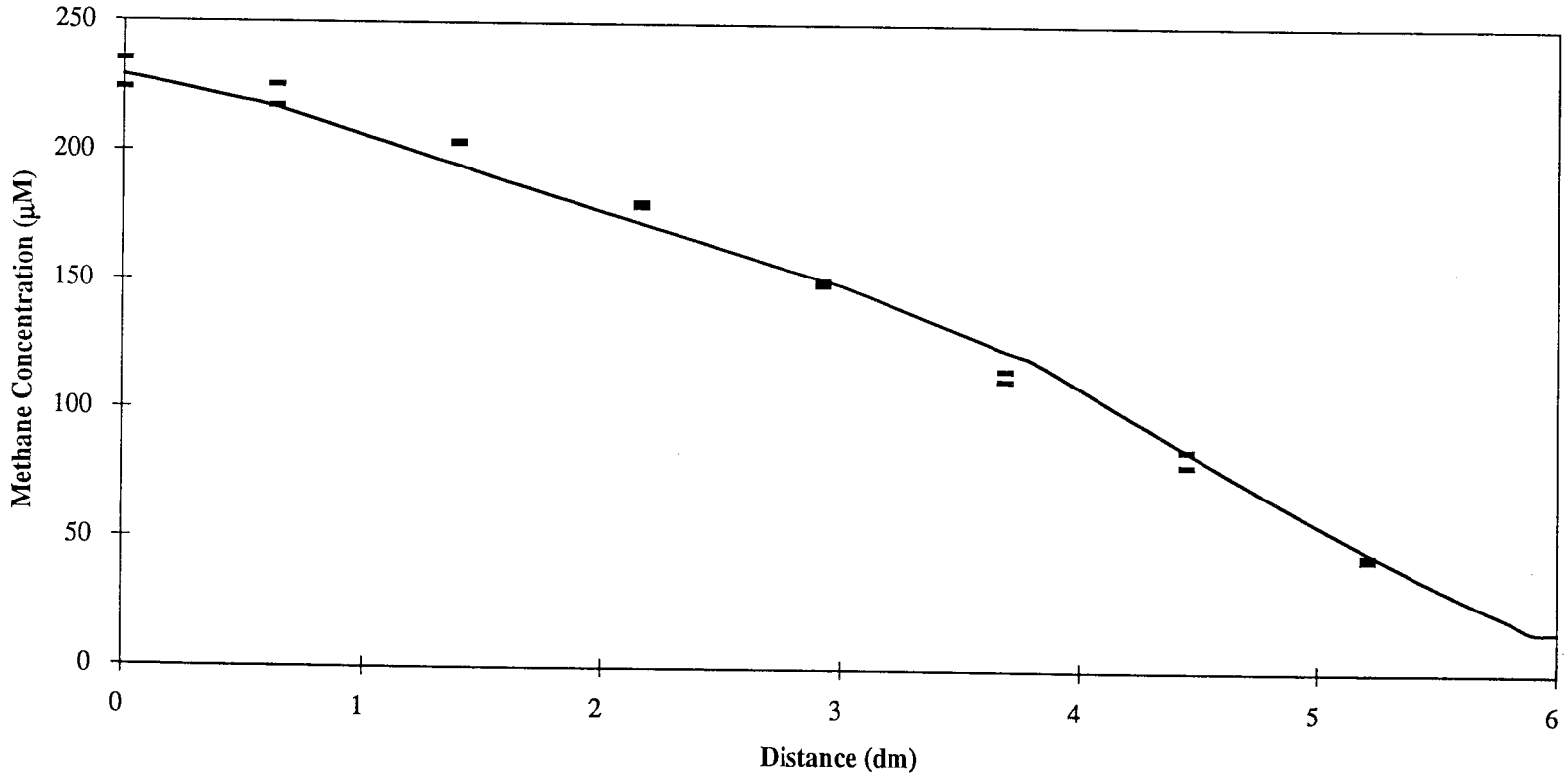

* Two samples were analyzed for [CH4] at each column sampling port. Dashes represent data. The line represents model predictions. All parameters used for model predictions are shown in Tables 5.1 and 5.3.

Figure 5.10. Comparison of Column Data to Model Simulations: Methane Concentrations at t = 3 Hours and t = 9 Hours After Commencement of Inlet Flow to Column Reactor*

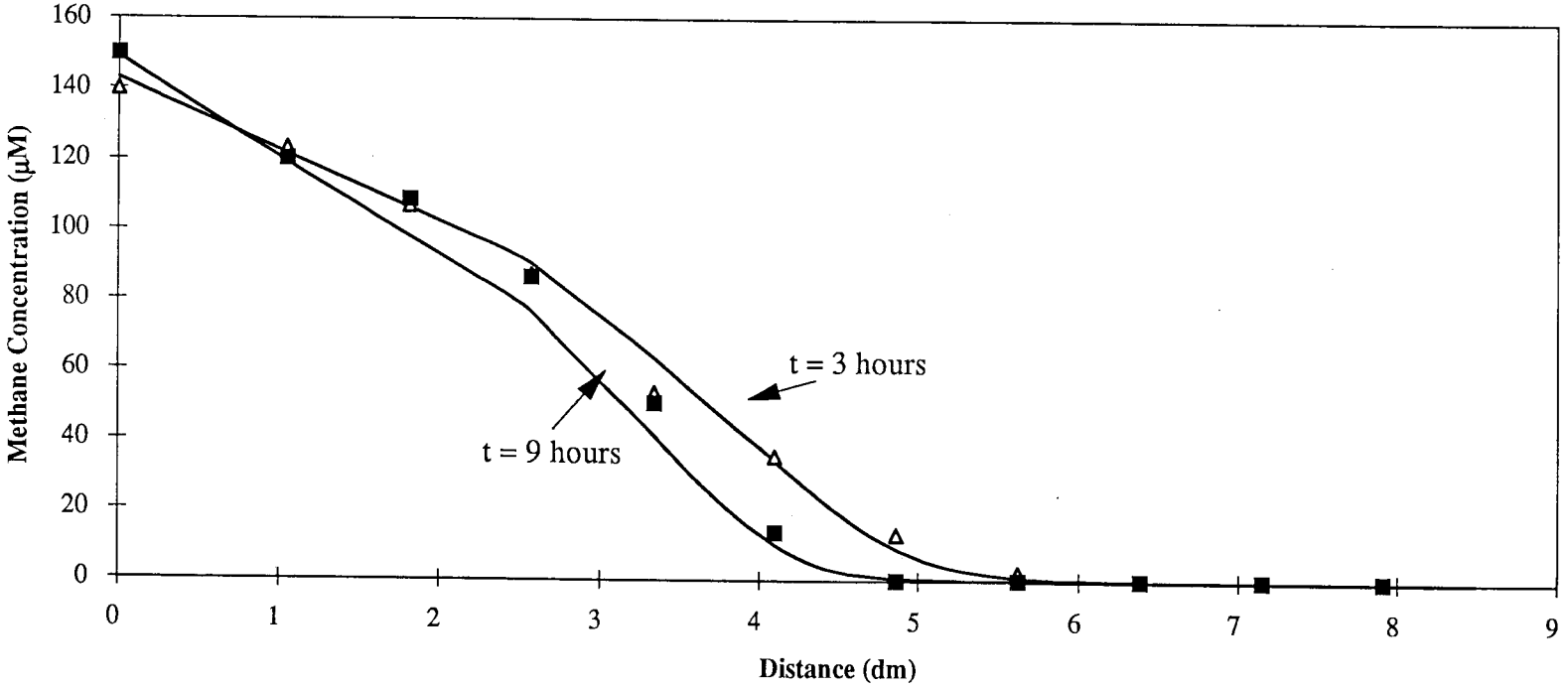

* Triangles represent samples analyzed at each column sampling port at t = 3 hours; squares represent samples analyzed at t = 9 hours. Solid lines represent model predictions. All parameters used for model predictions are shown in Tables 5.1 and 5.4.

Figure 5.11. Comparison of Column Data to Model Simulations: Methane Concentrations at t = 4 Hours and t = 14 Hours After Commencement of Inlet Flow to Column Reactor*

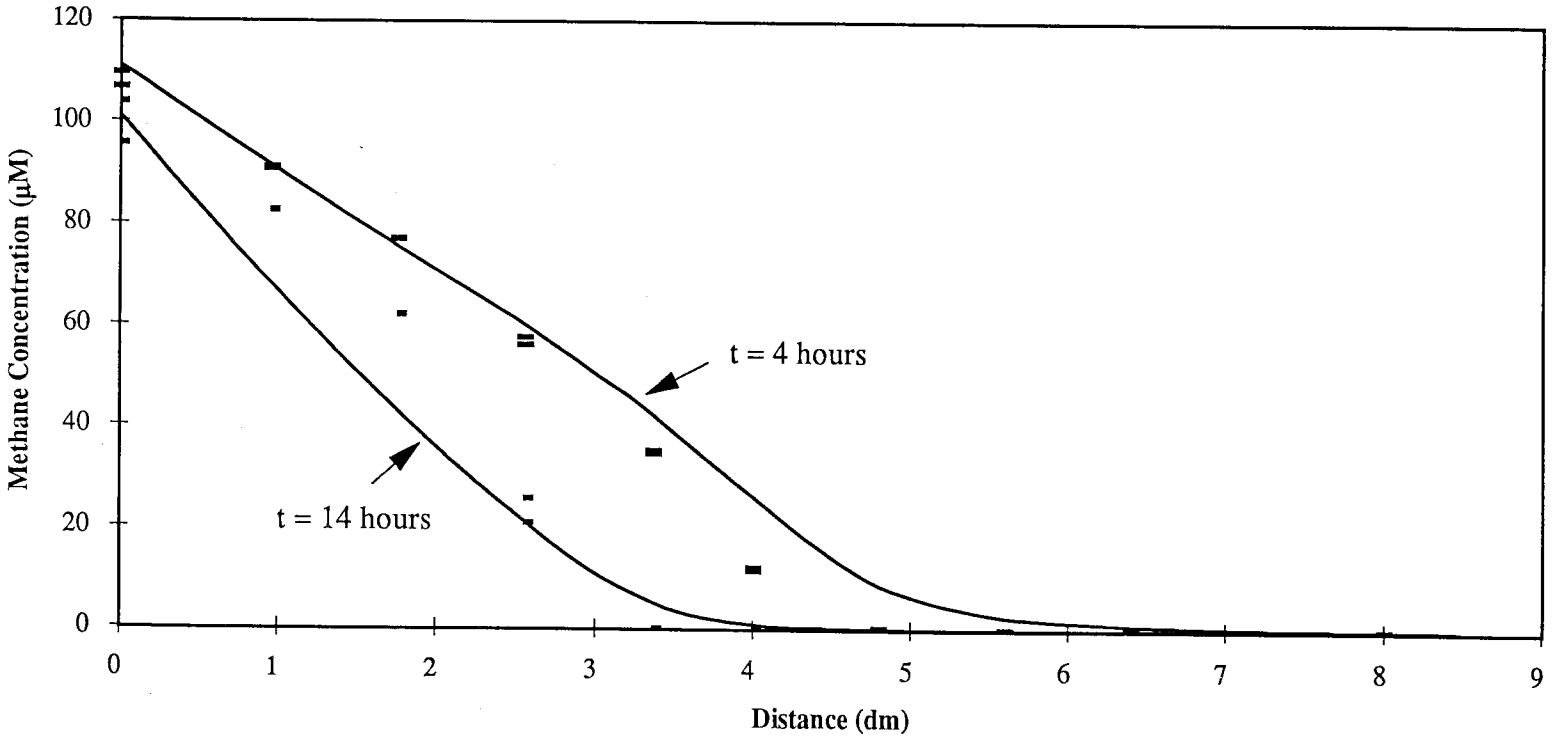

* Two samples were analyzed for [CH_4] at each column sampling port at each time point. Wide dashes represent samples analyzed at t = 4 hours; narrow dashes represent data at t = 14 hours. Solid lines represent model predictions. All parameters used for model predictions are shown in Tables 5.1 and 5.5.

Figure 5.12. Comparison of Column Data to Model Simulations: Methane Concentrations at t = 1, 8, and 15 Hours After Commencement of Inlet Flow to Column Reactor*

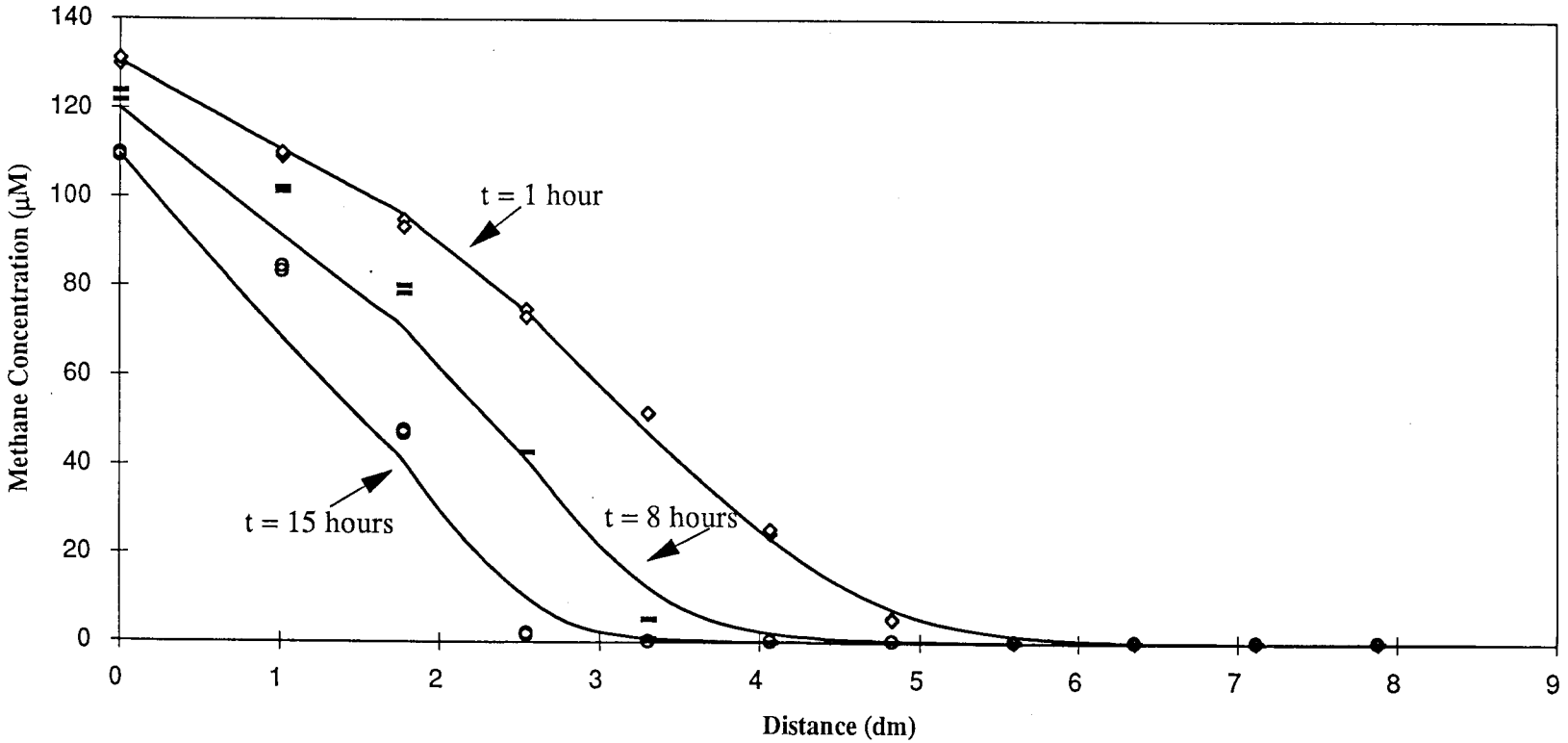

* Two samples were analyzed for [CH_4] at each column sampling port for each time point. Diamonds represent samples analyzed at t = 1 hour. Dashes represent data at 8 hours. Circles represent data at 15 hours. Solid lines represent model predictions. All parameters used for model predictions are shown in Tables 5.1 and 5.6.

Figure 5.13. Comparison of Model Predictions With and Without Mass Transfer Limitation, Using Column Reactor Data From Figure 5.12

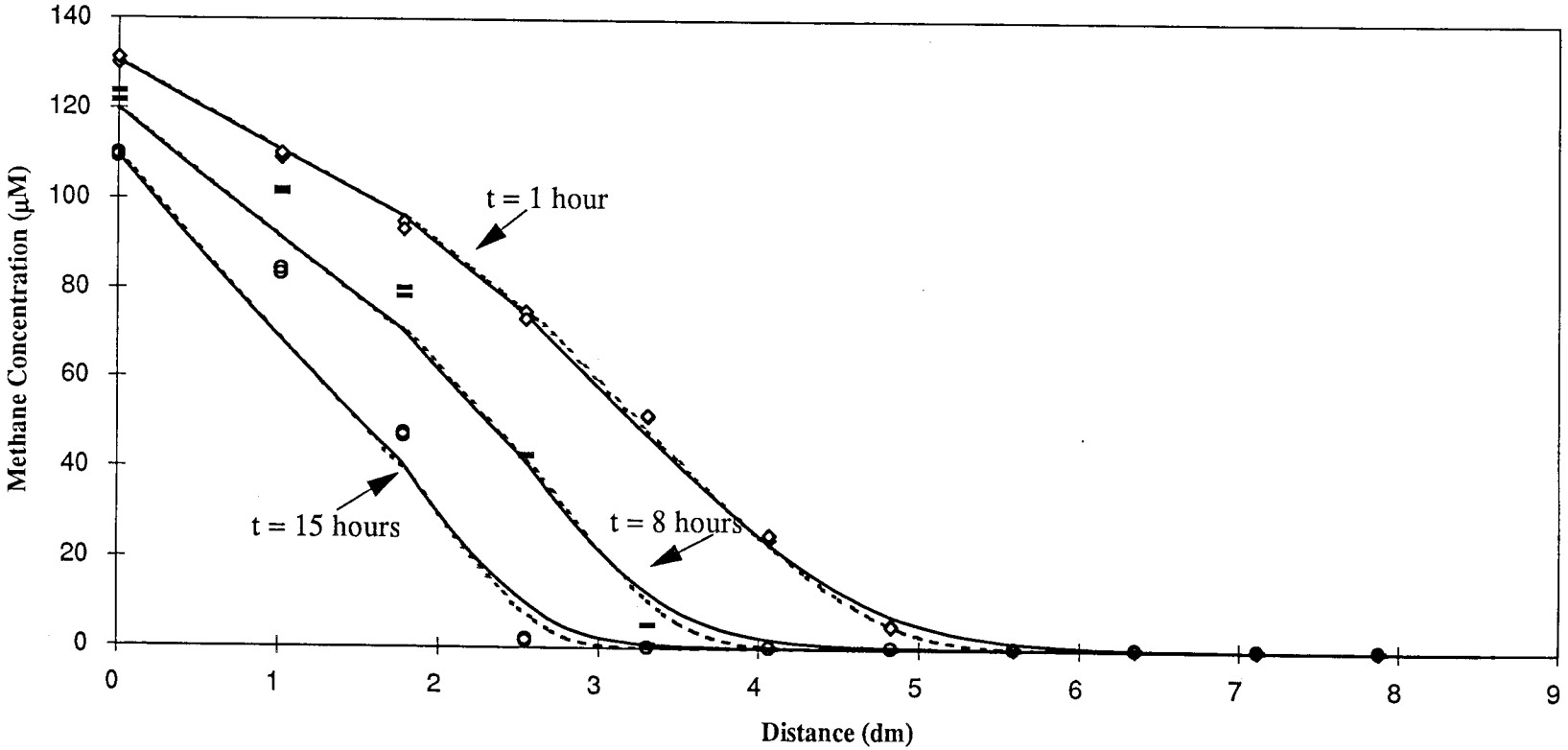

* Solid lines represent model predictions with mass transfer limitation included. Dashed lines represent model predictions with no mass transfer limitation. All parameters used for model predictions are the same as those used in Figure 5.12.

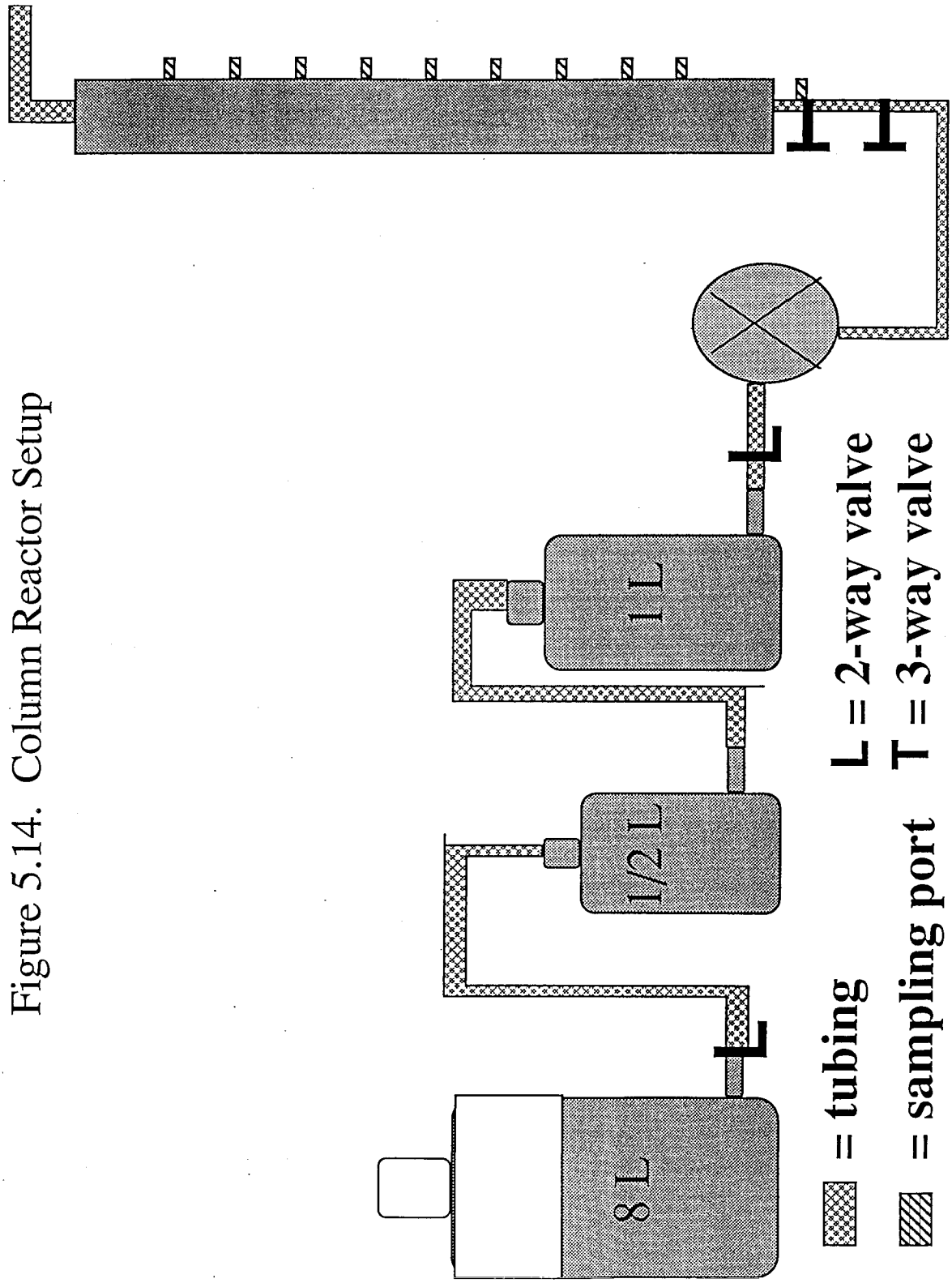

Figure 5.14. Column Reactor Setup

5.6 References

Drozd, J.W., Linton, J.D., Downs, J., & Stephenson, R.J. (1978). An *in situ* assessment of the specific lysis rate in continuous cultures of *Methylococcus* sp. (NCIB 11083) grown on methane. *FEMS Microbiology Letters, 4,* 311-314.

Nagai, S., Mori, T., & Aiba, S. (1973). Investigation of the energetics of methane-utilizing bacteria in methane- and oxygen-limited chemostat cultures. *Journal of Applied Chemistry and Biotechnology, 23,* 549-562.

Neidhardt, F.C., Ingraham, J.L., & Schaechter, M. (1990). *Physiology of The Bacterial Cell.* Sunderland: Sinauer Associates, Inc.

Pirt, S.J. (1965). The maintenance energy of bacteria in growing cultures. *Proceedings of the Royal Society of London Series B, 163,* 224-231.

Pirt, S.J. (1975). *Principles of Microbe and Cell Cultivation.* New York: John Wiley and Sons.

Sheehan, B.T., & Johnson, M.J. (1971). Production of bacterial cells from methane. *Applied Microbiology, 21,* 511-515.

Welty, J.R., Wicks, C.E., & Wilson, R.E. (1984). *Fundamentals of Momentum, Heat, and Mass Transfer.* New York: John Wiley and Sons.

Wilson, E.J., & Geankoplis, C.J. (1966). Liquid mass transfer at very low Reynolds numbers in packed beds. *Industrial and Engineering Chemistry Fundamentals, 5,* 9-14.

Chapter 6

Model Parametric and Dimensional Analysis, Groundwater Simulations, and Mass Transfer Limitation Analysis

6.1 Abstract

The effect of changing input parameter values for the model presented in Chapter 2 was studied. Of the five parameters analyzed, the maximum substrate utilization rate, V_{max}', and maximum specific growth rate, μ_{max}, were found to have the largest effect on model predictions. The Michaelis-Menten affinity coefficient and Monod half-maximum growth rate constant affected model predictions, but not as significantly as V_{max}' and μ_{max}. The longitudinal dispersion coefficient, D_L, displayed the least significant effect on model predictions. The mass transfer coefficient, k_c, affected model predictions when mass transfer became an important phenomenon. Dimensional analysis of the governing equations produced a Dahmköhler number which governed the onset of mass transfer limitation. This dimensionless group is $\frac{V_{max}'}{\alpha k_c C_o}$, the maximum substrate utilization rate / the mass transfer rate. Mass transfer becomes an important factor in model predictions when this Dahmköhler number is approximately 0.1 or greater. Simulations representing typical groundwater flows showed that the mass transfer limitation effect is greatest when the substrate concentration is less than or equal to the Michaelis-Menten affinity coefficient and Monod half-maximum growth rate constant.

6.2 Introduction

The model presented in Chapter 2 was shown to correctly predict methane concentrations throughout a column reactor over time in Chapter 5. Having demonstrated the model's predictive capabilities, the next step is using the model to obtain a better understanding of the physical processes in a natural groundwater system. In order to acquire this understanding I have evaluated the model's response to changes in parameters used for model simulations. In addition, I performed a dimensional analysis on the governing equations presented in Chapter 2 in order to identify the key dimensionless groups for the equations. Finally, I ran a series of groundwater flow simulations to identify when mass transfer limitation from the bulk fluid to particle surfaces begins to affect model predictions.

6.3 Methods

The program used for solving the set of governing equations presented in Chapter 2 and shown in Appendix A was used to evaluate how changes in input model parameters affect model predictions. One modification for groundwater flow simulations was made to the program. This was to have a single cell density throughout the length of the system at time $t = 0$. This modification was made because there is no reason to expect a large spatial variation in methanotroph cell densities before adding methane to a groundwater system. The spatial variation in cell density at $t = 0$ in the column reactor was due to experimental setup and was not meant to resemble a natural system.

6.4 Results

6.4.1 Dimensional Analysis

The governing equations presented in Chapter 2 are:

$$\frac{\partial C_B}{\partial t} = D_L \frac{\partial^2 C_B}{\partial x^2} - U \frac{\partial C_B}{\partial x} - \alpha X k_c (C_B - C_S) \qquad (2\text{-}23)$$

$$C_S = \frac{-(K_S + \frac{V_{max}'}{\alpha k_c} - C_B) + \sqrt{(K_S + \frac{V_{max}'}{\alpha k_c} - C_B)^2 + 4K_S C_B}}{2} \qquad (2\text{-}22)$$

$$\frac{\partial X}{\partial t} = \frac{\mu_{max} X C_S}{K_{S_{Monod_S}} + C_S} - aX \qquad (2\text{-}24)$$

Definitions for all variables are presented in Appendix B.

I have defined the following dimensionless parameters:

C_B^* = C_B/C_o

(bulk concentration/initial inlet concentration)

C_S^* = C_S/C_o

(concentration near particle surfaces/initial inlet concentration)

t^* = Ut/L

(velocity*time/length of column or length scale of aquifer)

x^* = x/L

(distance/ length of column or length scale of aquifer)

$X^* = X/X_o$

(cell mass concentration/initial cell mass concentration)

Substituting these dimensionless parameters into equations 2-22 through 2-24, I obtain:

$$\frac{\partial C_B^*}{\partial t^*} = \frac{D_L}{UL}\frac{\partial^2 C_B^*}{\partial x^{*2}} - \frac{\partial C_B^*}{\partial x^*} - \frac{\alpha X_o k_c L X^*}{U}\left(C_B^* - C_S^*\right) \tag{6-1}$$

$$C_S^* = \frac{-\left(\frac{K_S}{C_o} + \frac{V_{max}'}{\alpha k_c C_o} - C_B^*\right) + \sqrt{\left(\frac{K_S}{C_o} + \frac{V_{max}'}{\alpha k_c C_o} - C_B^*\right)^2 + 4C_B^*\frac{K_S}{C_o}}}{2} \tag{6-2}$$

$$\frac{\partial X^*}{\partial t^*} = \frac{L}{U}\left(\frac{\mu_{max} X^* C_S^*}{\frac{K_{S_{Monod\,S}}}{C_o} + C_S^*} - kX^*\right) \tag{6-3}$$

Seven dimensionless groups appear in these equations:

$$\text{Pe} = \frac{UL}{D_L} \tag{6-4}$$

$$\beta = \frac{\alpha k_c X_o L}{U} \tag{6-5}$$

(mass transfer rate / convection rate)

$$\text{Da}^1 = \frac{V_{max}'}{\alpha k_c C_o} \tag{6-6}$$

(maximum oxidation rate / mass transfer rate)

$$\gamma = \frac{K_S}{C_o} \quad (6\text{-}7)$$

(Michaelis-Menten affinity coefficient / initial inlet concentration)

$$\delta = \frac{K_{S_{Monod}}}{C_o} \quad (6\text{-}8)$$

(Monod half-maximum growth rate constant / initial inlet concentration)

$$Da^2 = \frac{L \mu_{max}}{U} \quad (6\text{-}9)$$

(maximum growth rate / convection rate)

$$Da^3 = \frac{La}{U} \quad (6\text{-}10)$$

(specific maintenance rate / convection rate)

Dividing equation 6-6 by equation 6-7 I obtain an additional Dahmköhler number:

$$Da^4 = \frac{V_{max}'}{\alpha k_c K_S} \quad (6\text{-}11)$$

(minimum oxidation rate / mass transfer rate)

Da^1 and Da^4 define whether a system will be mass transfer limited. If the substrate concentration the cells are exposed to is much greater than the Michaelis-Menten affinity coefficient, then cells consume substrate according to $V_{max}'X$ (see Chapter 2 Section 2.9). In this case, Da^1 defines the rate of substrate utilization / mass transfer rate. If the substrate concentration to which cells are exposed is much less than the Michaelis-Menten affinity coefficient, cells oxidize substrate according to $V_{max}'XC_S/K_S$ (see Chapter 2 Section 2.9). In this case Da^4 defines the rate of substrate

utilization / mass transfer rate. In most cases, the concentration will lie between the two extremes. The two Dahmköhler numbers can be used to ascertain whether mass transfer will limit the substrate oxidation rate.

6.4.2 Parametric Analysis

Figures 6.1 through 6.5 show the results for model simulations done with changes in model input parameters. Simulations were done using the main set of parameters for the final column experiment shown in Chapter 5. All parameter values used for simulations are shown in Table 6.1. The parameters evaluated for their effects on simulation predictions were V_{max}', K_S, $K_{S_{Monod_S}}$, μ_{max}, D_L and k_c. Each analyzed parameter was varied separately with the exception of K_S and $K_{S_{Monod_S}}$, which were varied simultaneously. Simulation predictions were graphed for three simulation time points: 1, 8 and 15 hours.

The first graph, Figure 6.1, shows the analysis for V_{max}'. This parameter sets the slope of concentration vs. distance at the column inlet and has a strong effect on model predictions. Three different values of V_{max}' are shown: 0.01, 0.013, and 0.1 μmol/hr/μg protein. The value of 0.013 μmol/hr/μg protein was used for the simulation of column experimental data. A 25% decrease in V_{max}' causes a measurable change in model predictions, as can be seen in Figure 6.1. The predictions for $V_{max}' = 0.01$ and $V_{max}' = 0.1$ are very different from the predictions for $V_{max}' = 0.013$.

The second graph, Figure 6.2, shows the analysis for the Michaelis-Menten affinity coefficient, K_S, and Monod half-maximum growth rate constant, $K_{S_{Monod_S}}$. These two parameters were varied simultaneously because one of the assumptions for

the model is that these two parameters should be equivalent. I found that K_S and $K_{S_{Monod_S}}$ have a measurable effect on model predictions, although the model's sensitivity to changes in these coefficients is less than the sensitivity to changes in V_{max}'. The values used for these coefficients in Figure 6.2 were 0.1, 8, and 50 μM. The value of 8 μM was used for predictions of column experimental data. At K_S and $K_{S_{Monod_S}}$ values of 50 μM, the slope of concentration vs. distance at the column inlet is approximately equal to the slope for V_{max}' = 0.01 μmol/hr/μg protein shown in Figure 6.1. However, the tailing of concentration towards the column outlet is much more significant when K_S and $K_{S_{Monod_S}}$ = 50 μM. When K_S and $K_{S_{Monod_S}}$ are set to 0.1 μM there are slight deviations from the predictions for K_S and $K_{S_{Monod_S}}$ = 8 μM. These parameters mainly affect the tailing towards the column outlet (as the concentration approaches K_S and $K_{S_{Monod_S}}$).

The next parameter evaluated was μ_{max}. Results are shown in Figure 6.3. The main effect changing μ_{max} has on model predictions is to change the rate of growth of cells and hence to change the rate of increased methane oxidation over time. Model predictions were very sensitive to changes in μ_{max}. The values used for model predictions shown in Figure 6.3 were 0.04, 0.08, and 0.15/hr. The μ_{max} value used for experimental data predictions was 0.08/hr. At t = 1 hour, there is not a wide variation in methane concentration predictions among the three μ_{max} values. However, by 8 hours, the simulations for the three values of μ_{max} show large differences. This is because the cells have had time to grow and display differences caused by changes in μ_{max}. The parameter μ_{max} has a strong effect on model predictions.

Figure 6.4 shows simulation results with variations in the longitudinal dispersion coefficient, D_L. The model is not very sensitive to changes in D_L for the parameter values used in these simulations. The values of D_L used for predictions were 0.12, 1.2, and 12 dm^2/hr. The value used for experimental data predictions was 0.12 dm^2/hr. There is no significant difference between model predictions for D_L = 0.12 dm^2/hr and D_L = 1.2 dm^2/hr. For D_L = 12 dm^2/hr there are slight but not very significant changes in model predictions compared to predictions for D_L = 0.12 dm^2/hr. The main effect of increasing D_L is increased tailing.

The last figure described in this section, Figure 6.5, shows model simulations for different values of the mass transfer coefficient, k_c. Changes in the mass transfer coefficient do not have a large effect on model predictions until k_c decreases below 1.5/dm. The values of k_c used for model predictions shown in Figure 6.5 were 1500, 1.5 and 0.15 dm/hr. The value used for experimental data predictions was 1.5 dm/hr. There is only a slight difference between simulation results for k_c = 1500 dm/hr and k_c = 1.5 dm/hr. However, for k_c = 0.15 dm/hr there are obvious deviations from the results for k_c = 1500 dm/hr and k_c = 1.5 dm/hr: tailing is significant when k_c = 0.15 dm/hr. This sudden shift in the effect of changes in k_c can be better understood by analyzing the first Dahmköhler number as k_c decreases from 1.5 dm/hr to 0.15 dm/hr. When k_c = 1.5 dm/hr, Da^1 = 0.07; the reaction rate is much slower than the mass transfer rate. For k_c = 0.15 dm/hr, Da^1 = 0.7; the reaction rate is of the same order of magnitude as the mass transfer rate. This mass transfer effect also significantly affects the cell growth rate because the growth rate is dependent upon the substrate concentration to which cells are exposed.

An important point to note here is that the effect of mass transfer limitation on substrate oxidation has approximately the same effect as an increase in the Michaelis-Menten affinity coefficient and Monod half-maximum growth rate constant. The simulations for K_S and $K_{S_{Monod_S}}$ = 50 μM shown in Figure 6.2 are very similar to the simulations for k_c = 0.15/dm shown in Figure 6.5. If researchers ignore mass transfer limitation effects when modeling substrate utilization in natural systems, higher than expected fitted values for K_S and $K_{S_{Monod_S}}$ may suggest that mass transfer should be included in the modeling. A model presented in a paper by Semprini *et al.* (1991) did not include mass transfer effects and the researchers used fitted K_S and $K_{S_{Monod_S}}$ values an order of magnitude higher than literature values in order for their model to correctly predict the measured data. This suggests that mass transfer might have been limiting the *in situ* methane utilization rates in their studies.

6.4.3 Groundwater Simulations: Mass Transfer Limitation

The final results section in this chapter covers simulations for flows characteristic of groundwater systems. The parameters used for model simulations were those given for a semi-confined groundwater system that had a solid phase composed of sand and gravel (Semprini *et al.*, 1991). The length scale studied was 3 m. This is the distance between groundwater wells in the site described by Semprini *et al.* (1991). Results are shown in Figures 6.6 through 6.11. Parameters used for model simulations are shown in Table 6.2. The first three figures show model predictions for methane concentration vs. distance for inlet concentrations equal to, an order of magnitude greater than, and two orders of magnitude greater than K_S and $K_{S_{Monod_S}}$.

The following three figures show cell density vs. distance for the same range of K_S and $K_{S_{Monod_S}}$ values as the first three figures. In all six figures, methane concentrations and cell densities are shown at three time points for three different mass transfer limitation conditions. The mass transfer conditions are: $k_c = \infty$ (no mass transfer limitation), k_c = 1 dm/hr and k_c = 0.1 dm/hr. These values correspond to $Da^1 = 0$, $Da^1 = 0.025$, and $Da^1 = 0.25$, respectively. The expected mass transfer coefficient, based on a correlation by Wilson and Geankoplis (1966) is approximately 0.7 dm/hr.

Predictions for both methane concentration and cell density vs. distance are similar for $k_c = \infty$ and k_c = 1 dm/hr in all the figures. There is less than 1 percent difference between predictions at each time point for these two values of the mass transfer coefficient. However, for k_c = 0.1 dm/hr, there is a divergence from the non-mass transfer limited predictions for all time points for the entire range of K_S and $K_{S_{Monod_S}}$ values. The deviations increase as K_S and $K_{S_{Monod_S}}$ approach the inlet concentration.

This is expected due to the mathematical forms of the methane uptake and cell growth kinetics equations. Both display saturation kinetics. Slight changes in concentration do not have a large effect on substrate utilization or cell growth for concentrations much greater than K_S and $K_{S_{Monod_S}}$. However, substrate oxidation and growth kinetics approach linear functions of concentration as the concentration approaches the values for K_S and $K_{S_{Monod_S}}$. Slight changes in concentration under these conditions have significant effects on the substrate oxidation and growth kinetics.

Another observation from these graphs is that cell densities do not vary greatly over the 3 m distance so long as the substrate concentration is approximately an order of magnitude greater than K_S and $K_{S_{Monod_S}}$. This can be seen most clearly by comparing Figure 6.9 with Figures 6.10 and 6.11. These are the cell density vs. distance simulation plots. Cell density is not constant with distance in Figure 6.9. This is the plot for $C_o=K_S=K_{S_{Monod_S}}$. The cell density is much larger near x=0 even when the methane concentration is 80 μM at the 3 m distance (See Figure 6.6.). In Figures 6.10 and 6.11 cell density is approximately constant with distance up to 90 hours. After this time, the methane concentration decreases to 0 before the 3 m point for the non-mass transfer limited cases. C_o was 20-fold greater than K_S and $K_{S_{Monod_S}}$ for the simulation shown in Figure 6.10 and 200-fold greater that K_S and $K_{S_{Monod_S}}$ in Figure 6.11. This result has important implications for *in situ* groundwater bioremediation. If site remediators want to maintain a uniform cell density for bioremediating a contaminated groundwater system, it would be necessary to ensure that the concentration of substrate for cell growth remained approximately an order of magnitude greater than the Monod half-maximum growth rate constant, $K_{S_{Monod_S}}$.

6.5 Conclusions

Seven dimensionless groups were defined by dimensional analysis of the governing equations for substrate transport in a groundwater system coupled with substrate oxidation by cells and cell growth. A full analysis was done on the effects of changing the dimensionless group representing the substrate utilization rate / mass

transfer rate (Da^1). In addition, a parametric analysis was done for five model parameters to obtain a better understanding of the phenomena governing model predictions. I found that changing values for V_{max}' and μ_{max} significantly affects model predictions. Model predictions are less sensitive, but still affected by changes in the values for K_S and $K_{S_{Monod_S}}$. The model is fairly insensitive to changes in D_L. The mass transfer coefficient becomes important when Da^1 is on the order of 0.1 or greater. I also found that model predictions for changes in values of K_S and $K_{S_{Monod_S}}$ mimic predictions for changes in the mass transfer coefficient when mass transfer becomes limiting.

Model predictions for groundwater flow conditions were found to be most sensitive to mass transfer limitation when the inlet concentration was near the Michaelis-Menten affinity coefficient and the Monod half-maximum growth rate constant. The mass transfer effect was seen for inlet concentrations greater than K_S and $K_{S_{Monod_S}}$ but it was not as profound. In all cases, mass transfer limitation was not significant until Da^1 approached a value of 0.1 or larger.

Table 6.1. Model Parameters for Figures 6.1 through 6.5

Parameter	Figure 6.1	Figure 6.2	Figure 6.3	Figure 6.4	Figure 6.5
C_o at t=0 (μM)	132	132	132	132	132
Change in Inlet Concentration (μM/hr)	-1.5	-1.5	-1.5	-1.5	-1.5
Column Length (dm)	8.6	8.6	8.6	8.6	8.6
V_{max}' (μmol/hr/μg protein)	0.01 - 0.1	0.013	0.013	0.013	0.013
K_s (mM)	8	1 - 50	8	8	8
μ_{max} (1/hr)	0.08	0.08	0.04 - .15	0.08	0.08
Specific Maintenance Rate a (1/hr)	0.02	0.02	0.02	0.02	0.02
D_L (dm^2/hr)	0.12	0.12	0.12	0.12 - 12	0.12
Velocity (dm/hr)	13	13	13	13	13
Mass Transfer Coefficient: k_c (dm/hr)	1.5	1.5	1.5	1.5	0.15 - 1500
Cell Surface Area per Mass of Cells (dm^2/μg protein)	0.001	0.001	0.001	0.001	0.001
Δt (hr)	0.001	0.001	0.001	0.001	0.001
Δx (dm)	0.02	0.02	0.02	0.02	0.02
Protein Concentration at t = 0 (μg/ml fluid) port 0 - port 1	20	20	20	20	20
port 1 - port 2	20	20	20	20	20
port 2 - port 3	30	30	30	30	30
port 3 - port 4	40	40	40	40	40
port 4 - port 5	40	40	40	40	40
port 5 - port 6	40	40	40	40	40
port 6 - port 7	40	40	40	40	40
port 7 - port 8	45	45	45	45	45
port 8 - port 9	45	45	45	45	45
port 9 - port 10	45	45	45	45	45

Table 6.2. Model Parameters for Figures 6.6 through 6.11

Parameter	Figure 6.6	Figure 6.7	Figure 6.8	Figure 6.9	Figure 6.10	Figure 6.11
C_o at t=0 (μM)	200	200	200	200	200	200
V_{max}' * (μmol/hr/μg protein)	0.005	0.005	0.005	0.005	0.005	0.005
K_s (μM)	200	10	1	200	10	1
μ_{max} (1/hr)*	0.06	0.06	0.06	0.06	0.06	0.06
Specific Maintenance Rate a (1/hr)	0.02	0.02	0.02	0.02	0.02	0.02
D_L (dm^2/hr)**	1	1	1	1	1	1
Velocity (dm/hr)	1	1	1	1	1	1
Mass Transfer Coefficient k_c (dm/hr)	0.1 - infinite	0.1 - infinite	0.1 - infinite	0.1 - infinite	0.1 - infinite	0.1 - infinite
Cell Surface Area per Mass of Cells (dm^2/μg protein)	0.001	0.001	0.001	0.001	0.001	0.001
Protein Concentration at t = 0*** (μg/ml fluid)	0.1	0.1	0.1	0.1	0.1	0.1
Δt (hr)****	0.01	0.01	0.01	0.01	0.01	0.01
Δx (dm)****	0.5	0.5	0.5	0.5	0.5	0.5

* The values for V_{max}' and μ_{max} were lowered for groundwater simulations compared to values used in column simulations because groundwater temperatures would be lower than 22°C, which was the temperature for column experiments.

** The longitudinal dispersion coefficient reported in Semprini *et al.* (1991) was used for these simulations.

*** The initial cell density used in the Semprini *et al.* paper simulations is also used in these simulations.

**** These values are larger than the values used for column simulations due to the longer time periods used for simulations. Several simulations were done with smaller values of Δt and Δx to ensure the numerical simulation would give the same results.

Figure 6.1. Column Simulation Parametric Analysis: Effect of the Maximum Methane Utilization Rate, V_{max}', on Model Predictions*

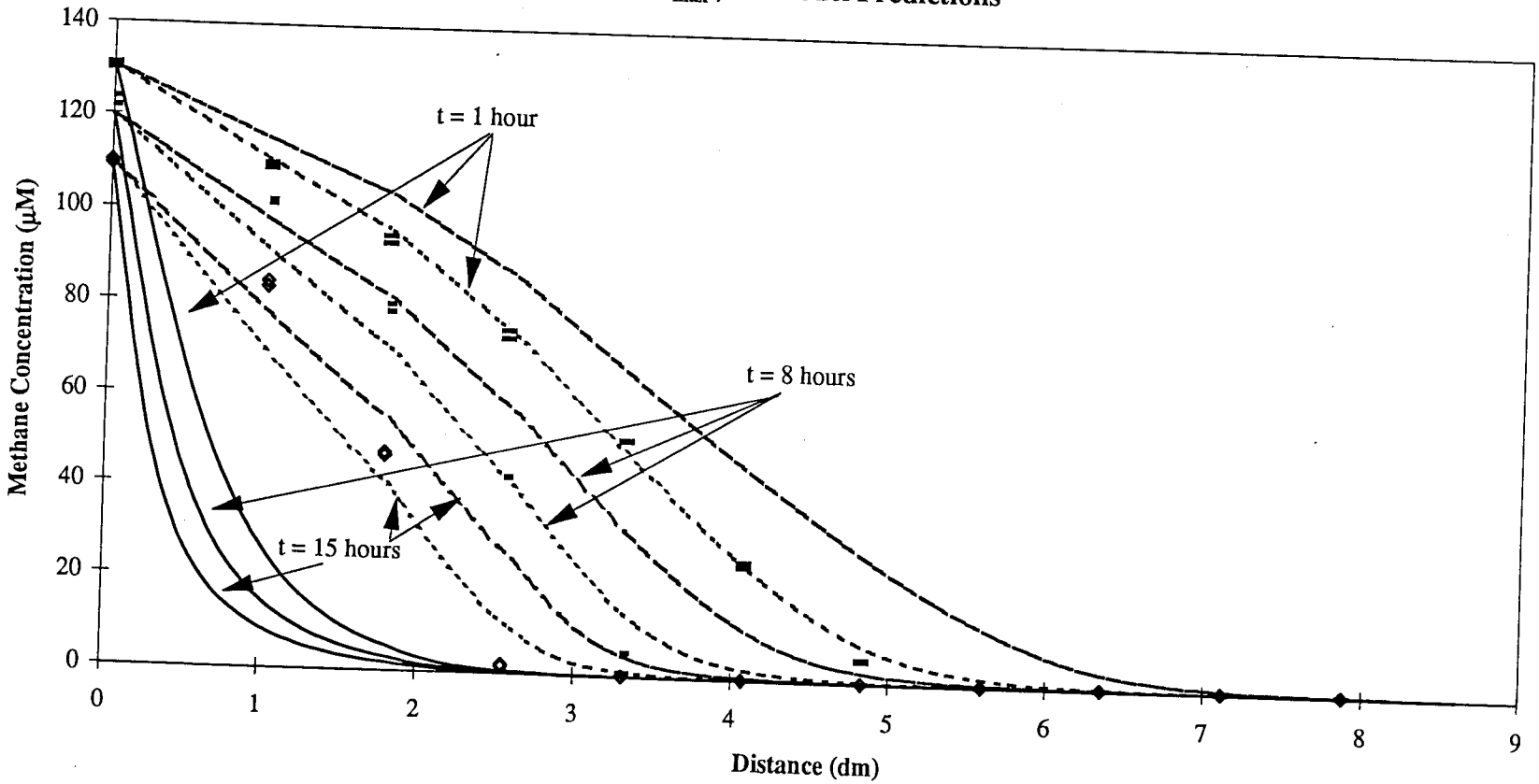

* Input parameters for simulations are shown in Table 6.1. Solid lines represent predictions with V_{max}' = 0.1 µmol/hr/µg protein. Short dashed lines represent predictions with V_{max}' = 0.013 µmol/hr/µg protein. Long dashed lines represent predictions with V_{max}' = 0.01 µmol/hr/µg protein. Symbols represent column experimental data presented in Chapter 5.

Figure 6.2. Column Simulation Parametric Analysis: Effect of the Michaelis-Menten Affinity Coefficient, K_S, and Monod Half-Maximum Growth Rate Constant, $K_{SMonod\text{-}S}$, on Model Predictions*

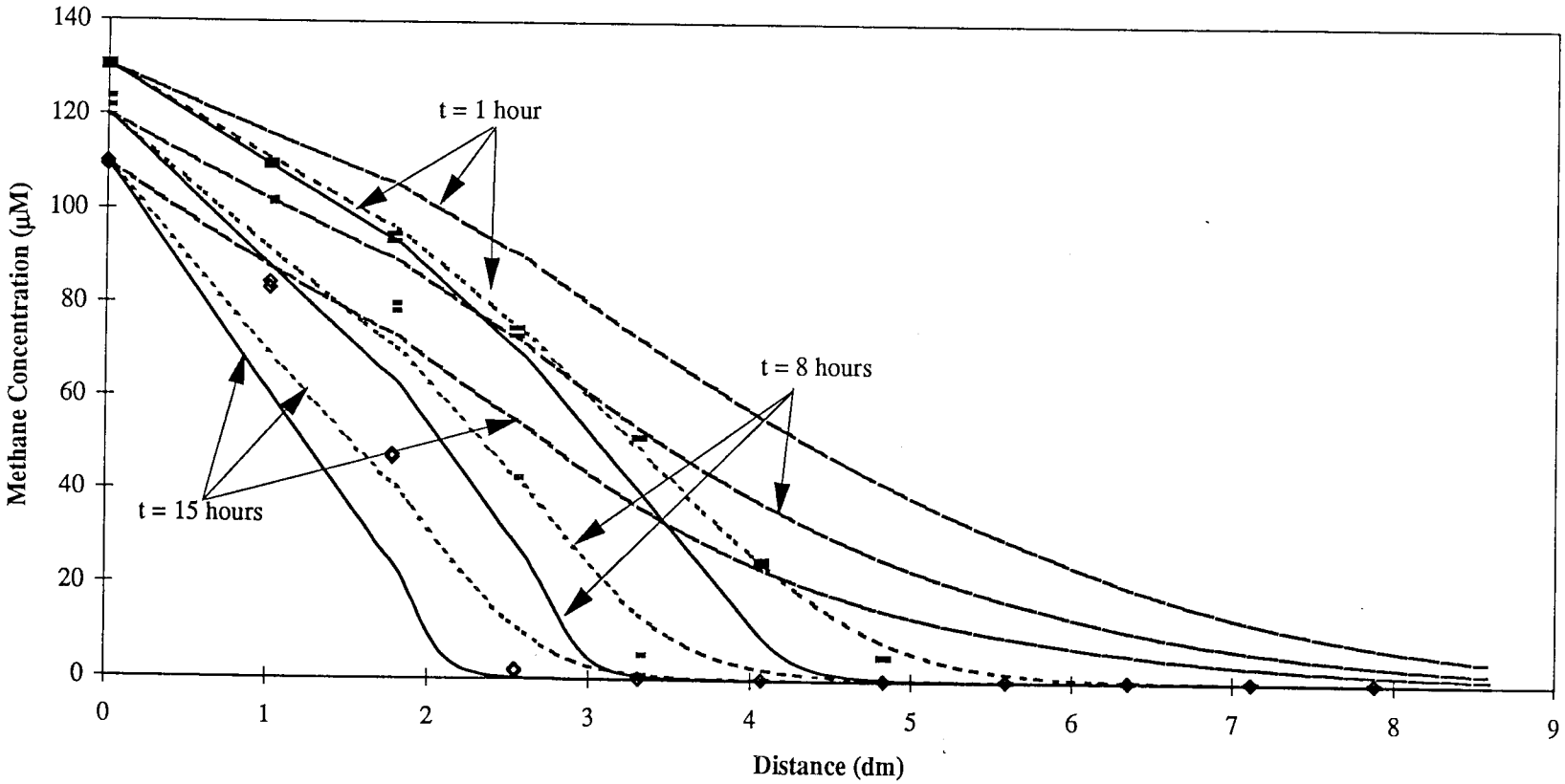

* Input parameters for simulations are shown in Table 6.1. Solid lines represent predictions with $K_S = K_{SMonod\text{-}S} = 0.1$ µM. Short dashed lines represent predictions with $K_S = K_{SMonod\text{-}S} = 8$ µM. Long dashed lines represent predictions with $K_S = K_{SMonod\text{-}S} = 50$ µM. Symbols represent column experimental data presented in Chapter 5.

Figure 6.3. Column Simulation Parametric Analysis: Effect of Maximum Specific Growth Rate, μ_{max}, on Model Predictions*

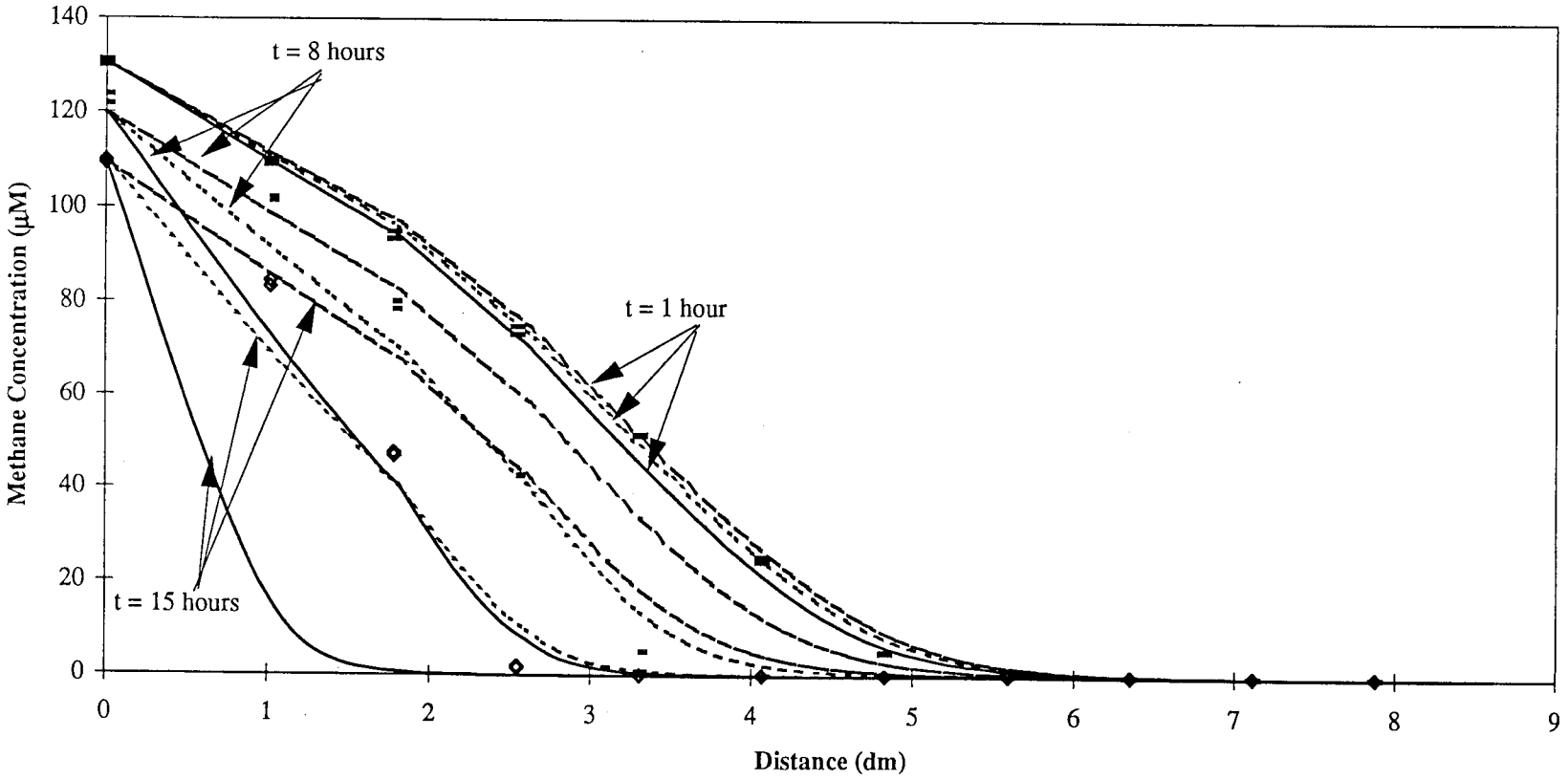

* Input parameters for simulations are shown in Table 6.1. Solid lines represent predictions with μ_{max} = 0.15/hr. Short dashed lines represent predictions with μ_{max} = 0.08/hr. Long dashed lines represent predictions with μ_{max} = 0.04/hr. Symbols represent column experimental data presented in Chapter 5.

Figure 6.4. Column Simulation Parametric Analysis: Effect of The Longitudinal Dispersion Coefficient, D_L, on Model Predictions*

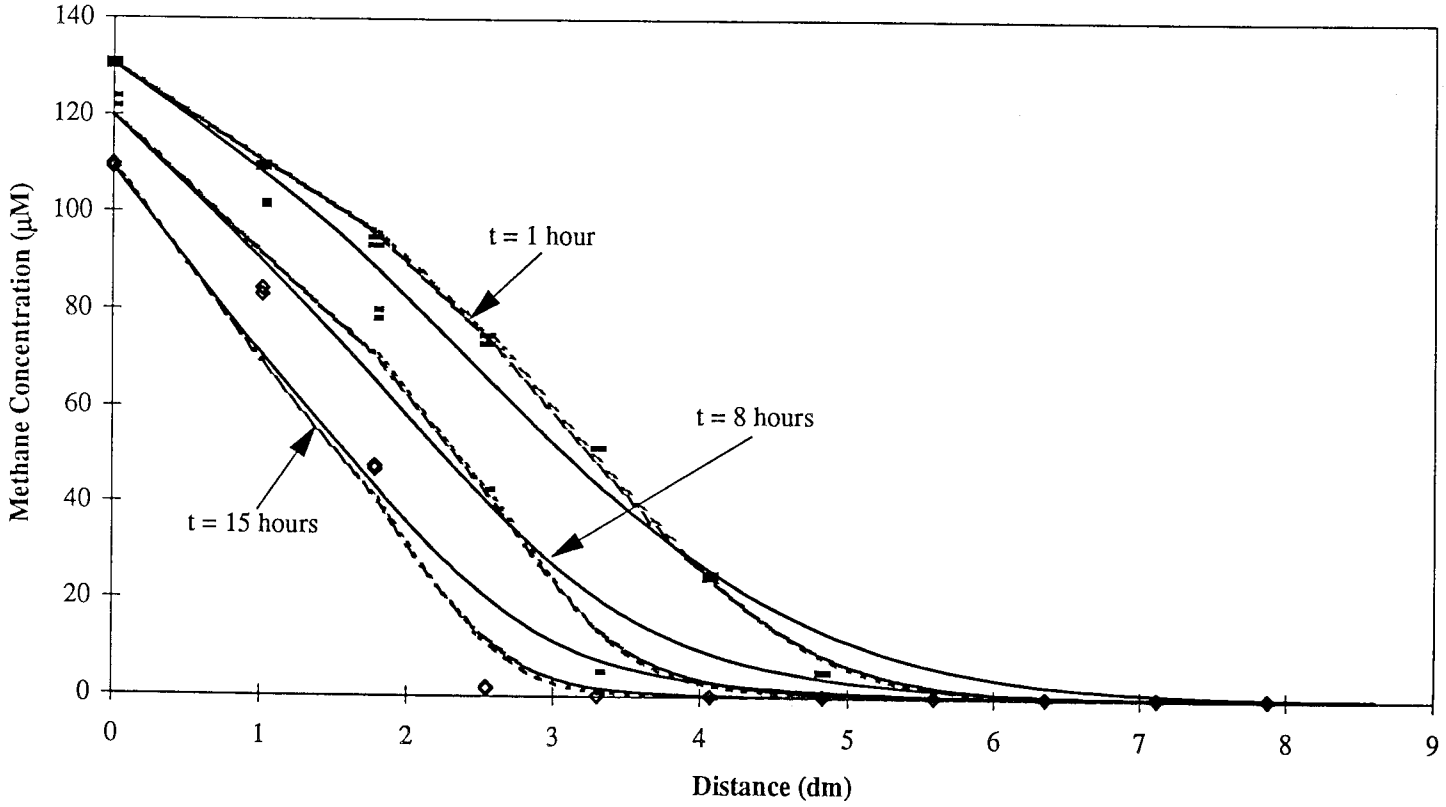

* Input parameters for simulations are shown in Table 6.1. Solid lines represent predictions with $D_L = 12$ dm^2/hr. Short dashed lines represent predictions with $D_L = 0.12$ dm^2/hr. Long dashed lines represent predictions with $D_L = 1.2$ dm^2/hr. Symbols represent column experimental data presented in Chapter 5.

Figure 6.5. Column Simulation Parametric Analysis: Effect of The Mass Transfer Coefficient, k_c, on Model Predictions*

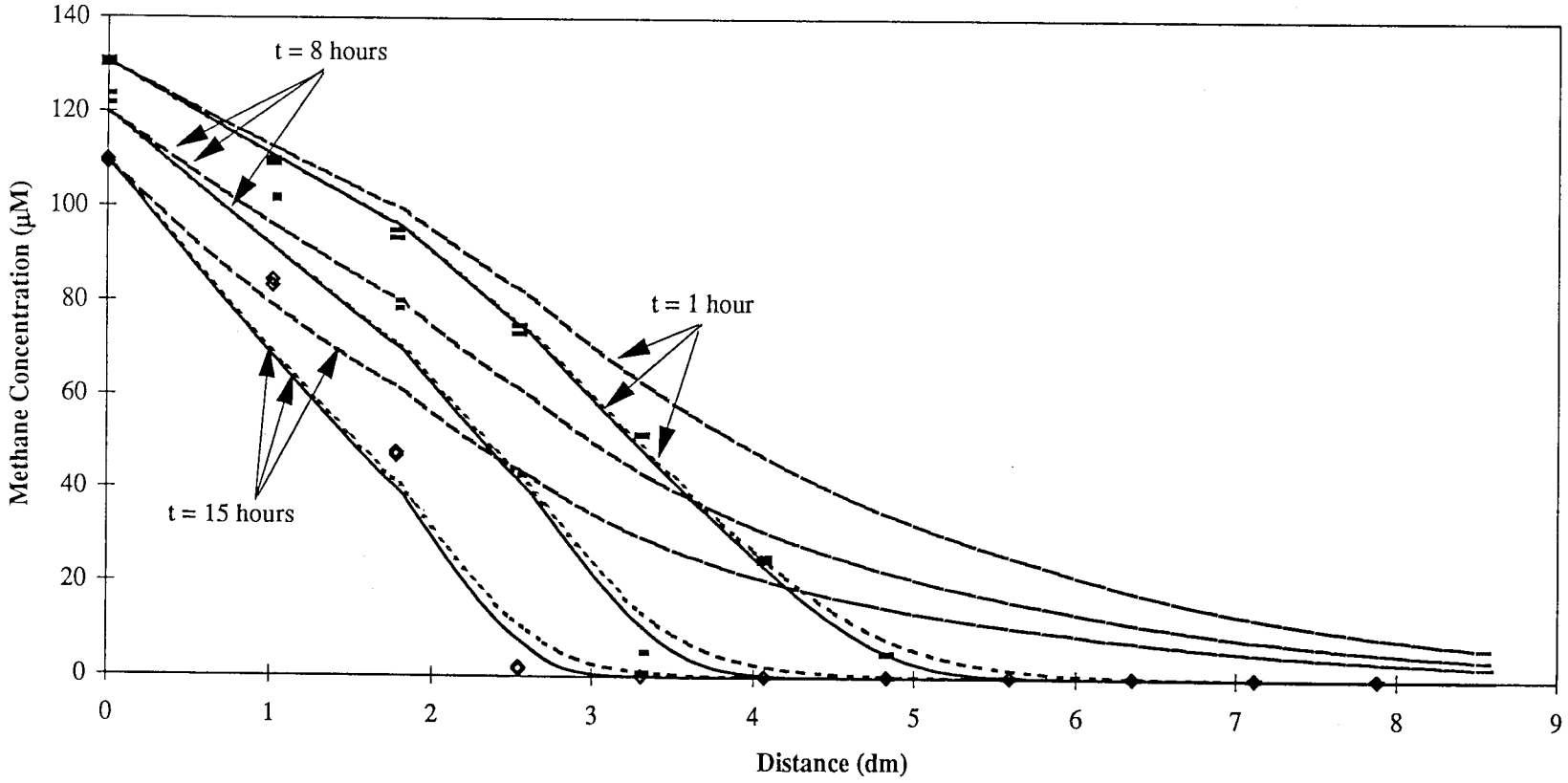

* Input parameters for simulations are shown in Table 6.1. Solid lines represent predictions with k_c = 1500 dm/hr. Short dashed lines represent predictions with k_c = 1.5 dm/hr. Long dashed lines represent predictions with k_c = 0.15 dm/hr. Symbols represent column experimental data presented in Chapter 5.

Figure 6.6. Groundwater Flow Simulations: Methane Concentration vs. Distance Over Time for $C_o = K_s$*

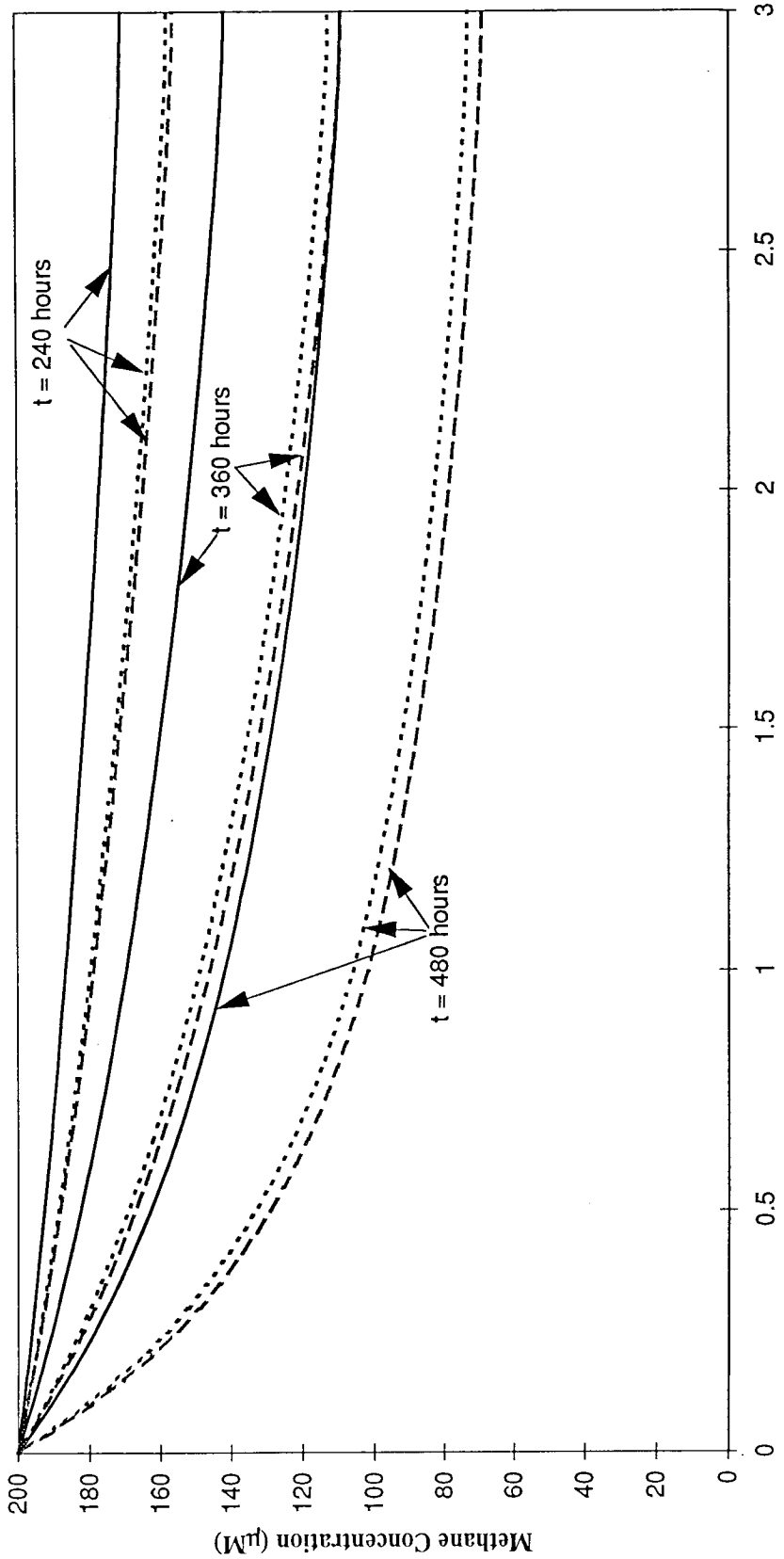

* All parameters used for model predictions are shown in Table 6.2. Solid lines represent predictions with k_c = 0.1 dm/hr. Short dashed lines represent predictions with k_c = 1 dm/hr. Long dashed lines represent predictions with k_c >> 1 dm/hr (simulation without mass transfer included).

Figure 6.7. Groundwater Flow Simulations: Methane Concentration vs. Distance Over Time for $C_o > K_s$*

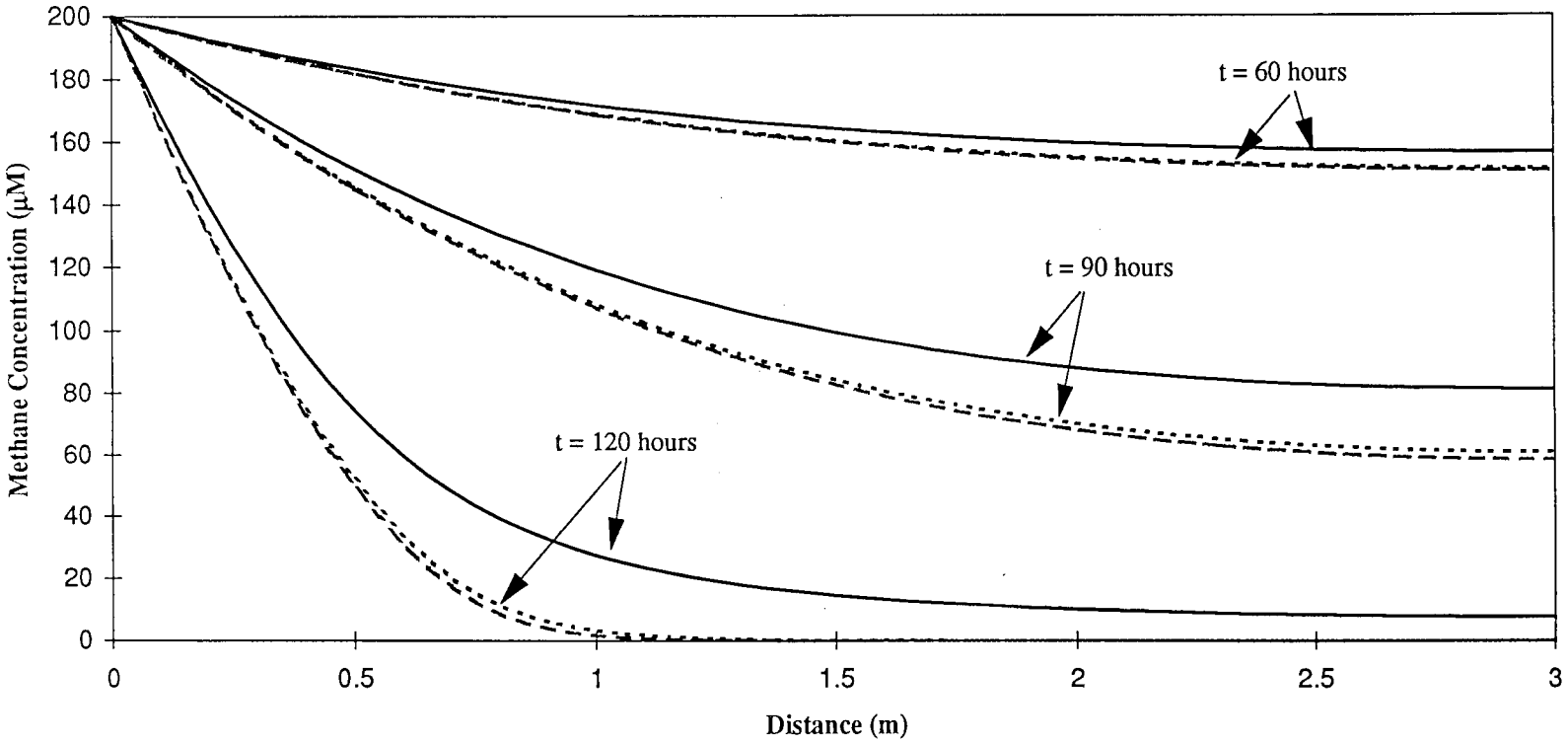

* All parameters used for model predictions are shown in Table 6.2. Solid lines represent predictions with $k_c = 0.1$ dm/hr. Short dashed lines represent predictions with $k_c = 1$ dm/hr. Long dashed lines represent predictions with $k_c >> 1$ dm/hr (simulation without mass transfer included). K_S was set to 10 μM.

Figure 6.8. Groundwater Flow Simulations: Methane Concentration vs. Distance Over Time for $C_o >> K_s$*

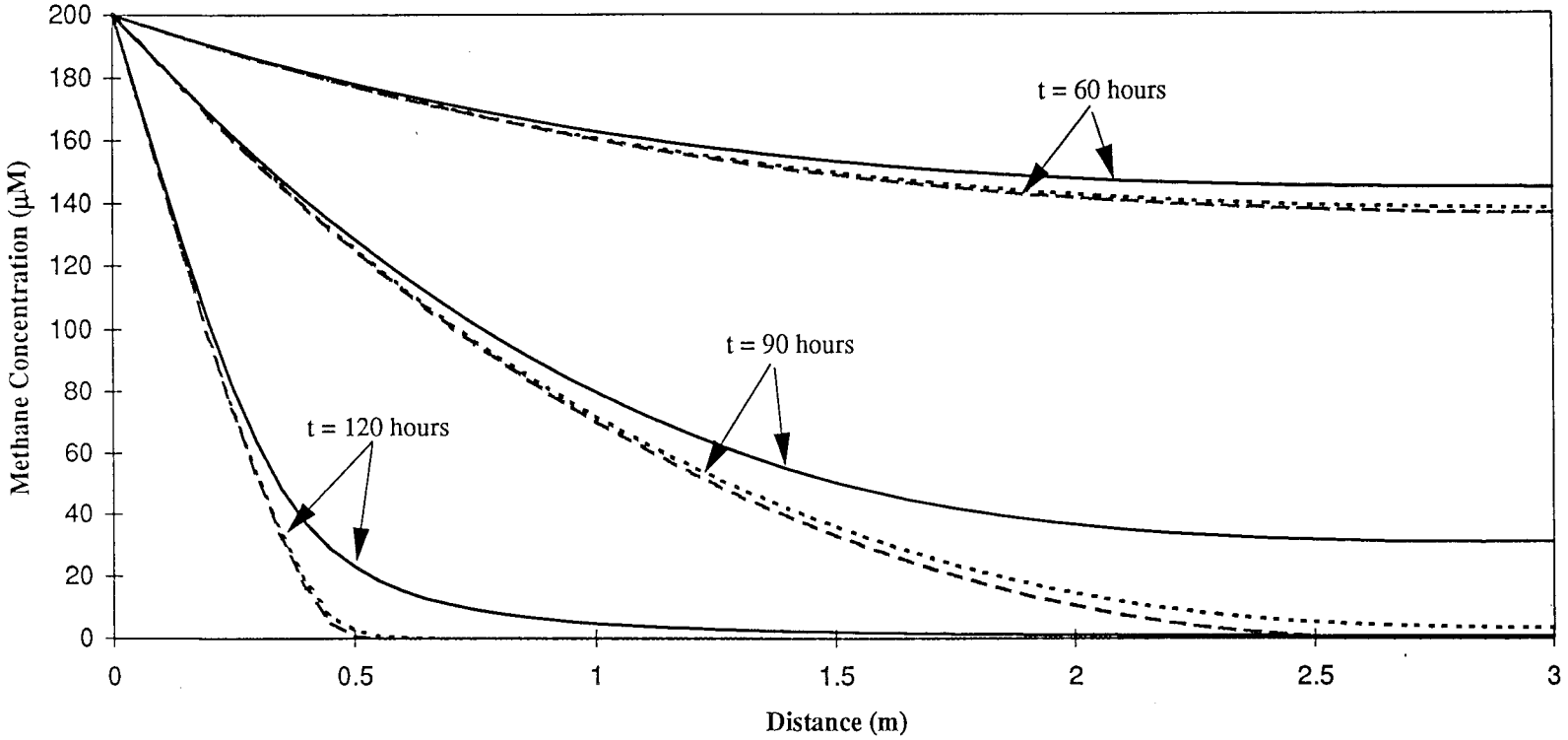

* All parameters used for model predictions are shown in Table 6.2. Solid lines represent predictions with k_c = 0.1 dm/hr. Short dashed lines represent predictions with k_c = 1 dm/hr. Long dashed lines represent predictions with $k_c >>$ 1 dm/hr (simulation without mass transfer included). K_S was set to 1 μM.

Figure 6.9. Groundwater Flow Simulations: Cell Density vs. Distance Over Time for $C_o = K_s$*

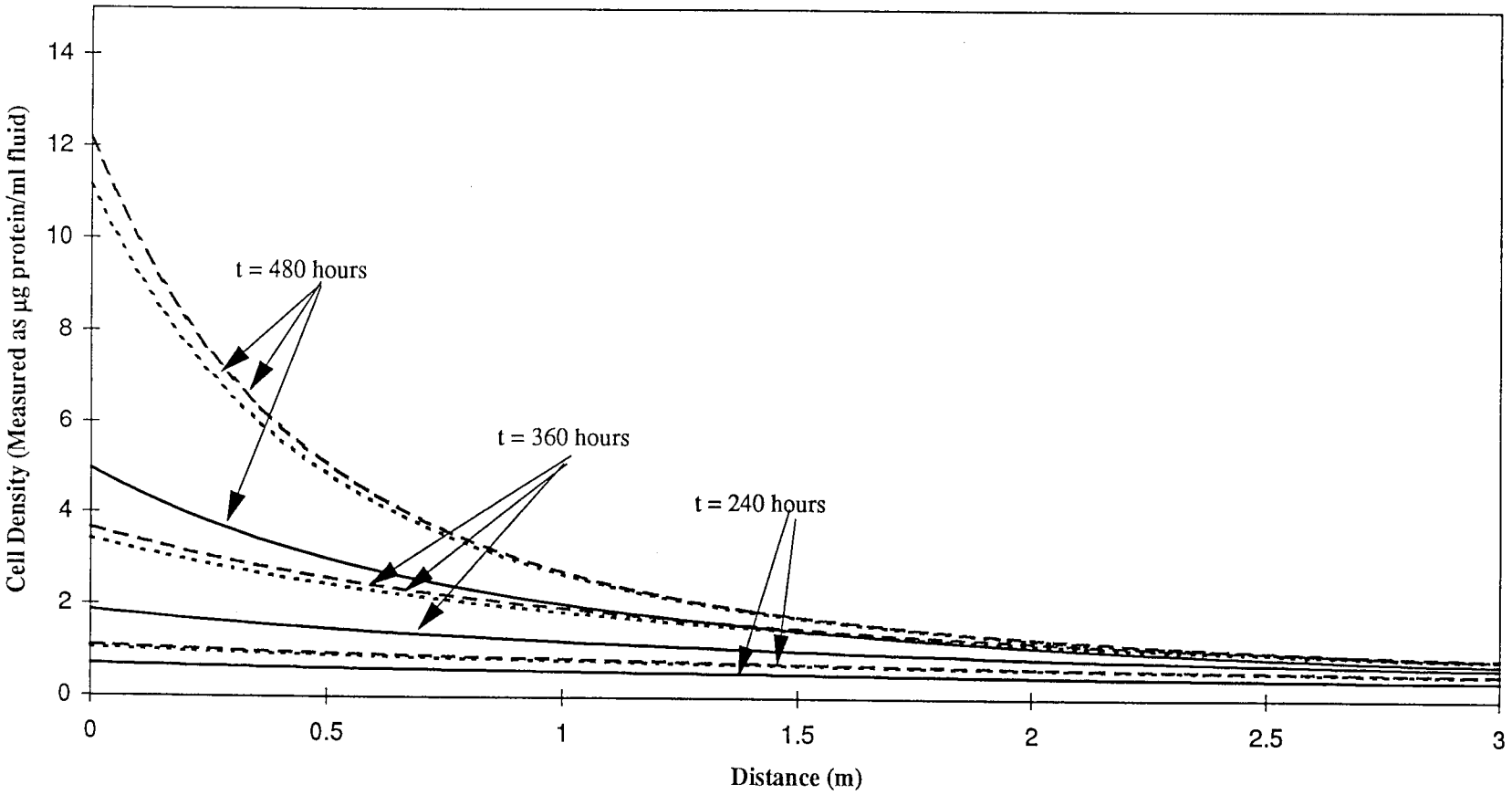

* All parameters used for model predictions are shown in Table 6.2. Solid lines represent predictions with $k_c = 0.1$ dm/hr. Short dashed lines represent predictions with $k_c = 1$ dm/hr. Long dashed lines represent predictions with $k_c >> 1$ dm/hr (simulation without mass transfer included).

Figure 6.10. Groundwater Flow Simulations: Cell Density vs. Distance Over Time for $C_o > K_S$*

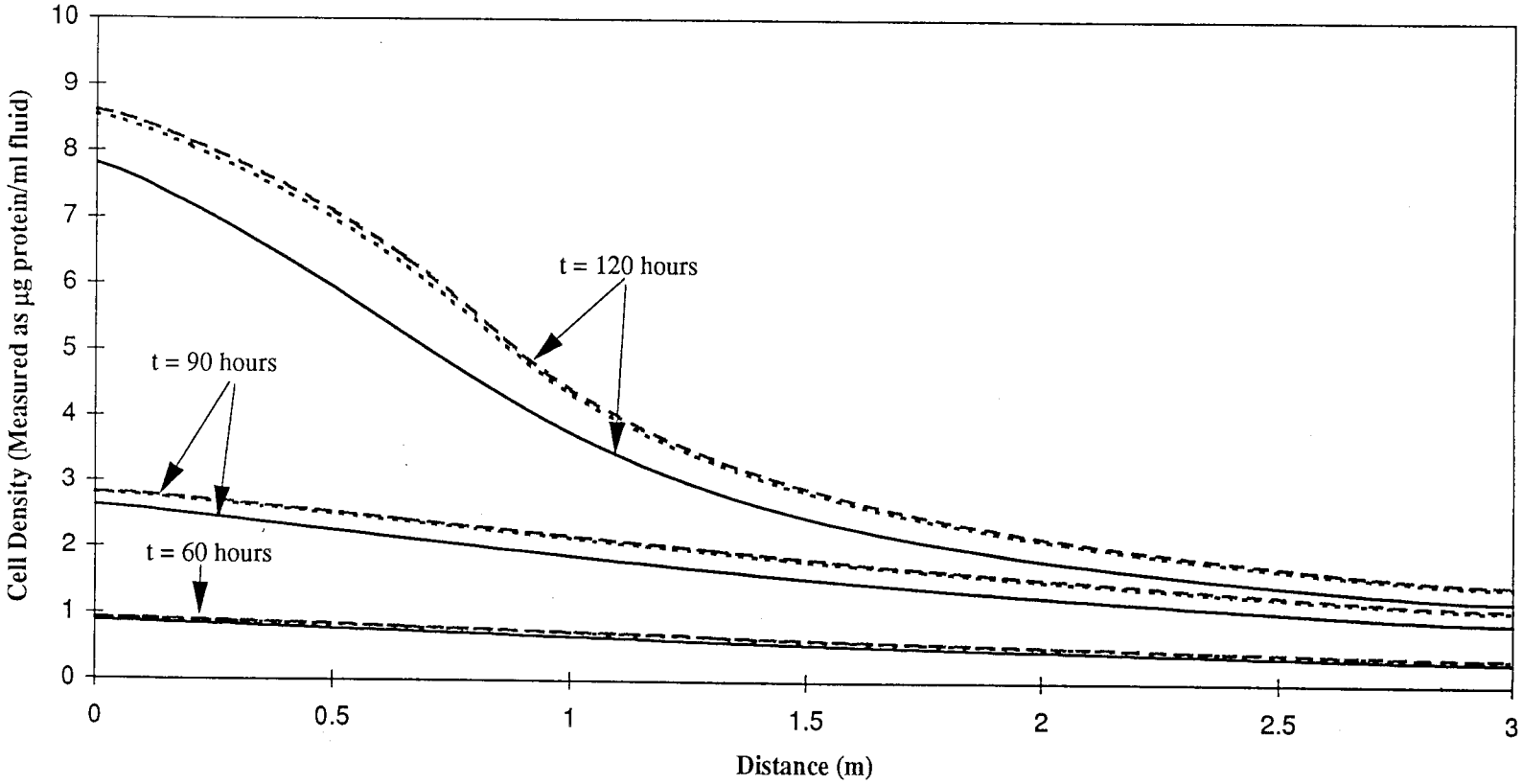

* All parameters used for model predictions are shown in Table 6.2. Solid lines represent predictions with $k_c = 0.1$ dm/hr. Short dashed lines represent predictions with $k_c = 1$ dm/hr. Long dashed lines represent predictions with $k_c >> 1$ dm/hr (simulation without mass transfer included). K_S was set to 10 µM.

Figure 6.11. Groundwater Flow Simulations: Cell Density vs. Distance Over Time for $C_o >> K_S$*

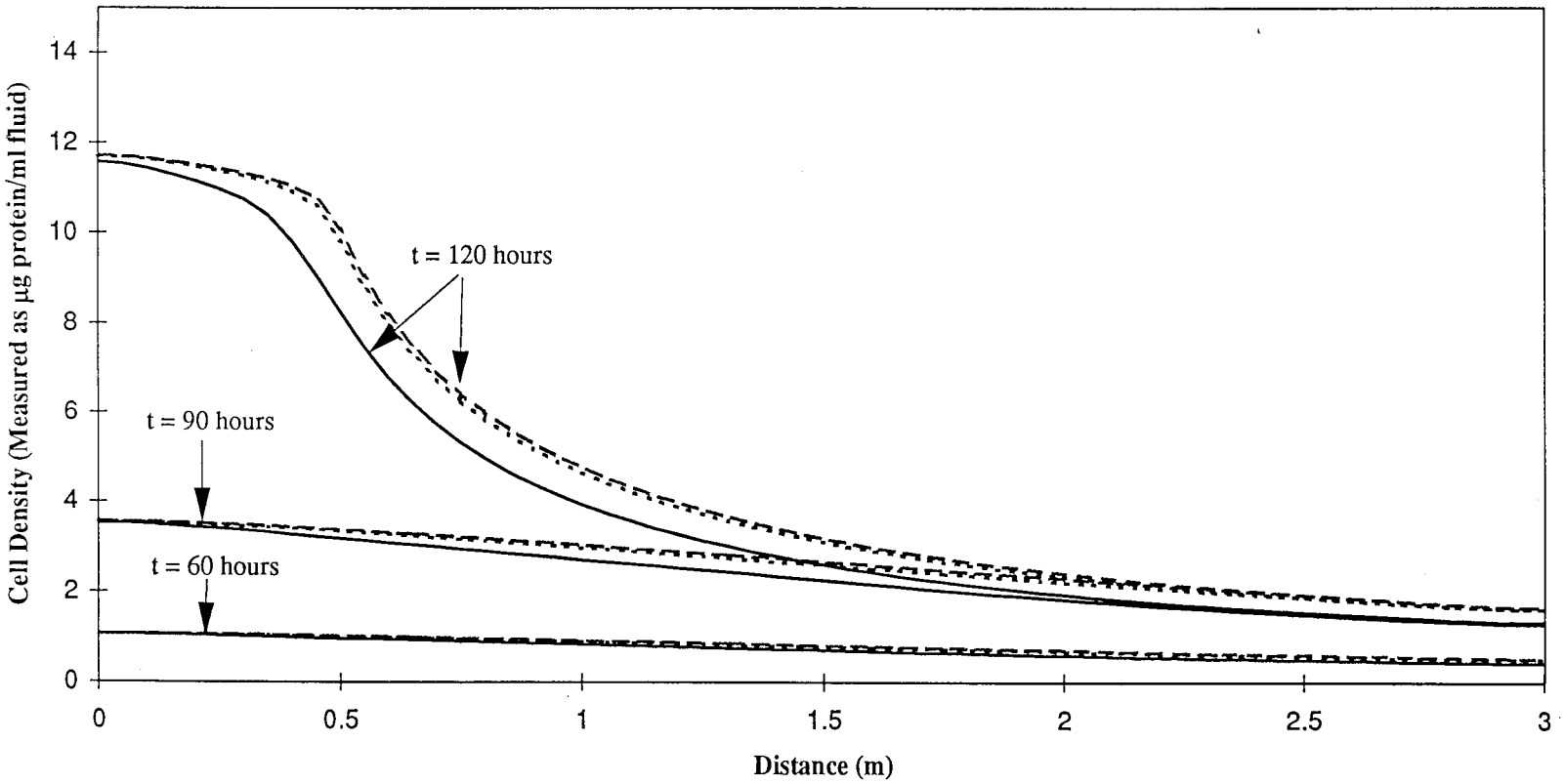

* All parameters used for model predictions are shown in Table 6.2. Solid lines represent predictions with $k_c = 0.1$ dm/hr. Short dashed lines represent predictions with $k_c = 1$ dm/hr. Long dashed lines represent predictions with $k_c >> 1$ dm/hr (simulation without mass transfer included). K_S was set to 1 µM.

6.6 References

Semprini, L., & McCarty, P.L. (1991). Comparison between model simulations and field results for *in situ* biorestoration of chlorinated aliphatics: part 1. biostimulation of methanotrophic bacteria. *Ground Water, 29,* 365-374.

Wilson, E.J., & Geankoplis, C.J. (1966). Liquid mass transfer at very low Reynolds numbers in packed beds. *Industrial and Engineering Chemistry Fundamentals, 5,* 9-14.

Chapter 7

Conclusions and Future Work

This thesis presented a description and analysis of the governing biological and physical aspects of enhancing bacterial growth for cometabolically bioremediating a contaminated groundwater system. In order to perform the analysis presented herein, several questions concerning reactor design for testing predictive models were answered. These pertained to the ability of methanotrophs to attach to washed Ottawa sand, the kinetics of methane utilization by the methanotroph *M. albus* BG8, and the physical characteristics of the reactor.

I found that of four methanotroph strains analyzed for their ability to attach to sand, only one strain displayed strong attachment characteristics. This strain, *M. albus* BG8, appeared to remain attached to sand even under harsh mixing conditions. This result is important for site remediators interested in designing above ground reactors for bioremediation. The result cannot be extrapolated to natural environments, however, because laboratory bacterial strains often have different physical characteristics than the same strain living in a natural system.

Past research has raised the question of whether and how copper affects the methane utilization kinetics of the particulate methane monooxygenase (pMMO). In addition, the kinetic parameters for methane utilization kinetics were needed as input parameters for model predictions. For these reasons, kinetic parameters were determined for *M. albus* BG8 cells for both high and low copper concentrations in cell growth medium. I found that copper did not have a statistically significant effect on the kinetic parameters for methane utilization for *M. albus* BG8 cells under the experimental conditions used.

Upon determining that *M. albus* BG8 cells attached well to pretreated sand, and ascertaining the methane utilization kinetic parameters of these cells, a column reactor was designed for testing the ability of a developed model to correctly predict methane concentrations in a plug flow reactor containing cells. The model included substrate transport, substrate oxidation by cells, and cell growth. I found that the model was able to correctly predict methane concentrations along the length of the column at different points in time.

Having shown the model's predictive ability, I analyzed the model's sensitivity to several input parameters. I found that the maximum methane uptake rate, V_{max}', and the maximum specific growth rate, μ_{max}, had the greatest effect on model predictions. Longitudinal dispersion had the smallest effect on predictions. The mass transfer coefficient had a minimal effect on model predictions until mass transfer became a limiting factor.

The mass transfer effect was studied in more detail to understand when mass transfer limitation has the strongest effect on model predictions. I found that when the growth substrate concentration approached the Michaelis-Menten affinity coefficient, K_S, mass transfer limitation had a larger impact on model predictions. This is expected because both methane uptake kinetics and cell growth kinetics are modeled as a saturation process. Far above the affinity coefficient, changes in substrate concentration do not have large effects on substrate utilization or cell growth because the kinetics approach zero-order kinetics. When the growth substrate concentration falls below the affinity coefficient, the substrate utilization and growth kinetics

approach first-order kinetics. Here, small changes in substrate concentration will affect both substrate utilization and cell growth.

This has important implications for site remediators considering using methanotrophs for bioremediation of trichloroethylene-contaminated aquifers. If remediators wanted to have uniform cell densities in systems undergoing remediation, it would be necessary to keep growth substrate concentrations far above the Michaelis-Menten affinity coefficient and Monod half-saturation growth rate constant. Predictive models such as the one presented in this thesis could be used to determine the necessary substrate concentrations needed to uphold this condition.

The obvious next step for this work would be to add trichloroethylene (TCE) degradation or oxygen limitation to the predictive model and to use the reactor described in this thesis to test the new model's predictive abilities. In addition, the reactor sand grains could be coated with chemicals that would enhance TCE adsorption in order to directly test adsorption models coupled with contaminant transport and oxidation by attached bacteria.

The reactor described herein is amenable to many changes. By changing reactor characteristics, the reactor can be used to answer more complex modeling questions pertaining to *in situ* bioremediation. Thus, I have presented not only a model for analyzing factors important for *in situ* bioremediation, but more importantly, I have developed a system which can be used to address additional questions pertaining to *in situ* bioremediation.

Appendix A

Fortran Program Used for Numerical Simulations

```
c     This program is designed to calculate the concentration of a
c     contaminant entering an aquifer at x=o fully mixed over a
c     cross-section.  The method for calculating the concentration
c     is the explicit finite difference method.
      program edye
c
cc
c
c
c
      dimension c(0:10000),temp(-1:10000),print(50),
     1 S(0:10000),stemp(0:10000),pro(0:10000),
     1 temppro(0:10000)
c
      real c,temp,d,e,tfinal,delt,delx,xfinal,dl,u,vmax,ks,
     1   first,secone,sectwo,second,third,t,pro01,pro12,pro23,
     1   pro34,pro45,pro56,pro67,pro78,pro89,pro910,
     1   pro1011,pro1112,pro1213,kc,b,a,cquad,S,
     1   temppro,pro,mumax,ksgrowth,slope,alpha,k1,
     1   k2,k3,k4,stemp,cmid,secnum,kme
c
      integer i,o,l,m,n,k,print,timeprint,p,l1,l2
c     c
c     c
c     c
      open(60,file='conct1.prn',status='new')
      print*,'Enter values for D,U,Vmax,ks, and L.'
      read*,dl,u,vmax,ks,xfinal
      print*,'Enter values for mumax and Y*maintenance energy.'
```

```
read*,mumax,kme
print*,'Enter the value for Ks for growth.'
read*,ksgrowth
print*,'enter values for alpha and the mass transfer coeff.'
read*,alpha,kc
print*,'Enter values for the protein concentration from'
print*,'port 0 to port one in ug protein/ml void space.'
read*,pro01
print*,'Enter proconc for port 1 to port 2.'
read*,pro12
print*,'Enter proconc for port 2 to port 3.'
read*,pro23
print*,'Enter proconc for port 3 to port 4.'
read*,pro34
print*,'Enter proconc for port 4 to port 5.'
read*,pro45
print*,'Enter proconc for port 5 to port 6.'
read*,pro56
print*,'Enter proconc for port 6 to port 7.'
read*,pro67
print*,'Enter proconc for port 7 to port 8.'
read*,pro78
print*,'Enter proconc for port 8 to port 9.'
read*,pro89
print*,'Enter proconc for port 9 to port 10.'
read*,pro910
print*,'Enter proconc for port 10 to port 11.'
read*,pro1011
print*,'Enter proconc for port 11 to port 12.'
read*,pro1112
```

```
      print*,'Enter proconc for port 12 to port 13.'
      read*,pro1213

c
c     c
      print*,'How long to evolve, delta time     '
      read*,tfinal,delt

      print*,'At how many times would you like data printed?'
      print*,'The maximum number is 50.'
      read*,timeprint

       do 30 i=1,timeprint
       print*,'At what time (in hours) would you like printed
     1 data? Please enter an integer only.'
       read*,print(i)
30      continue

c     c
       print*,'Enter the initial concentration'
       read*,c(0)
c     c  calculate the concentration of substrate at the
c       surface of particles at x=0:
       b=vmax/kc/alpha-c(0)+ks
       a=1.
       cquad=-ks*c(0)
       S(0)=(-b+(b**2.-4.*a*cquad)**0.5)/(2.*a)
       print*,'Enter the concentration gradient slope.'
       read*,slope
c
```

```
c
      Print*,'Input delta x        '
      read*,delx
c     c
c     c
      d=xfinal/delx

      write(*,*) 'the total number of x steps is:',d
c
c       calculate the total number of steps for x and the
c       number of steps between printed data.
c
      l=ifix(d+0.00001*d)
      m=ifix(l/50)

      write(60,*) 'These data were obtained with qw_menx4.'
      write(60,*) 'The total number of x steps is:',l
      write(60,*) 'The steps are printed every',m,'steps.'
c
c       set the initial time to 0.0
c
       t=0.
c
c       set the initial concentration in the
c       bulk fluid phase and near particle surfaces to
c       0.0 for all points in the column except the initial
c       point, at x=0.0.  These are the values for all
c       x at t=0.0
c
c
```

```
      do 200    k=1,l
c
c
          c(k)=0.
          S(k)=0.
c
c
200   continue
c
c
      write(60,*) ' c(0)= ',c(0)
      write(60,*) 'Concentration Gradient slope =',slope
      write(60,*) 'final time = ',tfinal
      write(60,*) 'delta time = ',delt
      write(60,*) 'total length = ',xfinal
      write(60,*) 'delta x =',delx
      write(60,*) 'Vmax prime = ',vmax
      write(60,*) 'maximum specific growth rate =',mumax
      write(60,*) 'maintenance*Yield =',kme
      write(60,*) 'Dl=',dl
      write(60,*) 'kc=',kc
      write(60,*) 'alpha=',alpha
      write(60,*) 'velocity = ',u
      write(60,*) 'Ks =',ks
      write(60,*) 'Ks for growth =',ksgrowth
      write(60,*) 'Protein concentrations from port 0 to port 10'
      write(60,*) 'in ug protein/ml void volume are:'
      write(60,270) pro01,pro12,pro23,pro34,pro45,pro56,pro67,pro78,
     1 pro89,pro910
c     c
```

```
c
270   format(10(f7.3,1x))
c
c      calculate the total number of time steps, n
c
      n=int((tfinal+0.0000001*tfinal)/delt)
c     c


c      first distance in the column from port 0 to port 1 is 4 inches,
c      or 10 cm, or 1 dm.  substract 0.00001 from xfinal to avoid
c      integer - real number problems

      l1=(l/(xfinal-0.00001))*1
      write(*,*) 'l1 = ',l1
c
c      every other distance from port to port in the column is 3 inches
c      or 0.76 dm.  Add 1 to l2 to correct roundoff errors on the
c      calculation

      l2=(l/(xfinal))*0.76+1
      write(*,*) 'l2 = ',l2
c
c       set up the initial protein concentrations.
      do 290     k=0,l1
           pro(k)=pro01
290      continue
      do 291         k=l1+1,l1+l2
         pro(k)=pro12
291       continue
       do 292    k=l1+l2+1,l1+2*l2
```

```
      pro(k)=pro23
292     continue
      do 293 k=l1+2*l2+1,l1+3*l2
        pro(k)=pro34
293     continue
      do 294 k=l1+3*l2+1,l1+4*l2
        pro(k)=pro45
294     continue
      do 295 k=l1+4*l2+1,l1+5*l2
        pro(k)=pro56
295     continue
      do 296 k=l1+5*l2+1,l1+6*l2
        pro(k)=pro67
296     continue
      do 297 k=l1+6*l2+1,l1+7*l2
         pro(k)=pro78
297     continue
      do 298 k=l1+7*l2+1,l1+8*l2
        pro(k)=pro89
298     continue
      do 299 k=l1+8*l2+1,l1+9*l2
         pro(k)=pro910
299     continue
      do 300 k=l1+9*l2+1,l1+10*l2
         pro(k)=pro1011
300     continue
      do 301 k=l1+10*l2+1,l1+11*l2
        pro(k)=pro1112
301     continue
      do 302 k=l1+11*l2+1,l1+12*l2
```

```
      pro(k)=pro1213
302   continue


   do 800   i=1,n,1
c
c     i starts at 1 because all the concentrations have been
c     set up for all x at t=0.0 above.  So the first calculation
c     is for t=t+delt, i=1.
c     set time to the time at which new concentrations
c     are being measured.

      t=t+delt
c
   do 305   k=0,1,1
c
c     set up temporary variables for Cbulk, Cs, and X
c     the "temp" represents the value at each point in
c     space k at the time (i-1)*delt.  The temp(k)
c     values are used to calculate the new concentrations
c     at each point in space, k, at the current time i*delt.
c
      temp(k)=c(k)
      stemp(k)=S(k)
      temppro(k)=pro(k)

c
305   continue
c
c     set up the temporary Cbulk before the inlet for calculating
```

```
c     dc/dx at the second node (x=delx) (the first node is x=0)
c
      temp(-1)=temp(0)
c
c     calculate the concentrations for all x at time i*delt
c
     do 310    k=1,l-1
c
c     this is Dd2c/dx2 - uses forward time centered space scheme
c     from Numerical Recipes
c
      first=dl*(temp(k-1)-2.*temp(k)+temp(k+1))/delx/delx*delt
c
c     this is -udc/dx - uses Quick method from Leonard
c
      secone=1./8.*temp(k-2)-7./8.*temp(k-1)
      sectwo=3./8.*temp(k)+3./8.*temp(k+1)
      second=-u*(secone+sectwo)/delx*delt
c
c     try the Lax method.
c       secone=-u*(temp(k+1)-temp(k-1))/2./delx
c       sectwo=(temp(k+1)-2.*temp(k)+temp(k-1))/2./delt
c       second=(secone+sectwo)*delt
c
c     upwind differencing:   p. 630 in Numeric Recipes
c
c      second=-u*(temp(k)-temp(k-1))/delx*delt
c
      third=-kc*alpha*temppro(k)*1000.*(temp(k)-stemp(k))*delt
c
```

```
c
c
c
      c(k)=first+second+third+temp(k)
310   continue

c     dc/dx=0 at x=L, set c(x=L-delx)=c(x=L)
      c(l)=c(l-1)
c     c(0)=Co-slope*time
      c(0)=temp(0)+slope*delt



c     calculate the new Csurface at time i*delt, also
c     calculate the new protein concentrations, X
c
      do 355 o=0,l,1

c     use the quadratic formula for S.

      b=vmax/(alpha*kc)-c(o)+ks
      a=1.
      cquad=-ks*c(o)

320       S(o)=(-b+(b**2.-4.*a*cquad)**0.5)/(2.*a)
c
c     if S(o) is low enough such that
c     mumax(S/Ks+S)<kme, then dX/dt =0, otherwise
c     dX/dt=(mumax*S/(Ks+S)-kme)X

      if(mumax*S(o)/(ks+S(o)).lt.kme) then
```

```
      pro(o)=temppro(o)

      else

c     Calculate the linear interpolation for Csurface at time
c     t=1/2((i-1)delt + i*delt)
c
      cmid=(stemp(o)+S(o))/2.
c
c     calculate the Runge-Kutte parameters for integrating
c     dX/dt

      k1=(temppro(o)*(mumax*stemp(o)/(ksgrowth+stemp(o))-kme))*delt
      k2=((temppro(o)+k1/2.)*(mumax*cmid/(ksgrowth+cmid)-kme))*delt
      k3=((temppro(o)+k2/2.)*(mumax*cmid/(ksgrowth+cmid)-kme))*delt
      k4=((temppro(o)+k3/2.)*(mumax*S(o)/(ksgrowth+S(o))-kme))*delt
c
c     calculate the new protein concentration at t=i*delt
      pro(o)=temppro(o)+k1/6.+k2/3.+k3/3.+k4/6.


c     this is the endif for the test of
c     mumax*S/(Ks+S)<kme
      endif

355   continue
c
c     we want to print out results at the times specified above.

      do 370 p=1,timeprint
```

```
      if(ifix(t*1000.).eq.1000*print(p)) then
      write(60,*) 'time= ',t
      write(60,*)'Protein concentrations from port 0 to port 10'
      write (60,*) 'in ug protein/ml fluid are:'
      write(60,270) pro(l1),pro(l1+l2),pro(l1+2*l2),pro(l1+3*l2),
     1  pro(l1+4*l2),pro(l1+5*l2),pro(l1+6*l2),pro(l1+7*l2),
     1  pro(l1+8*l2),pro(l1+9*l2)

      write(60,360) (c(k),S(k),pro(k),k=0,l,l/50)
360   format(f11.4,5x,f11.4,5x,f7.3)

      endif
370     continue
c
c
800   continue

c
c
    end
c
```

Appendix B

List of Variables

a = specific maintenance rate $\left(\frac{1}{t}\right)$

a' = gas-liquid interfacial area per unit volume fluid $\left(\frac{1}{l}\right)$

C = concenteration of dissolved gas in the bulk liquid $\left(\frac{m}{l^3}\right)$

C* = concentration of dissolved gas at a gas-liquid interface in equilibrium with gas at the interface $\left(\frac{m}{l^3}\right)$

C_B = substrate concentration in the bulk fluid phase $\left(\frac{m}{l^3}\right)$

C_o = substrate concentration at x=0 and t=0 $\left(\frac{m}{l^3}\right)$

C_S = substrate concentration near the surface of a particle $\left(\frac{m}{l^3}\right)$

D = substrate diffusion coefficient $\left(\frac{l^2}{t}\right)$

d_c = cell decay oxygen demand $\left(\frac{m_{oxygen}}{m_{cell}}\right)$

D_L = longitudinal dispersion coefficient $\left(\frac{l^2}{t}\right)$

F = substrate to oxygen utilization ratio for cell growth $\left(\frac{m_{oxygen}}{m_{substrate}}\right)$

f_d = biodegradable fraction of cells (-)

j_D = Chilton-Colburn j-factor (-)

k_c = mass transfer coefficient $\left(\frac{l}{t}\right)$

k_L = liquid flim mass transfer coefficient $\left(\frac{l}{t}\right)$

K_m = Michaelis-Menten affinity coefficient for a pure enzyme $\left(\frac{m}{l^3}\right)$

K_S = Michaelis-Menten affinity coefficient for whole cells $\left(\frac{m}{l^3}\right)$

$K_{S_{Monod_o}}$ = Monod oxygen concentration at half-maximum growth rate $\left(\frac{m}{l^3}\right)$

$K_{S_{Monod\,S}}$ = Monod substrate concentration at half-maximum growth rate $\left(\frac{m}{l^3}\right)$

MUR = methane uptake rate $\left(\frac{m}{l^3 t}\right)$

$N_{substrate}$ = flux of substrate from the bulk fluid to a particle surface $\left(\frac{m}{l^2 t}\right)$

O = oxygen concentration $\left(\frac{m}{l^3}\right)$

Ra' = observed rate of absorption per unit volume fluid $\left(\frac{m}{l^3 t}\right)$

Re' = Reynolds number in terms of a particle diameter, superficial mass velocity of fluid, and fluid viscosity (-)

S = substrate concentration $\left(\frac{m}{l^3}\right)$

Sc = Schmidt number (-)

t = time

U = velocity $\left(\frac{l}{t}\right)$

V = velocity of reaction $\left(\frac{m}{l^3 t}\right)$

V' = velocity of reaction normalized to cell mass $\left(\frac{m_{substrate}}{m_{cells} t}\right)$

V_L = liquid volume (l^3)

V_{max} = maximum velocity of reaction $\left(\frac{m}{l^3 t}\right)$

V_{max}' = maximum velocity of reaction normalized to cell mass $\left(\frac{m_{substrate}}{m_{cells} t}\right)$

x = distance (l)

X = cell mass concentration $\left(\frac{m}{l^3}\right)$

Y = cell yield coefficient $\left(\frac{m_{cells}}{m_{substrate}}\right)$

α = surface area of cells exposed to fluid per unit mass of cells $\left(\frac{l^2}{m}\right)$

δ = particle diffusion boundary layer thickness (l)

ε = porosity (-)

μ = specific growth rate of cells $\left(\frac{1}{t}\right)$

μ_{dec} = specific decay rate of cells $\left(\frac{1}{t}\right)$

μ_{max} = maximum specific growth rate of cells $\left(\frac{1}{t}\right)$